NERC Scientific Facilities and Technology
Ion Microprobe Facility

University Of Edinburgh
NERC Ion Microprobe Facility

2007 Annual Science Report

Ion Microprobe Facility
School of Geosciences
Kings Buildings
West Mains Road
Edinburgh
EH9 3FE

https://www.edweb.ed.ac.uk/geosciences/facilities/ionprobe

Contents

	from $\delta^{18}O$ by SIMS analysis of quartz cement in Cambrian sandstones, Baltic Basin
N. Oskarsson	Volatiles in magmas quantified by Ion-probe analysis of silicate inclusions
E. Passmore, J. Maclennan & J.G. Fitton	Investigating volatile saturation pressures and degassing in the plumbing system of the 1783 AD Laki fissure eruption
D.M. Pyle, S.J.Collins & J. Maclennan	The melt inclusion record of magma degassing at Etna, Sicily
A.J. Ridgwell & D.N. Schmidt	Ocean acidification during the Palaeogene hyperthermals
D. N. Schmidt	Variation of boron isotopes and trace elements in foraminifers: biomineralisation or ecology?
V.C. Smith, J. Blundy & J.L. Acre	Open system processes recorded in plagioclase phenocrysts from Nevado de Toluca, Mexico
N.A. Starkey & J. Maclennan	Melt inclusions in a Baffin Island high-$^{3}He/^{4}He$ picrite: source variability or crustal contamination
C.D. Storey and C.J. Hawkesworth	Probing the birth and growth of continents via isotopic records in titanite
M. Talikka, S. Vuori, R. Lahtinen	Geochemistry and boron isotopic composition of tourmalines from gold-bearing and barren rocks in SW Finland – a pilot study
R.J.M. Taylor, S.L. Harley, R.W. Hinton & S. Elphick	Distribution of trace elements between zircon, garnet and melt: a key to understanding crustal events and processes
C. W. Thomas & P.C.J. Donoghue	Trace element analysis of Neoproterozoic metazoan embryos
M. Walter& G.P Bulanova	The carbon isotopic composition of diamonds from Juina, Brazil
D.F. Wiggers de Vries, G.R. Davies, D.G. Pearson & G.P Bulanova	Understanding the processes that control diamond formation and their growth histories: a mineralogical, carbon, nitrogen and Re-Os isotope study
P.M Wynn, I.J. Fairchild & A. Baker	Annual sulphate abundance cycles and secular sulphur isotope variations in speleothems

Lithium isotopes in foraminferal hosted calcite

R. Abell[1] & T. Elliott[1]

[1]Department of Earth Sciences, University of Bristol, Bristol BS8 IRJ, UK

Overview

Elemental distributions within foraminiferal tests have been shown to be complex and it is not necessarily simple to reconstruct palaeo information from their measurement [1]. We wished to similarly investigate the *in situ* variability of Li isotopes and Li/Ca, to assess its robustness as a palaeo-proxy with which to gain information of variations in the Li geochemical cycle.

The SIMS analyses carried out using the single collector Cameca ims 4f. A 10 to 20 nA $^{16}O^-$ primary beam focused to 10 - 20 µm spot size spluttered positive secondary ion (^{6}Li for 5 seconds and ^{7}Li for 2 seconds) from the resin mounted foraminifera (see appendix). Repeat analysis (n=16) of glass standard BCR2 gives and external reproducibility of ± 2.3 ‰ (2 σ) and 11 analyses of a desmophyllum coralline standard (PS69/318-1 from the Haxby Seamounts) ± 2.0 ‰ (2 σ). This natural carbonate standard provides a matrix-matched standard with which to overcome instrument mass fractionation. Bulk measurements of this standard were performed via MC-ICP-MS at the University of Bristol, Department of Earth Sciences and was found to have a δ^7Li = 27.0 ‰. In addition to measuring Li isotopes, we monitored ^{7}Li, ^{26}Mg, ^{30}Si, ^{27}Al ^{44}Ca ^{55}Mn and ^{88}Sr concentrations and filtered data to remove analysis containing clay contamination.

Results

Figure 1 shows the average results of the SIMS analysis from two *G.truncatulinoides* 2_1A, 2_1B and 2_1E (sample 2_1A re-polished to analyse twice) one sample of *G.tumida* and three samples of *G.sacculifer* with pooled data are plotted on Figure 1. The average values plotted show good agreement with the trend of δ^7Li and Li/Ca in bulk values of foraminifera. Namely decreasing Li/Ca with increasing δ^7Li and an offset to lower Li/Ca values with species *G.tumida* [2]

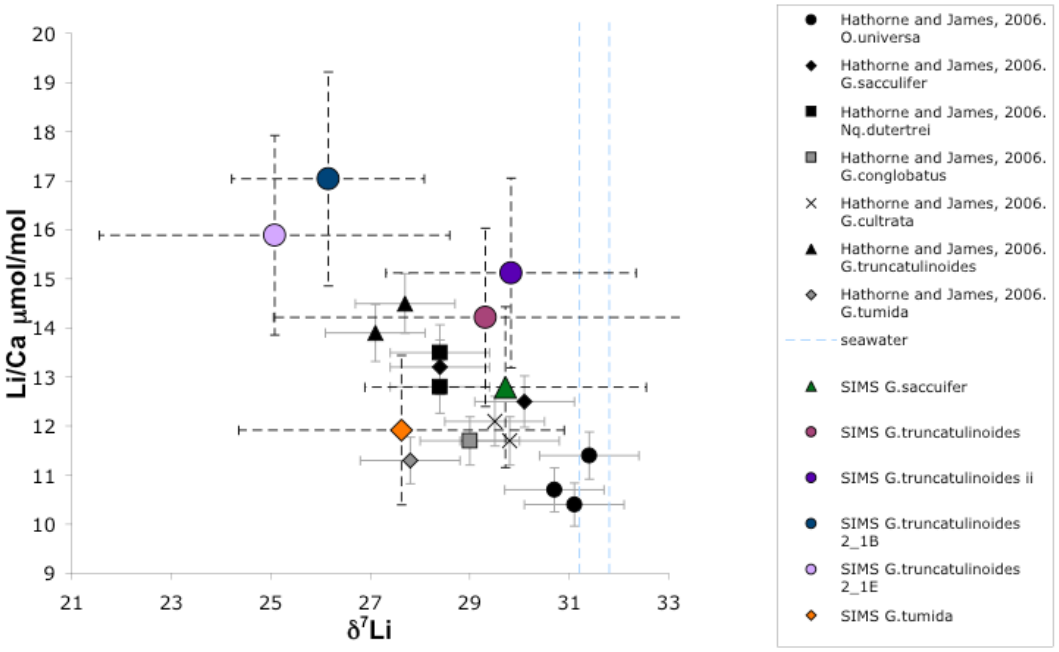

Figure 1. SIMS analysis of 3 species of recent foraminifera from this study (2σ) and compared with published MC-ICP-MS and ICP-MS values [2].

We document not only the previous species-specific variation [2] but also uniquely intra species variation of the SIMS analysis of *G.truncatulinoides* (figure 2). Figure 2 shows the individual δ^7Li and Li/Ca analysis of *G.truncatulinoides,* which shows a similar trend in the single specimens to the multi-species trend of figure 1. The SIMS analysis of *G.truncatulinoides* samples both ontogenetic (development stage) chamber carbonate (produced at varying depths during migration of the specimen during chamber foramation) and also gametogenic (reproductive stage) calcite precipitated in the final stages of the specimen's life cycle. The different depth habitats that *G.truncatulinoides* occupy during its different chamber formation represent dissimilarity in environmental parameters that are experienced during calcification (e.g. water chemistry, temperature and light availability).

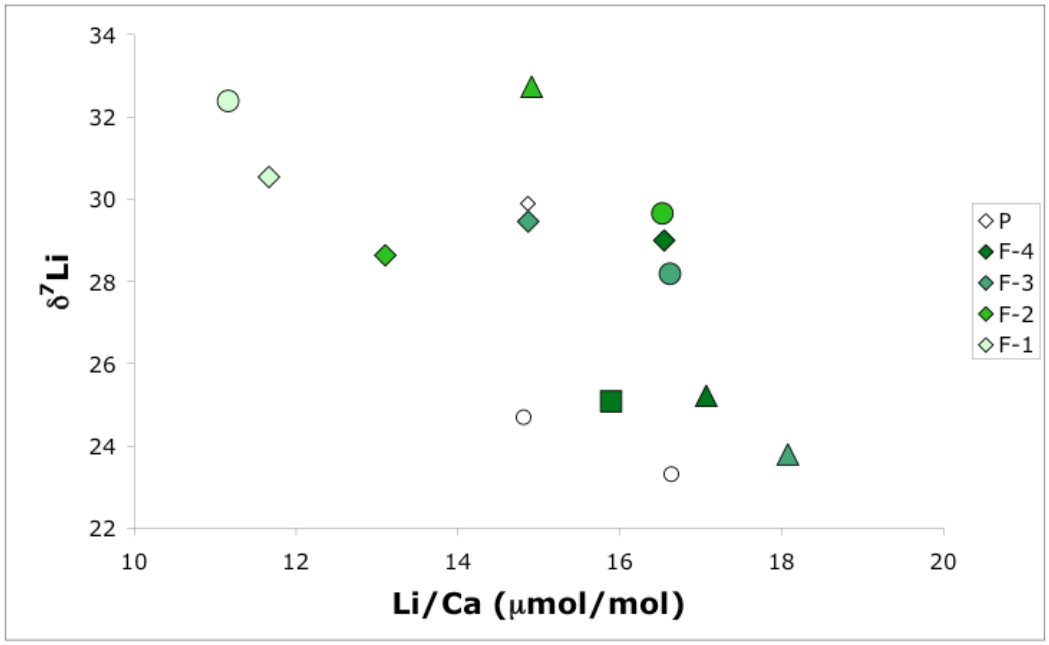

Figure 2. SIMS analysis of average chamber values (final chamber, f-x. P = procolith) from 4 samples of recent *G.truncatulinoides*.

The different Li isotope ratios and Li/Ca (figure 2) suggest that environmental parameters affect the measured Li/Ca and δ^7Li as this species migrates through the water column, and are likely the cause of the general trend apparent in figure 1. This alludes to a complicated process of Li incorporation that is metabolically or physiologically mediated as found in other more traditional proxies. If temporal foraminiferal archives are to be interpreted in terms of the variations in the Li geochemical cycle [2], this environmental effect must be separated to reveal the true Li composition of seawater.

References

[1] J. Erez Reviews in Mineralogy and Geochemistry 54 (2003) 115-149.
[2] E.C. Hathorne, O. Alard, R.H. James, and N.W. Rogers. Geochemistry Geophysics Geosystems 4, 12.

Coral calcifying fluid pH (indicated by $\delta^{11}B$) and skeletal $\delta^{18}O$ and Sr/Ca in coral skeletons

N. Allison[1]& A. A. Finch[1]

[1]School of Geography and Geosciences, University of St. Andrews, St. Andrews KY16 9AL, UK

Introduction

Coral skeleton geochemistry reflects the environmental factors prevailing at the time of deposition and the analysis of fossil skeletons offers a method to reconstruct past climate e.g. skeletal Sr/Ca ratios indicate sea surface temperatures (SSTs) while $\delta^{18}O$ combines information on SST and seawater $\delta^{18}O$ (reflecting ice volume and local precipitation). However SIMS $\delta^{18}O$ and Sr/Ca analyses indicate that skeletons are much more geochemically heterogeneous than expected indicating the importance of other, non climatic factors on skeletal geochemistry (*1*). Understanding the cause of this heterogeneity is essential for the effective development of coral skeletons as climate indicators. To further our understanding of processes affecting skeletal chemistry we have used SIMS to measure $\delta^{11}B$ in a coral previously analysed for Sr/Ca and $\delta^{18}O$ by SIMS. The $\delta^{11}B$ of experimentally precipitated calcite reflects the pH at which precipitation occurs (*2*) and hence $\delta^{11}B$ of coral aragonite encodes fluid pH at the calcification site. The pH at the coral calcification site will directly or indirectly affect the geochemistry of the precipitating skeleton. For example pH affects the $\delta^{18}O$ of the dissolved inorganic carbon (DIC) used for calcification (*1*).

Results and discussion

We used SIMS to measure $\delta^{11}B$ across an annual growth band of a Hawaiian *Porites* coral skeleton. We positioned the primary beam over areas previously analysed for $\delta^{18}O$ and Sr/Ca by SIMS. We used the equation of Sanyal et al. 1996 (*3*) to estimate the fluid pH at the time of calcification from skeletal $\delta^{11}B$. The $\delta^{11}B$ across the annual transect ranges from 21.6 to 28.3‰, equivalent to a pH range of ~8.1 - 8.8 at the calcification site. This is in good agreement with actual measurements of the fluid between the coral tissue and the skeleton which indicate a pH range of ~8 (under dark conditions) to ~9 (in the light,*4*). Sr/Ca does not correlate significantly with $\delta^{11}B$ at low pH (<8.45, equivalent to $\delta^{11}B$ of ~24.5) but we observe a correlation between Sr/Ca and calcification site pH at higher pH (pH>8.45, Figure 1a). $\delta^{18}O$ and $\delta^{11}B$ do not show a significant correlation over any pH range (Figure 1b).

Our data indicate that Sr/Ca and calcification site pH are inversely correlated at high pH. It is likely that this reflects the role of the enzyme calcium adenosine triphosphatase (Ca-ATPase) in calcification. The coral skeleton precipitates from a calcifying fluid, the composition of which is determined by active and passive transport processes (Figure 2). Ambient seawater is able to permeate to the calcification site (*5*) either through diffusion through the coral skeleton or via fluid transport through vacuoles and/or pericellular channels. The [Ca] at the calcification site is increased by Ca transport mechanisms including calcium channels and by the enzyme Ca-ATPase. Ca-ATPase pumps

Figure 1. Correlations between skeletal $\delta^{11}B$ and a) Sr/Ca and b) $\delta^{18}O$. Typical errors (2σ) are shown. The lines are linear regressions through sections of the data.

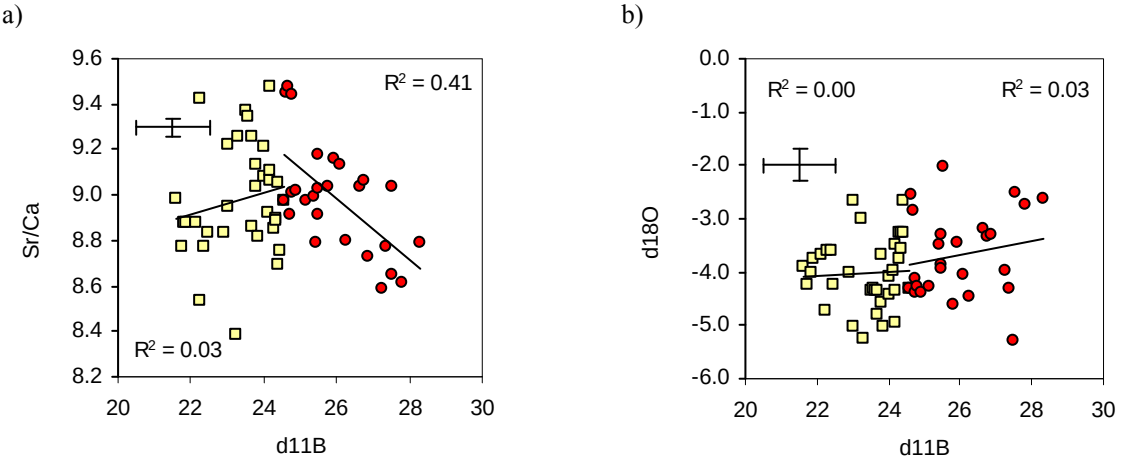

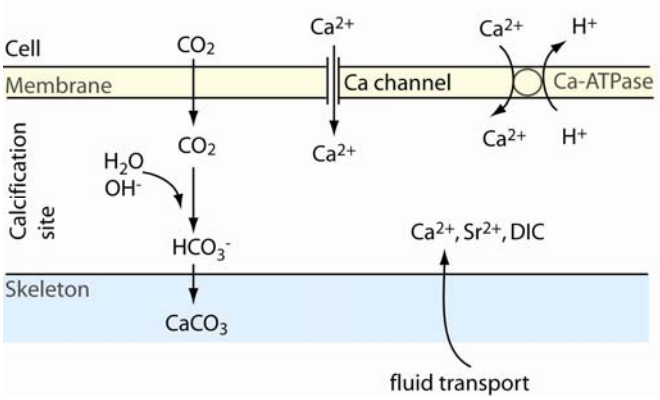

Figure 2. Simple summary of major routes of Sr, Ca and DIC transport to the calcification site and effects of pH changes. Note seawater may enter the calcification site through diffusion through the coral skeleton (as shown), via pericellular channels or through vacuole transport. For clarity these latter pathways are omitted from the image.

Ca^{2+} in and H^+ out of the calcification site, thereby increasing the pH of the calcifying fluid. The final Sr/Ca composition of the calcifying fluid will also reflect the transport of Sr to the calcification site. Sr^{2+} has a similar ionic radius to Ca^{2+} and may substitute in place of Ca in transport processes. However it is likely that subtle variations in the efficiency of the transport of the 2 ions will occur e.g. Ca^{2+}-ATPase has a higher affinity for Ca^{2+} than for Sr^{2+} (*6*) so the Sr/Ca ratio in the calcifying fluid will decrease during periods of high Ca-ATPase activity.

The observed correlation between Sr/Ca and $\delta^{11}B$ at high calcification site pH is consistent with the model for the role of Ca-ATPase in calcification. During periods of rapid calcification e.g. under optimal light conditions, Ca-ATPase activity is high, Ca^{2+} is rapidly pumped to the calcification site and H^+ is extruded resulting in a high pH in the calcifying fluid. Sr is less efficiently transported than Ca by the enzyme and the Sr/Ca of the calcifying fluid is effectively reduced. However the relationship between Sr/Ca and $\delta^{11}B$ is not observed over the lower pH range. It is reasonable to assume that calcification is slower at these low pHs and it is possible that the contribution of Ca-ATPase to Ca transport is negligible under these conditions. Ruthenium red, a Ca-ATPase inhibitor, reduces calcification rates by ~40% in the coral *Galaxea fascicularis* (*7*), indicating that significant calcification is maintained when the enzyme is inactive. We observe significant Sr/Ca heterogeneity in regions of the skeletons deposited at both high and low pH and observe a large range in Sr/Ca (>0.5mmol mol-1) deposited at any single pH value. This indicates that Sr/Ca heterogeneity is generated by other processes besides the activity of Ca-ATPase. The role of other Ca (and Sr) transport processes in generating this heterogeneity remains to be resolved.

We observe no significant relationship between $\delta^{18}O$ and $\delta^{11}B$ over the whole pH range. At present the current view of coral calcification (e.g. 8) suggests that skeletal oxygen is largely derived from molecular CO_2. This diffuses passively across the biological membrane which separates the coral tissues and the calcification site (Figure 2) and reacts with H_2O or OH^- in the calcifying fluid to produce bicarbonate, HCO_3^-, which precipitates with Ca^{2+}. The DIC produced by CO_2 reactions becomes enriched in ^{16}O as pH increases and CO_2 hydroxylation increasingly dominates over hydration (*8*). Our data do not support the view that skeletal O is largely CO_2 derived. We hypothesise that much of the DIC used in calcification enters the calcification site by fluid transport and is already in isotopic equilibrium with seawater. This is mixed with CO_2-derived DIC to offset the $\delta^{18}O$ of the skeleton to more negative values than observed in inorganically precipitated aragonite. $\delta^{18}O$ heterogeneity in the coral aragonite is driven by variations in the relative contributions of DIC from seawater and from metabolic CO_2.

References

[1] Rollion Bard C. et al., Earth. Planet. Sci. Lett., 2003 275-288.
[2] Sanyal A. et al. Geochim. Cosmochim. Ac, 64 (2000) 1551-1555.
[3] Sanyal A. et al. Paleoceanography. 11 (1996) 513-517.
[4] Al-Horani F.A. et al., Mar. Biol., 142 (2003) 419-426.
[5] Braun A. and Erez J., Eos Trans., American Geophysical Union, 85 (47) (2004), B14B-04.
[6] Yu X and Inesi G, J. Biol. Chem., 270 (1995) 4361-4367.
[7] Marshall A.T., Science 271 (1996), 637-639.
[8] McConnaughey T.A., Coral Reefs, 22 (2003) 316-327.

The petrogenetic evolution of the Lochnagar pluton diorites: an integrated SIMS quartz, zircon and whole-rock oxygen isotope approach

S.K. Appleby[1]

[1]School of GeoSciences, University of Edinburgh, Edinburgh EH9 3JW, UK

Introduction

Zircon is a common accessory mineral in granitoid rocks. In contrast to whole-rock oxygen isotopes zircon is insensitive to hydrothermal alteration and fractional crystallisation during cooling due to slow oxygen diffusion rates and high closure temperatures, and hence retains its $\delta^{18}O$ from the time of crystallisation [1, 2, 3]. Previous SIMS oxygen isotope analysis of zircons found in diorites of the Scottish late Caledonian Lochnagar pluton showed that zircon crystals analysed of different intrusive phases form homogeneous as well as heterogeneous populations with respect to zircon $\delta^{18}O$. In the latter variation was observed predominantly between, but also within individual crystals. This was interpreted to be evidence for isotopic disequilibrium between zircon and the current host rock. In addition, as $\delta^{18}O$ in zircon only changes following open-system processes it suggested the dioritic magmas experienced magma mixing with material of differing oxygen isotope composition.

Quartz, which commonly crystallises later than zircon in a magma's evolution, is also known to be resistant to isotopic modification and to preserve its $\delta^{18}O$ from the time of crystallisation [4].

Integrating zircon, quartz and whole-rock oxygen isotope data is a useful tool to establish the state of equilibrium between zircon, quartz and their current host rock, and the magma's petrogenetic evolution from the time of zircon crystallisation to sub-solidus alteration.

The specific objectives of this project were to carry out in-situ oxygen isotope analysis on quartz crystals from two samples known to be homogeneous (Cul nan Gad diorite = CnG) and heterogeneous (Allt Darrarie diorite = AD1) in zircon $\delta^{18}O$ in order to:

- determine the scale of heterogeneity in quartz crystals.
- potentially find further evidence for magma mixing.
- assess the state of equilibrium between quartz, zircon and their host rock.

Results

Only minor variation was observed in quartz crystals. CnG diorite quartz oxygen isotope data range from 10.4 ‰ to 11.4 ‰ (mean: 10.9 ± 0.5 ‰ (2SD, n=22)) and AD1 diorite data from 11.3 ‰ to 12.3 ‰ (mean: 11.7 ± 0.6 ‰ (2SD, n=27). Values from both samples display unimodal distributions and all data, but one analysis of a possibly altered area, lie within error of the mean. A systematic change between grain centres and rims of between different grain sizes was not observed.

Discussion & Conclusions

In contrast to SIMS zircon $\delta^{18}O$ data, quartz oxygen isotope data of both diorites yield unimodal oxygen isotope populations. Hence, quartz data of the AD1 diorite provide no evidence of magma mixing.

Following an empirical equation [5] the equilibrium fractionation factor between quartz and zircon (Δ(Qtz-Zrc)) is 2.3 ‰ at 800°C (typical magmatic temperature at which minerals co-exist). However, in the CnG this value is much higher at 4.9 ± 1.1 ‰. Due to the complexity of the data comparison of the AD1 quartz and zircon data yields a spread of Δ(Qtz-Zrc) values between 5.6-3.6 ± 1.0 ‰. Hence, in both diorites the data provide strong evidence for isotopic disequilibrium between quartz and zircon **(Figure 1)**. Some authors have found that quartz does not preserve its oxygen isotope composition as well as zircon. However, the lack of oxygen isotope heterogeneity along cracks and crystal boundaries, and between crystals of differing size suggests that in the Lochnagar diorites the higher quartz values were not caused by e.g. alteration or diffusion. A possible explanation is that quartz precipitated from late-stage fluids possibly after zircon ceased to crystallise and certainly well after the magma mixing events recorded in the zircon oxygen isotope data.

Previous comparison of zircon and whole-rock oxygen isotope data suggested that, in contrast to zircon and quartz, zircon and whole-rock appear to be in isotopic equilibrium in the CnG diorite **(Figure 1)**. An explanation for this is that the modal percentage of quartz in this rock is less than 5 %,

hence not enough to shift the whole-rock out of equilibrium. In the AD1 diorite the state of equilibrium is less clear due to the large variation observed in zircon $\delta^{18}O$. However, the fact that whole-rock $\delta^{18}O$ is lower than zircon $\delta^{18}O$ may indicate that the whole-rock underwent hydrothermal alteration.

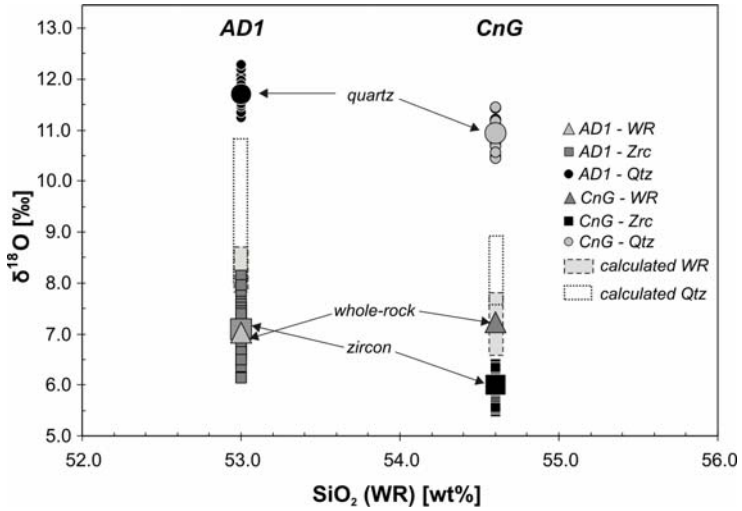

Figure 1. Evaluation of equilibrium between zircon (Zrc), quartz (Qtz) and whole-rock (WR).
AD1: Zircon is not in equilibrium with quartz or whole-rock. Measured whole-rock is too low to be in equilibrium with zircon, which suggests it was affected by hydrothermal alteration after zircon crystallisation.
CnG: Zircon and quartz are not in equilibrium as measured quartz $\delta^{18}O$ is considerably higher than the calculated quartz value, which suggests quartz crystallised late in sequence. Zircon and whole-rock are in equilibrium. Low modal percentage of elevated quartz in whole-rock (< 5 %) did not shift whole-rock out of equilibrium.

To summarise, even though the Cul nan Gad and Allt Darrarie diorites both belong to the Lochnagar pluton they had differing petrogenetic evolutions. The Cul nan Gad diorite appears to have a relatively simple history with zircons crystallising from a homogeneous melt with respect to zircon $\delta^{18}O$, quartz precipitating late from late-stage fluids, and no evidence for hydrothermal alteration. In contrast, the AD1 diorite has a much more complex history. Zircon $\delta^{18}O$ heterogeneity suggest that the evolving magma experienced magma mixing and/or assimilation during zircon growth, like in the CnG diorite quartz also crystallised late, hence shows no evidence of open-system processes. The current host rock in not in equilibrium with zircon, which indicates it underwent sub-solidus hydrothermal alteration.

References

[1] M.H. Dodson, Contrib. Min. Pet. 40 (1973) 259-274.
[2] E.B. Watson & D.J. Cherniak, EPSL 148 (1997) 527-544.
[3] J.W. Valley, RMG 53 (2003) 343-385.
[4] J.W. Valley & C.M. Graham, Contrib. Min. Pet. 124 (1996) 225-234.
[5] J.W. Valley, I.N. Bindemann & W.H. Peck, Geochim. Cosmochim. Acta 67 (2003) 3257-3266.

Investigating the role of recycled crust in generating radiogenic Pb isotope signatures in the mantle

R. Avanzinelli[1] & T. Elliott[1]

[1]Department of Earth Sciences, University of Bristol, Bristol BS8 IRJ, UK

Overview

The objective of this study was to exploit the observation of large variability of Pb isotopic ratios in melt inclusions [1] and couple this with trace element analyses and volatile contents. In this manner we hoped to characterise the endmembers that go to make bulk lava samples and understand their origins. Specifically we wished to test if radiogenic Pb isotope ratios in some oceanic basalts were plausibly explained by recycled oceanic crust by linking Pb isotopic signatures with key incompatible trace element ratios (e.g. Ba/Nb) and volatile contents (mainly water and CO_2).

Background

The samples for our study came from La Palma, Canaries. We have a large collection of La Palma samples, characterised petrographically, chemically and isotopically. Moreover, in collaboration with Dr. I. Nikogosian (University of Utrecht), the melt inclusions (dominantly hosted in mafic, Fo>80, olivines) of a number of these samples have been investigated in some detail. La Palma provides an interesting location, as its whole rocks have radiogenic Pb isotopic compositions that show a greater relative variation ($^{206}Pb/^{204}Pb$ 19.2-20.0) than the somewhat more extreme island of Mangaia ($^{206}Pb/^{204}Pb$ 21.5-21.9). The latter has been the previous focus of *in situ* Pb isotope work. We thus anticipated at least comparable isotopic variability to the considerable range evident in Mangaia melt inclusions.

The analyses were undertaken in three one-week sessions. The first two one-week session were performed in 2006. Initially Pb isotope ratios were measured on as many potentially suitable inclusions using the Cameca 1270. Subsequently the same inclusions were reanalysed for a suite of incompatible trace elements (Ti, Rb, Sr, Y, Zr, Nb, Ba, La, Ce, Nd, Pb, Th, U) using the Cameca 4f. In all 32 silicate melt inclusions were analysed together with 5 sulphide inclusions. In the only session in 2007 the inclusions, previously analysed Pb isotopes and trace elements, were analysed for volatile contents (CO2, H2O, F, Cl) using the Cameca 4f.

Results

Water contents in the analysed melt inclusions varied from 0.03 wt.% to 0.6 wt.%, values comparable with those measured in melt inclusions from Hawaii [2], but lower than those measured for submarine glasses, again from the Hawaiian chain [3,4]. These sometimes-low water contents suggest a significant role for H loss via diffusion. Hydrogen diffusion is confirmed by measurements of H_2O contents in the olivine crystals enclosing the melt inclusion. Indeed, olivine shows H_2O content comparable with the lowest values measured in the melt inclusions. The high variability of H_2O abundances in melt inclusion is somehow reduced when inclusions from the same rock samples are considered. Data from LP02 (4 melt inclusions measured) range from 0.3 wt.% to 0.6 wt.% H_2O, whilst inclusions from LP41 (9 measurements) varies from 0.03 wt.% to 0.06 wt.%, with only one melt inclusion at 0.15 wt. % H_2O. This suggests that the measured water contents are not primary values, but reflect the cooling and degassing history of the magmas.

CO_2 analyses proved difficult and their reliability is still to be properly evaluated. An initial problem was posed by the large amount of MgO in the matrix and the consequent large interference of $^{24}Mg^{2+}$ on the peak of ^{12}C: working in high resolution we were able to discriminate the two peaks monitoring the effect of the $^{24}Mg^{2+}$ tail with both tail measurement on standards and samples (normally negligible).

This procedure yielded good results for standards (sisson51, RB497 and a MORB standard) but further problems arose when the melt inclusions were analysed. We noticed that some measurements yielded anomalously high values, normally when the analysis was performed in the same spot of the previous Pb isotope and trace element measurement or, even more, in the proximity of the pit holes of previous

laser ablation analyses. We interpreted this feature to be related to surface contamination occurring during the repeated coating of the samples, as also suggested by the instability (i.e. decreasing) of the ^{12}C signal during the analyses. To avoid this effect we considered only analyses with stable ^{12}C signal and we performed, where possible, the measurements on clean (i.e. not previously analysed) melt inclusion surfaces.

The CO_2 contents range from 200 to 7000ppm, with most of the melt inclusions having between 1000 and 2000ppm. These values are higher than those measured for both melt inclusion and submarine glasses at Hawaii [2-4]. In this case CO_2 determination in the olivine crystals yielded low values (<50ppm), suggesting limited C loss via diffusion, as anticipated. The variability among melt inclusions from the same samples was similar to the variability for the data set as a whole, in contrast to H.

F and Cl contents varied from 1000ppm to 4000ppm and from 100ppm to 800ppm, respectively. As for CO_2, Cl and F absolute abundances are higher than those measured by Hauri et al. [2] in melt inclusions from Hawaii. This is in keeping with the more alkalic nature of La Palma and incompatible behaviour of these volatiles.
Not surprisingly, no correlation was observed between any of these volatile elements and Pb isotope or trace element ration, casting more doubt on the primitive nature of the measured data.

Concluding Remark and suggestions.
In measuring volatile elements in melt inclusion we encountered several problems that we believe are related to sample selection and treatment. The low values of H_2O indicate hydrogen loss during slow cooling of the sub-aerial erupted lavas. In order to obtain primary water content in melt inclusion we suggest that sample as quenched as quickly as possible to be analysed (e.g. submarine or quenched scoriae). As for CO_2 analyses we recommend performing volatile analyses on fresh melt inclusion surface (possibly before any other analyses), in order to minimize possible surface contamination. Despite the problems, a reference dataset has been generated for low degrees of mantle melting, yielding minimum constraints on volatile contents.

References
[1] A. Saal et al., Earth Planet. Sci. Lett. 240 (2005) 605-620.
[2] Hauri et al., Chem. Geol. 183 (2002) 115-141.
[3] Dixon et al., J. Pet. 38 (1997) 911-939.
[4] Dixon & Clague, J. Pet. (2002) 627-654.

The composition and volatile content of kimberlite magmas

R.A. Brooker[1], R.S.J. Sparks[2], M. Field[3] & J. Kavanagh[2]

[1]Department of Earth Sciences, University College, Gower Street London, WC1E 6BT, UK
[2]Department of Earth Sciences, University of Bristol, Wills Memorial Building, Bristol BS8 1RJ, UK
[3]De Beers MRM R & D Group, Mendip Court, Bath Road, Wells, Somerset, BA5 3DG, UK

The problem with kimberlites

The composition of kimberlite magmas has been a long-standing and sometimes contentious issue in petrology. While there is agreement that kimberlites must represent ultrabasic melts with significant quantities of CO_2 and H_2O, there are few accurate constraints on the actual composition or the volatile content. These problems arise with kimberlites more than any other rocks due to high levels of xenolithic contamination and strong pervasive alteration in the form of serpentisation, with many of kimberlites also representing the pyroclastic remnants of an explosive decompressed magma. Reconstructing the compositions is thus difficult and to a considerable extent dependent on assumptions about how textures and minerals assemblages might be interpreted. The best rocks to consider for parental compositions are the aphanitic, hyperbyssal quenched intrusives found in dykes and sills that may still retain their volatile component. Estimating the volatile contents as a function of depth represent a key issue for understanding the dynamics of kimberlite eruptions as the system 'blows' through to form the ubiquitous diatreams that charcterise kimberlite volcanology [1].

This project involves experiments to investigate phase relations in three proposed kimberlite compositions that cover a wide range of silica content, with an emphasis on the possible volatile contents that these magmas could carry to near surface environments (depths of <3km or pressures of 1 kbar). The first composition is based on a generic kimberlite reconstructed from a large number of analyses by Le Roex et al [2], with relatively high SiO_2 in the range 30-35% and MgO in the range 25 to 30%. These generic compositions are claimed to carry about 12 wt% CO_2 plus 7wt% H_2O as they approach the earth's surface. Our second composition is based on an actual rock composition with a similar silica content (34 wt%) from Jericho mine in Canada [3], which appears to be a fresh, quenched hyperbyssal rock and has some useful analytical data on the crystal phase assemblage, temperature of growth (1030-1170°C,[4]), depth of emplacement (<1km) and volatile content (13 wt% CO_2, 7 wt% H_2O). Our third composition is more contentious and has a much lower silica content. This is based on our textural observation that serpentisation can profoundly change the bulk composition of kimberlites in open-system hydrothermal metamorphic reactions [5]. In particular igneous calcite has been destroyed and in relative terms Mg and Si are enriched during serpentinization. We thus suspect that the published compositions of serpentinised kimberlites (nearly all kimberlites show this alteration to some extent) are not representative of the original magma. Our low silica composition is a reconstruction of the Wesselton Sills kimberlite based on the idea that these magmas may have originally had much lower SiO_2 and MgO contents of 15-20% and 5-15% respectively and higher CO_2 around 10-25%. In terms of silica and CO_2 contents, this composition (Sparks Reconstruction) is transitional between a silica-rich kimberlite and a silica-free carbonatite. The presence of primary hydrous phases grown such as phlogopite early in the history of kimberlites demonstrates that water was dissolved in the melt, and exsolved magmatic water may initiate the hydrothermal systems that produce serpentinisation as the system solidifies and cools below 400°C.

Our two main objectives were to survey the volatile content that these three melt (or magma) compositions can carry to shallow depths and to see if the any crystalline phase assemblages were affected by the CO_2:H_2O ratio in a way that could be used to infer the original volatile content of the magma before post-emplacement alteration. In particular, we will see if we can reproduce the phase assemblage observed in the Jericho rock from the analysed bulk rock composition, at the suggested depth, temperature and volatile ratio.

Experimental observations

Initial experiments on the more 'silicic' kimberlite compositions of LeRoex and the rock from Jericho were carried out at 1-2 kbar (=3-7km) with water, CO_2 and water-CO_2 mixtures. At temperatures of

1225-1275°C (well above estimates for kimberlite magmas), both these higher silica kimberlites had a surprisingly small amount of glass present (20-40%) amongst abundant olivine, spinels and minor monticellite. This represents a very low amount of melt for these kimberlite magmas when it is considered that field evidence shows emplacement as a low viscosity, very mobile fluids, not a 'crystal-rich mush'. All the volatile bearing experiments released a significant proportion of their loaded volatiles after quenching suggesting the volatile content found in the rocks cannot be dissolved in the magma at 3km, let alone the shallower emplacement depths. This also shows that the maximum amount of dissolved volatiles cannot reduce the liquidus of these magmas to the lower temperature estimates. In contrast to these results, the experiments on the lower silica 'transitional' kimberlite show a much lower liquidus with 70% melt at 1275 and 40% at 1100°C. These results suggest a more carbonatitic, pre-serpentinization composition has more potential to exist as a fluid magma near the surface. To better understand the relationship between bulk composition and the volatile effect on the liquidus, together with quantification of the volatile carrying capacity of these magma compositions it is essential to analyse the volatile content of the quenched glasses in these experiments. Melt pools are too small for traditional IR analysis and the ion probe is clearly the analytical tool of choice. However, we needed to develop techniques and calibrations for CO_2 and H_2O analysis in our kimberlitic melt compositions, at the concentrations we expect to measure and with a beam size to match our experimental melt pocket size.

Ion Probe Results

An extensive range of 50 previously bulk analysed CO_2-bearing glasses allowed the development of a reliable calibration and methodology for ion probe analysis of CO_2 to compliment previously calibrated H_2O methods. The data in Fig 1 show the CO_2 and H_2O contents of the experimental kimberlitic glasses as a function of pressure/depth. It is clear that for the silica-rich kimberlites even 100% melt could not carry the volatile contents observed in the rocks to shallow depths. When it is considered that these melts represent less than 50% of the total magma, then the discrepancy is far worse. Although the more carbonatitic kimberlite (Sparks reconstruction) composition appears to carry the most CO_2 and this is combined with a higher melt fraction at even lower temperatures than 1275°C, this is still not as high as the natural rocks. It would appear than some different compositions (perhaps even more carbonatitic) may be required to transport the observed CO_2 content close to the surface. The solubility of water also appears very low, even compared to more common magma compositions (basalts to rhyolites) and this also applies to the more carbonatitic kimberlite. It has been suggested that water solubility is higher than this in pure carbonatites [6]. These results appear to support a more carbonatitic composition at the time of emplacement of kimberlites OR the addition of these volatiles from a separate vapour phase that accompanies the magma (low T metamorphic reactions).

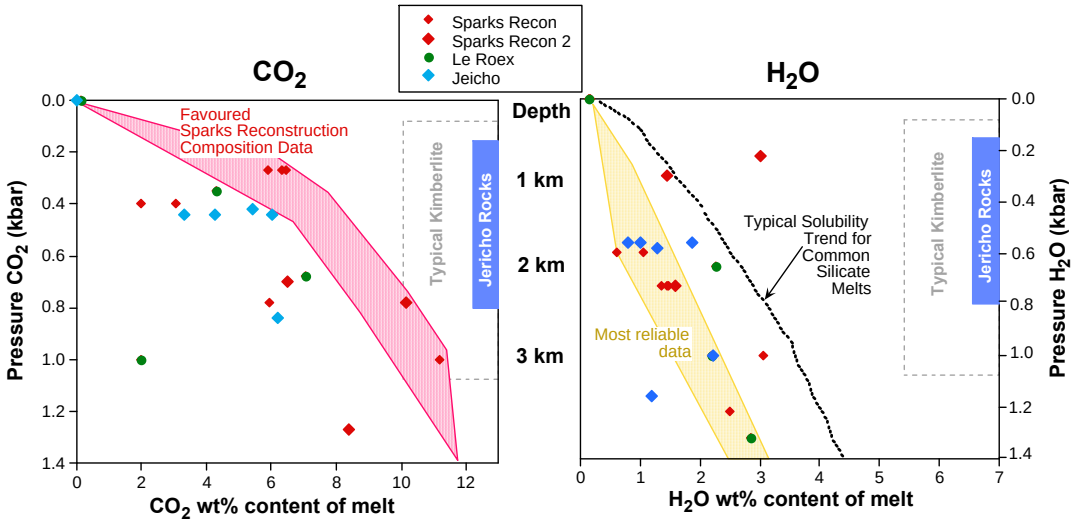

Fig 1. Volatile content measured by ion probe in the glasses from experiments on various kimberlite compositions (see text). Volatile pressures are calculated using bulk reconstructions of the vapour

phase in experiments. The estimate volatile content typical for generic kimberlites and the measured values for Jericho are indicated along with estimates of emplacement depth.

References

[1] Sparks, R.S.J., Baker, L., Brown, R.J., Field, M., Schumacher, J., Stripp, G. & Walters, A. J. Volcanol. Geotherm. Res. 155, (2006) 18-48.
[2] Le Roux, A.P., Bell, D.R., Davis, P., J. Petrol. 44, (2003) 2261-2286.
[3] Price, S.E., Russell, J.K. & Koplova, M.G. J. Petrol. 41, (2000) 789-808
[4] Fedortchouk, Y. & Canil, D. J. Petrol. 45, (2004).1725-1745
[5] Stripp, G.R., Field, M., Schumacher, J. C., Sparks, R.S.J. & Cressey, G J. Metamorphic Geol. 24, (2006) 515-534.
[6[Keppler, H. Am. Mineral 88, (2003) 1822-1824.

Lithium Isotope Constraints on Crustal Anatexis

I.S. Buick[1] & S. Kasemann[2]

[1]Research School of Earth Sciences, The Australian National University, Acton, ACT 0200, Australia
[2] School of GeoSciences, University of Edinburgh, Edinburgh EH9 3JW, UK

Introduction

SIMS-based investigations of mantle rocks or mantle-derived melts have recently shown that, at temperatures in excess of 1000˚C, extreme (20-40‰) intra-grain kinetic fractionation of δ^7Li may occur as a result of the relaxation of lithium concentration gradients and the different diffusivities of ^{6}Li and ^{7}Li. As a result, kinetic fractionation of δ^7Li in minerals such as clinopyroxene and olivine may render them unsuitable for use as isotopic tracers. In metasedimentary and felsic magmatic rocks Li abundances ([Li]) in minerals such as cordierite, biotite and garnet occur at the 1-100 ppm level. Compared to mantle-derived materials, there are few SIMS δ^7Li data from minerals in metasedimentary rocks, and it is unclear whether kinetic isotopic fractionation is a problem at temperatures relevant to high-grade metamorphism and anatexis e.g. c. 650-900˚C. As a result, this pilot study sought to assess the extent of kinematic fractionation: a) during prograde low-pressure/high-temperature anatexis of metapelites from Mt. Stafford (central Australia); and b) during fractional crystallisation of peraluminous pegmatites, also from central Australia.

Metapelites from Mt. Stafford experienced anatexis beginning in the andalusite stability field and formed peritectic cordierite due to dehydration melting of Qtz+Bt+Sil. Most high-grade restitic metapelites contain low boron contents (<10-20 ppm), as typically seen in other terrains where melt has been extracted. A subset are extremely boron-rich ([B] = c. 500-4000 ppm). They experienced similar cordierite-producing reactions as B-poor "normal" metapelites except that tourmaline was a reactant and B-rich minerals such as werdingite and grandidierite were products.

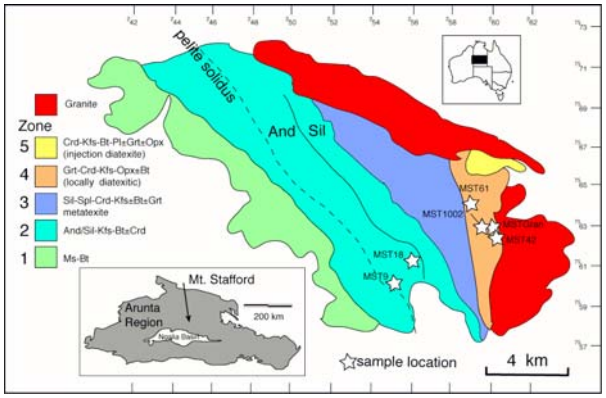

Figure 1: Geology of Mt. Stafford, central Australia

Results

Cordierite δ^7Li data were collected across peritectic cordierite in anatectic metapelities formed at ~700˚C and ~800˚C. Cordierite grains from B-poor migmatites showed little intra-grain variation in [Li], as measured by LA-ICP-MS at the ANU. $\delta^7Li_{(Crd)}$, corrected for matrix effects related to X_{Mg} (Kasemann, unpub. data): a) vary in a narrow range of typically just in excess of analytical uncertainty (Figs 2 & 3); b) show little difference in the $\delta^7Li_{(Crd)}$ obtained from migmatites formed at relatively low temperatures (c. 700 ˚C), and those at the highest granulite grades (c. 800 ˚C); c) show typically show low δ^7Li values (c. -13‰ to -9.5‰) for "normal" low-[B] bulk compositions and significantly higher δ^7Li values (c. +2‰ to +5‰) for rare [B]-rich bulk compositions (Fig. 3)l and d) have apparent $\Delta^7Li_{(Bt\text{-}Crd)}$ of ~+12-15 ‰ in both [B]-poor and [B]-rich bulk compositions.

δ^7Li data were also collected across Mn-rich garnets of late magmatic (c. 650-700 ˚C) origin from peraluminous pegmatites emplaced during the c. 440-300 Ma Alice Springs Orogen. The garnets show core to rim decreases in a range of trace elements, including [Li], [Y], [Ti] and [HREE], consistent with growth during a Rayleigh fractionation process (LA-ICPMS data from the ANU). Despite a [Li] concentration gradient to drive kinetic fractionation, $\delta^7Li_{(Grt)}$ shows little variation (Fig. 4).

Discussion

The uniformityof $\delta^7Li_{(Crd)}$ in the [B]-poor anatectic metapelites suggests that kinetic fractionation of δ^7Li has not occurred in rocks that experienced c. 700-800 ˚C peak temperatures and subsequent slow

cooling. The similarity in the low δ^7Li values obtained from peritectic cordierite in upper amphibolite and granulite-facies [B]-poor rocks results from the fact that at low pressures (c. 3.5 kbar at Mt. Stafford) the major cordierite producing reaction, modelled at Qtz + Bt + Sil = Crd+ Kfs + Liq, occurs in a range of metapelitic bulk compositions in the narrow temperature range ~670-690 ˚C ie this reaction went to completion at temperatures just below those reached by MST18 in Fig. 2, and along the prograde heating path at >100˚C below the maximum temperature experienced by MST42. Preservation of the $\delta^7Li_{(Crd)}$ set in along the prograde path in MST42 further suggests that $\delta^7Li_{(Crd)}$ is robust to diffusive resetting at temperatures relevant to anatexis. The maintentance of distinctly different $\delta^7Li_{(Crd)}$ in anatectic rocks that have different bulk compositions ([B]-poor v. [B]-rich protoliths) provides further supporting evidence for the refractory behaviour of Li isotopes in cordierite. This suggests that $\delta^7Li_{(Crd)}$ could be a useful tracer of a range of processes in metamorphic and antectic rocks e.g. the origin of xenocrystic v. magmatic cordierite in S-type volcanics

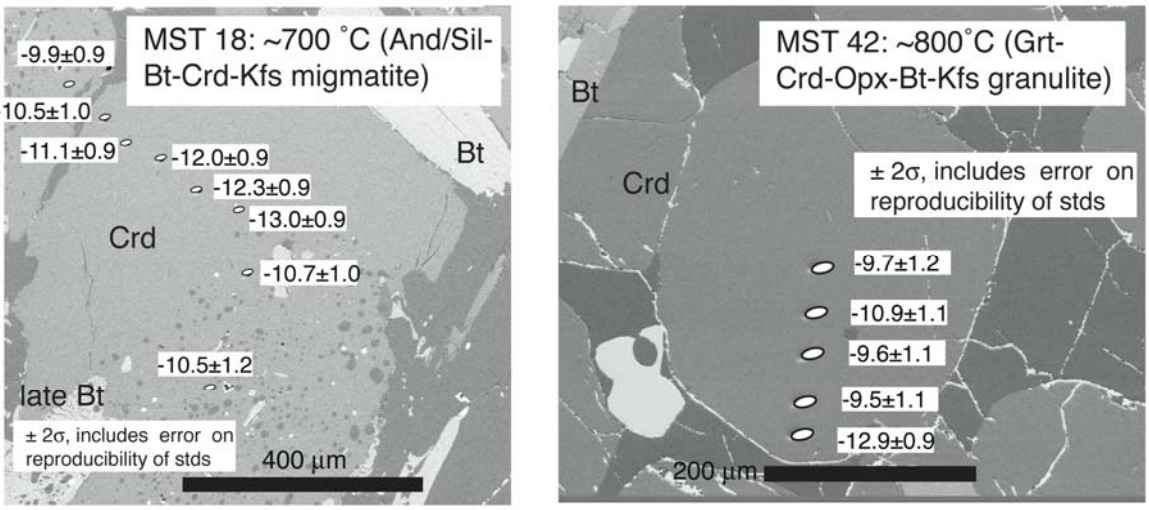

Figure 2: SIMS δ^7LI traverses across cordierite from c. 700˚C and c. 800 ˚C anatectic metapelites, Mt. Stafford.

Similarly, the preservation of [Li] zoning, and the lack of systematic variation in $\delta^7Li_{(Grt)}$ in late magmatic garnet from the peraluminous pegmatite suggests that this mineral is also likely to be unaffected by kinetic fractionation of Li isotopes, at least at low anatectic temperatures (650-700 ˚C).

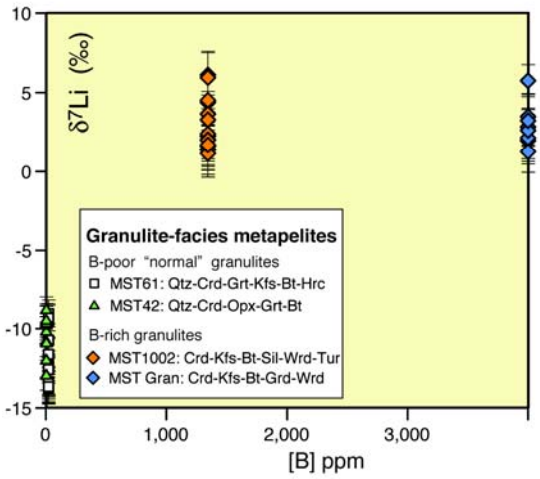

Figure 3: $\delta^7Li_{(Crd)}$ v. whole rock [B] content, Mt. Stafford

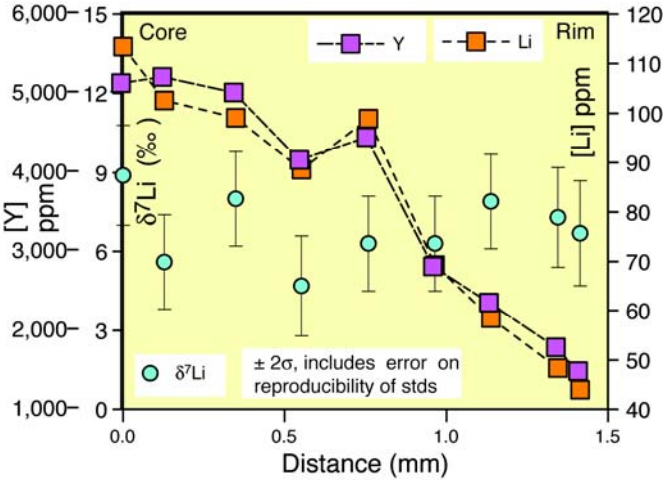

Figure 4: core to rim zoning in $\delta^7Li_{(Grt)}$, [Li], [Y]; late magmatic garnet from peraluminous pegmatite, central Australia.

U-Pb dating of lunar baddeleyite

Ray Burgess[1], Vera Fernandes[2] & Katherine Joy[3]

[1]School of Earth, Atmospheric and Environmental Sciences, University of Manchester, Manchester M13 9PL
[2]Berkeley Geochronology Center, Berkeley, CA 94709, U.S.A.
[3]Department of Earth Sciences, University College London, London, WC1E 6BT

Aim

The purpose of the work was to undertake a pilot study of U-Pb dating of baddeleyite (ZrO_2) in basaltic lunar meteorite La Paz 02205 (LAP 02205). Isotopic dating of this meteorite had previously given a whole-rock Ar-Ar age of 2.94 ± 0.01 Ga [1] and a U-Pb phosphate age of 2.93 ± 0.15 Ga [2], slightly younger than the Sm-Nd isochron age of 3.02 ± 0.02 Ga [3]. Since the Ar-Ar and U-Pb phosphate systems are more susceptible to disturbance events (especially shock) it was considered possible that the slightly younger ages may reflect the time of a later impact event consistent with the presence of thin melt veins in the meteorite. One aim of the study was therefore to use U-Pb dating of baddeleyite in LAP 02205 to discriminate between these processes by testing for concordance with the Ar-Ar or Sm-Nd ages. The U-Pb ages would also help to resolve another important issue related to source pairing of LAP 02205 with lunar basalt meteorite NWA 032 (2.779 ± 0.014 Ga [4]). A further aim was to determine whether baddeleyite is a suitable mineral for U-Pb dating of lunar samples. Lunar zircons are rare and baddeleyite as an alternative has advantages of having abundant U, negligible initial common Pb, only rarely occurring as xenocrysts, and experiences negligible Pb loss over time. It is a common accessory phase in lunar basalts so it has the potential to provide a new means of reliably dating the crystallisation ages of these rocks.

Results and Discussion

A section of LAP02205 was examined using scanning electron microscopy and the electron microprobe to identify Zr-rich grains assumed to be baddeleyite (Fig. 1). Zr-rich minerals were abundant in areas of mesostasis, as expected for these late-stage crystallisation products. Several areas of the section were investigated using the Cameca ims-1270 ion microprobe including some close to impact melt veins. Ion microprobe analysis of the Zr-rich grains revealed that the large majority were in fact zirkelite $(Ca,Th,Ce)Zr(Ti,Nb)_2O_7$, with lesser amounts of baddeleyite and a phosphate phase, probably apatite or merrillite. During ion microprobe analyses, baddeleyite and zirkelite could be distinguished on the basis of the higher Th/U>1 and Hf content of the latter mineral.

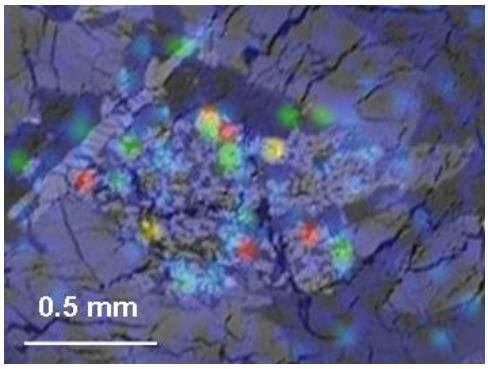

Fig. 1 BSE image showing a small area of mesostasis ("swiss cheese" texture) in LAP 02205 with superimposed Zr elemental map. Coloured spots indicate the presence of Zr-rich minerals.

U-Pb dating was hampered by the small size the baddelyite and zirkelite grains which were all ≤10 microns, and therefore smaller than the primary ion beam. In addition, there is no suitable zirkelite age standard to take account of U/Pb fractionation in this mineral. For these reasons, age determinations were restricted to $^{207}Pb/^{206}Pb$ ages following a minor correction for common lead based on ^{204}Pb. Data are shown in Fig. 2 for 15 zirkelite and baddeleyite grains with no evidence for a systematic difference between them, or their proximity to impact melt veins. The weighted mean $^{207}Pb/^{206}Pb$ age is 2.996 ± 0.040 Ga (2σ) which is close to the Sm-

Nd isochron age determined for this meteorite. This would imply that the slightly younger Ar-Ar and U-Pb phosphate ages may have been partially disturbed by a later shock event. It also indicates that LAP 02205 is ~200 Ma older than NWA 032,

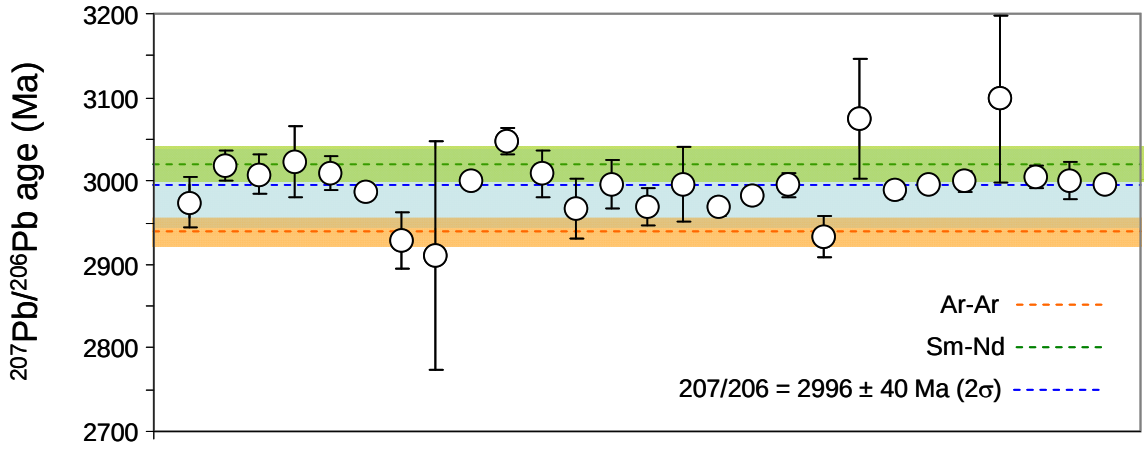

Fig. 2. 207Pb/206Pb ages of zirkelite and beddeleyite in LAP 02205. Ar-Ar ages and Sm-Nd age determinations are shown for comparison.

While LAP 02205 contained abundant baddeleyite and zirkelite grains that can be successfully dated using Pb-Pb methods, they are too small for precise U-Pb age determinations. This limits the widespread use of this mineral for dating of lunar basalts.

References

[1] V.A. Fernandes, R. Burgess & A. Morris, Geochim. Cosmochim Acta (submitted).
[2] M. Anand, L.A. Taylor, C. Floss, C.R. Neal, K. Terada & S. Tanigawa, Geochim. Cosmochim Acta 70 (2005), 246-264.
[3] L.E. Nyquist, C.-Y. Shih, Y. Reese & D.D. Bogard, Lunar Planet. Sci. XXXVI (2005), #1374.
[4] V.A. Fernandes, R. Burgess & G. Turner, Meteorit. Planet Sci. 38 (2003), 555-564.

Disentangling biological, ontogenetic and environmental influences on oxygen isotope composition of brachiopod and bivalve shells

M. Cusack[1], A. Pérez-Huerta[1] & P. Dalbeck[1]

[1]Department of Geographical & Earth Sciences, University of Glasgow, Glasgow G12 8QQ, UK

Introduction

Marine biomineral carbonates record environmental information such as ambient seawater temperature that can be interpreted using proxies such as oxygen isotope composition or Sr/Ca or Mg/Ca ratios. These carbonates are not passive recorders of such environmental data since they are produced under exquisite biological control that determines mineral type, polymorph, structure and crystallography. To ensure accurate interpretation of environmental data, it is imperative to gain a detailed understanding of how biological control influences environmental data. This project uses the NERC Ion Probe facility to measure stable oxygen isotope (^{18}O) composition of brachiopods and bivalves. The sharp microstructural and crystallographic changes within these biominerals requires the high spatial resolution of the ion probe (Cameca ims-1270).

There is a sharp transition between the outer (primary) layer and inner (secondary) layer of Rhynchonelliform brachiopods which have low Mg-calcite shells (Figure 1). The secondary layer is in oxygen isotopic equilibrium with seawater [1, 2]. Auclair et al [3] used micro-sampling to demonstrate that, in *Terebratalia transversa*, there is no switch to isotopic equilibrium concomitant with the sharp transition from the primary to secondary layer. Instead there is a progression towards oxygen isotope equilibrium towards the innermost shell. This has important implications for the use of brachiopods as seawater temperature proxies since it implies that, not only is it essential to sample secondary layer calcite but also to measure the isotopic composition of shells that have reached sufficient maturity that the inner calcite has achieved isotopic equilibrium with ambient seawater. This project uses SIMS analyses to determine the consistency of this trend in *T. transversa* and *Terebratulina retusa*.

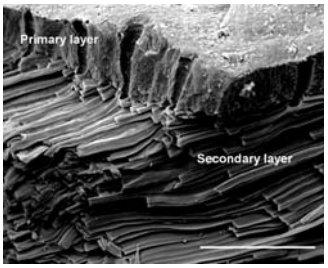

Figure 1 Secondary electron image of a fracture section of *T. retusa* shell. Scale bar=10 µm.

A characteristic of bivalve molluscs is their ability to produce different polymorphs of calcium carbonate (calcite and aragonite) (Figure 2). The oxygen isotope composition of specimens from a full ontogenetic suite of *Mytilus edulis* were measured in order to determine the relationship between ontogeny, crystallographic orientation (obtained using electron backscatter diffraction, EBSD at University of Glasgow) and isotopic composition in both calcium carbonate polymorphs.

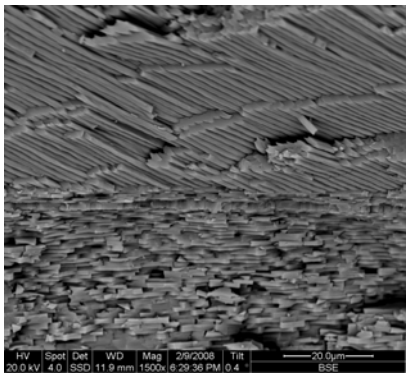

Figure 2. Secondary electron image of calcite (top) and aragonite (bottom) in a fracture section of *M. edulis*. Scale bar = 20 µm.

Results

Oxygen isotope composition of both *T. transversa* and *T. retusa* becomes heavier from outer to inner shell (Figure 3).

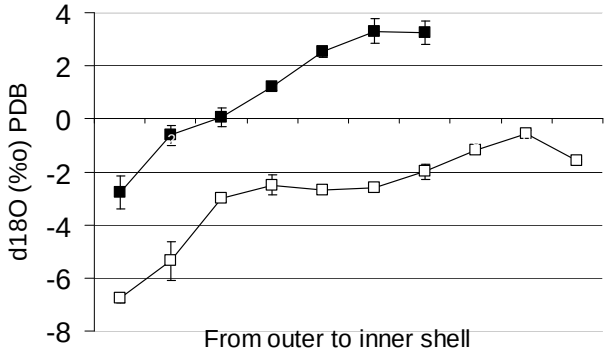

Figure 3. Oxygen isotope composition ($\delta^{18}O$) ‰ PDB from the outer (left) to innermost (right) secondary layer of the ventral valve of *T. retusa* (filled squares) and *T. transversa* (open squares). Mean values and standard deviations from three transects.

Line transects from the outer to inner shell of the blue mussel (*Mytilus edulis*) reveal distinct differences between the polymorphs as well as within the individual layers as summarised in Figure 4).

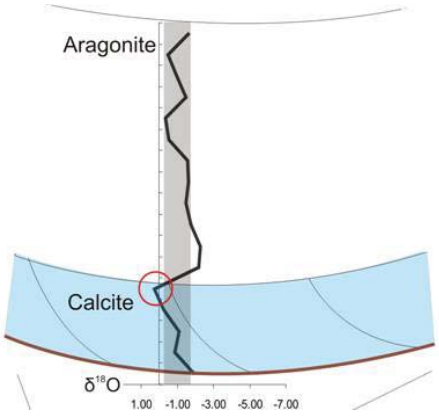

Figure 4. Transect from the outer shell surface (bottom) to the inner shell (top). Considerable variation within the layers as well as crossing polymorph interfaces.

These variations in the profile obtained via SIMS coincide with variations in the crystallography determined using EBSD [4].
In brachiopod calcite and *M. edulis* calcite and aragonite, there is a consistent shift of ~3‰ between conventional mass spectrometry data and the SIMS data. Since variations in strontium concentration tend to distort $\delta^{18}O$ measured using SIMS, the low strontium variation in these shells make them ideal for SIMS analyses.

Conclusions

In Rhynchonelliform brachiopods, the trend towards isotopically heavier calcite throughout the secondary layer of *T. transversa* is confirmed using SIMS and now demonstrated in *T. retusa*. The implication here is that the secondary layer of mature specimens of Rhynchonelliform brachiopods are in isotopic equilibrium with seawater and thus, inclusion of more juvenile material may distort proxy data.
In *M. edulis*, large shifts in $\delta^{18}O$ in short periods, which cannot be accounted for by environmental changes, suggest a kinetic effect in both polymorphs of *M. edulis*. Faster growing calcite in early stages of shell development could prevent equilibrium being achieved in some regions across the shell thickness.
Our own electron probe micro analysis (EPMA) data reveal a shift in Mg concentration coincident with the change in $\delta^{18}O$ and refinement of crystallographic orientation. This should be investigated further as this could be central to the relationship between kinetics and oxygen isotope and trace element proxies such as Mg/Ca ratios. Another area that may merit further investigation is the fact that $\delta^{18}O$ values in the calcite layer trend toward more negative values with older stages of ontogeny.

References

[1]Carpenter, S.J. & Lohmann, K.C., Geochim. Cosmochim. Acta 59 (1995) 3748-3764.
[2] Parkinson, D. Curry, G.B. Cusack, M. & Fallick, A.E. Chem. Geol. 219 (2005) 193-235.
[3] Auclair, A.-C. Joachimski, M.M. & Lécuyer, C., Chem. Geol. Isot. Geosci. 202 (2003) 59-78.
[4] Dalbeck, P. England, J. Cusack, M. Lee, M.R. & Fallick, A.E., Eur. J. Mineral. 18 (2006) 601-609.

Mg/Ca ratios in sequential chambers of the foraminifera *Streptochilus* from the Arabian Sea

K. Darling & S. Kasemann[1]

[1]School of GeoSciences, University of Edinburgh, Edinburgh EH9 3JW

Volatile contents of unusual eruptions of the Yellowstone hotspot track

B. Ellis[1], M. Branney[1] & T. Barry[2]

[1]Geology Department, University of Leicester, Leicester, LE1 7RH, UK
[2]Volcano Dynamics Group, CEPSAR, Open University, Milton Keynes, MK7 6AA England, UK

The Snake River Plain of southern Idaho and northern Nevada, USA, represents the Miocene record of the Yellowstone hotspot. The explosive and effusive rhyolitic eruptions from the hotspot during this period are sufficiently different to conventional rhyolitic Plinian, ignimbrite-forming and dome-building eruptions elsewhere that they have been defined as a new style of volcanic activity [1]. This new style of activity, Snake River-type volcanism, is typified in part by large-volume, intensely rheomorphic, ignimbrites produced from magmas with high estimated magmatic temperature (c. 900°C and higher). The ignimbrites are also atypical in respect to their oxygen isotopic characteristics, being exceptionally depleted in $\delta^{18}O$ [2]. The sources of these eruptions, which may represent large caldera systems are obscured by later effusions of basalt. The rhyolitic ignimbrites contain no hydrous phenocryst phases, and are thought to have had low pre-eruptive water contents, yet they still erupted in a highly explosive manner, and were fluidal enough to be highly rheomorphic upon aggradation from a pyroclastic density current.

The aim of this work is to determine the pre-eruptive volatile contents of the magma by the analysis of melt inclusions, to test whether the water contents of these magmas were indeed lower than in other, more typical, rhyolitic volcanic products. A second aim is to test whether there is any correlation between the pre-eruptive volatile content in the magma and the subsequent style of eruption e.g. whether the magma resulted in a lava or a pyroclastic deposit. To do this, a number of rhyolitic lavas and ignimbrites that erupted closely in time from similar magma batches were chosen for study.

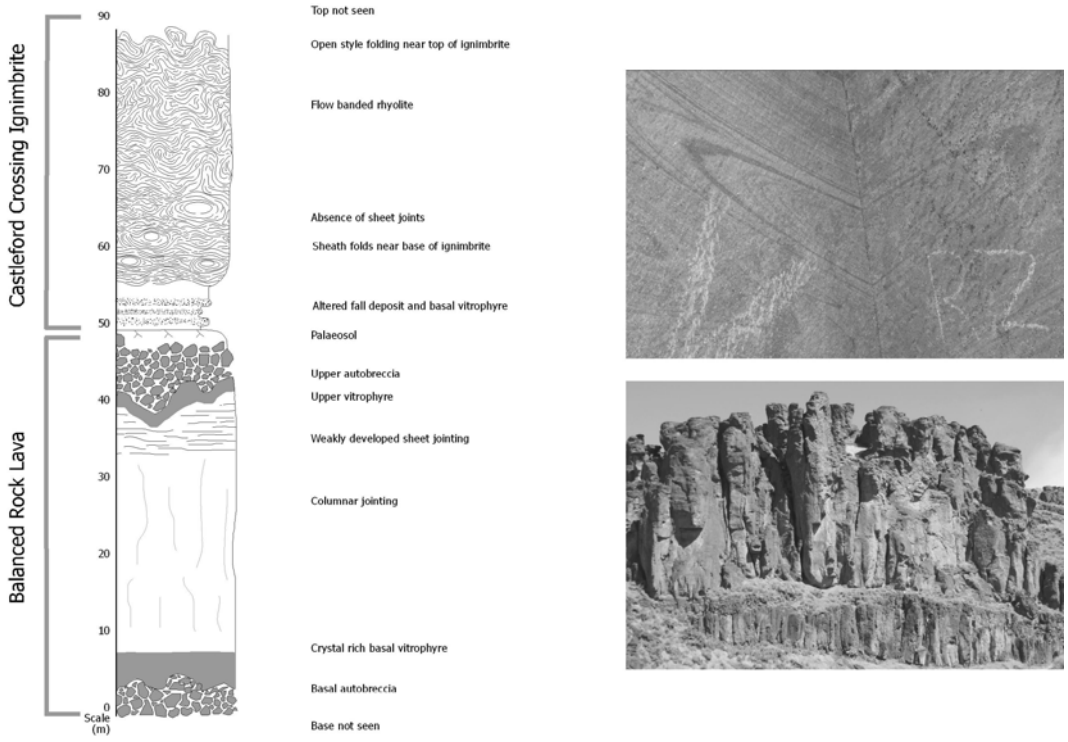

Figure 1. Log showing the relationship between two of the units in this study. Photographs on the right show sheath folds in the base of the Castleford Crossing Ignimbrite (above;1 metre field of view), and the outcrop appearance of the Balanced Rock Lava (below).

More than 70 melt inclusions from 6 units were analysed along with groundmass glass, to determine the volatile contents of the magmas. The pre-eruptive water contents of the Snake River-type volcanic products were found to be lower than those of conventional rhyolitic volcanism (Figure 2; Snake River c. 1.6 to 4 wt% with conventional rhyolitic volcanism ranging from 3 to 7 wt% [3]). This agrees well with the general absence of hydrous mineral phases in Snake River Plain ignimbrites and lavas and the high magmatic temperatures inferred from a variety of mineral thermometers.

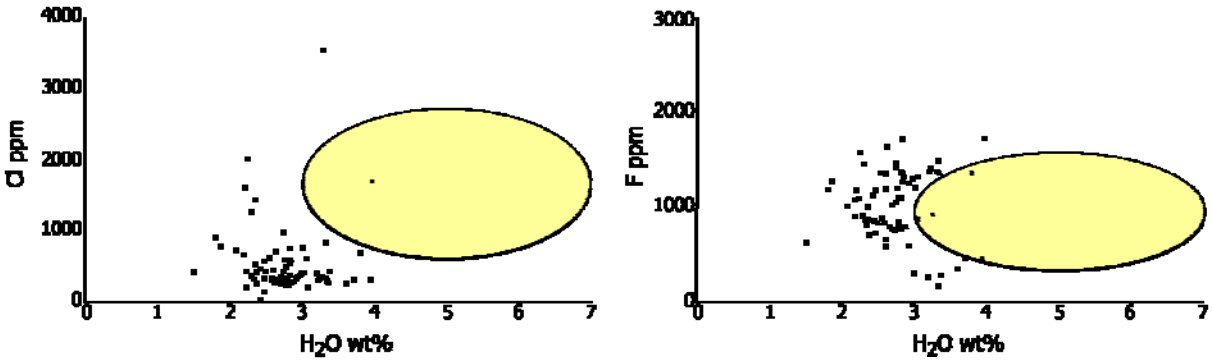

Figure 2. Plots of Cl and F (ppm) versus H_2O (wt %) from melt inclusions within Snake River-type ignimbrites and rhyolite lavas (represented by data points) compared to Plinian-type high silica rhyolites from elsewhere around the world (represented by yellow field) based on 24 studies of melt inclusions in rhyolite [3].

The pre-eruptive water content does not appear to be the control on eruptive style, with both lavas and ignimbrites having similar water contents in melt inclusions; something which has been suggested from other areas (e.g. Pantelleria, Mayor Island).

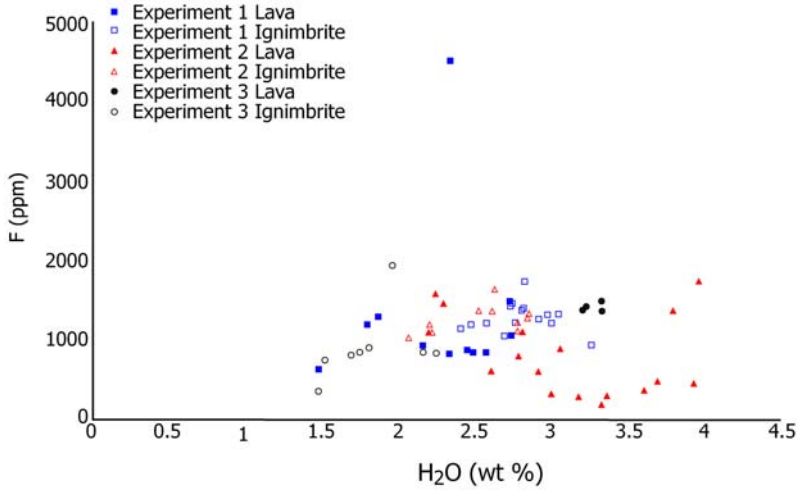

Figure 3. Water and fluorine contents in melt inclusions from pairs of lavas and ignimbrites from the experiments in this study. This figure shows that the pre-eruptive water content in these magmas was not the controlling factor in terms of subsequent eruptive style.

Halogen contents remain relatively constant between the melt inclusions and the groundmass glass, suggesting that F and Cl are retained during these eruptions. This retention of F and Cl may help in reducing the viscosity of the erupted products and promote the intense rheomorphism common to Snake River-type ignimbrites.

References

[1] Branney M.J., Bonnichsen B., Andrews G.D.M., Ellis B., Barry T.L. & McCurry M. Bull. Volc. 70 (2008) 293-314.
[2] Boroughs S., Wolff J., Bonnichsen B., Godchaux M. & Larson P. Geology 33 (2005) 821-824.
[3] Lowenstern J.B. (1995) in: Thompson, J.F.H. (ed.) Magmas, Fluid and Ore Deposits. Mineral. Assoc. Can. Short Course 23, 71-99.

In-Situ Li and B Isotopic Measurements on the Italian Alkaline Volcanism

D. Gagnevin[1], S. Conticelli[2] and J.S. Daly[1]

[1]School of Geological Sciences, University College Dublin, Belfield, Dublin 4, Ireland
[2]Dipartimento di Scienze della Terra, Universita degli Studi di Firenze, Via La Pira, 4, I-50121 Firenze, Italy

Aims

The central theme of this research is to test whether Lithium (Li) and Boron (B) can be used as tracers of mantle enrichment processes below the Italian peninsula. The region is a classic example of alkaline (potassic to ultrapotassic) magmatism in a post-collisional, subduction-related, setting. The extraordinary variety of rock types (from silica-saturated to silica-undersaturated) has been attributed to modification of the lithospheric mantle by various fluids/melts (mantle metasomatism) derived from the subducting lithosphere [1,2,3,4,5,6,7].

Li and B isotopes have the potential to trace the fate of such metasomatic fluids/melt [8,9] in the source region below the Tuscan and Roman Magmatic Provinces (TMP and RMP, respectively). In particular, we want to assess the possible differences in Li and B isotopic composition among Tuscan-type (silica-saturated) and Roman-type (silica-undersaturated) magmas, as well as the extent of Li diffusive equilibration, which may hamper the recognition of the primary high-temperature metasomatic signals recorded in the crystals and host lavas [10,11,12].

Method and samples

This study is focusing on the Capraia (TMP), Torre Alfina (TMP), Sabatini (RMP) and Vulsini (RMP) volcanic systems. In-situ isotopic (δ^7Li, δ^{11}B) and trace element (Li, B, P) analyses were carried out by ion microprobe on mineral phases (mostly on olivine for consistency) from andesitic (Capraia; sample CP101), shoshonitic (Capraia; sample CP101), lamproitic (Torre Alfina sample VS29), tephritic (Sabatini; sample BR29) to basanitic (Vulsini; sample VS139) lavas. Olivine crystals were also analysed for δ^7Li and trace elements in a dunitic mantle xenolith in Torre Alfina (sample VS27). Despite Li was the main strategy at this early stage of investigation, δ^{11}B SIMS analyses are also reported in some crystals.

Results

The main results for Li are summarised as follows:

- There are large δ^7Li variations in olivine (δ^7Li = -36.7 to 14.9‰), which also corresponds to large variations in the Li concentration (3-22 ppm) (Fig. 1).
- Such variability can occur at the single crystal scale: for example, δ^7Li in the olivine crystal from Sabatini varies from -34.2 to 1.4‰ (Fig. 1b).
- Olivines from Capraia, Sabatini and Vulsini have light signatures (δ^7Li < 0‰ in most cases; Fig. 1b, d), while olivines from the lamproite VS29 have heavier signatures (δ^7Li > 0‰ in most cases; Fig. 1a).
- The δ^7Li core to rim transect in olivine from the dunite xenolith (Fig. 1c) is similar to the host Torre Alfina lavas (Fig. 1a) and have heavy δ^7Li in the core region (value up to 13.5‰).
- Overall, the rims display a limited range of isotopic variation (δ^7Li =-5.5 to -3.9‰) compared to variations observed in the core regions (Fig. 1).
- There are complex co-variations between δ^7Li and trace elements (Li, B, P) (Fig. 2). There is a positive correlation between Li and δ^7Li that is defined by olivine in the lamproite, while data are more scattered for Sabatini and Vulsini (RMP; Fig. 2a).
- The plagioclase crystal from Capraia has a rather restricted range of variations (δ^7Li =-5.9 to –2.2‰).

The main results for B are summarised as follows:

- As a whole, δ^{11}B (-14.1 to -0.7‰) and B (0.1 to 5.4 ppm) are less variable than δ^7Li and Li.
- Despite relatively large errors, there are resolvable core to rim differences in δ^{11}B (Fig. 1a, b). δ^{11}B tends to increase towards the rim in Sabatini (Fig. 1b).
- There is no clear difference in δ^{11}B between the lamproite sample VS29 and other lavas.
- δ^{11}B variations are generally correlated with trace element variation, including B (Fig. 2).

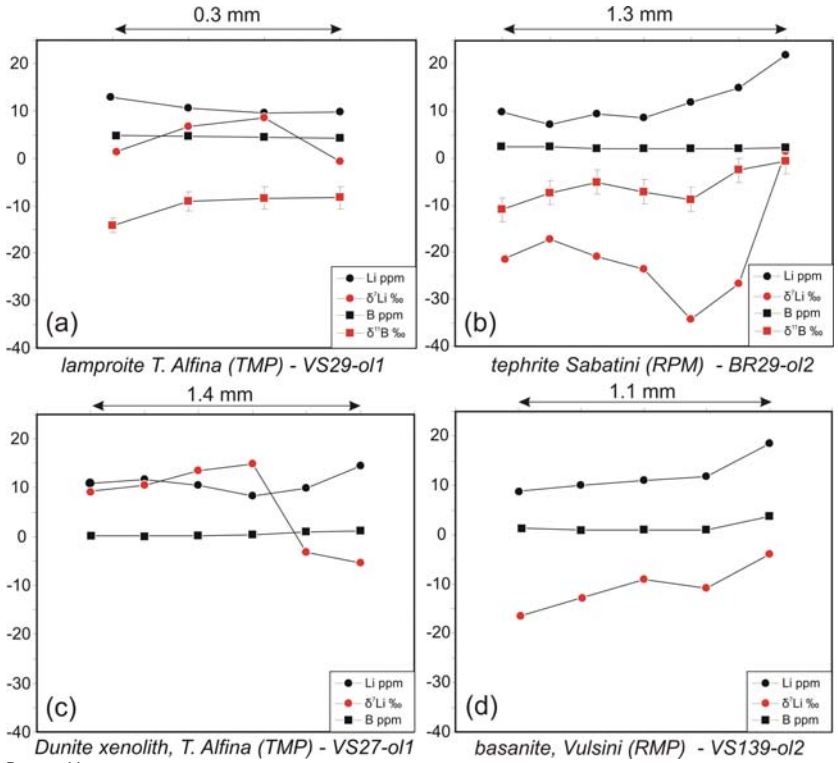

Fig. 1: Selected δ^7Li, δ^{11}B and trace elements olivine zoning patterns for the Torre Alfina, Sabatini and Vulsini volcanic centres.

Discussion and conclusion

A fundamental difference between olivines in leucite-bearing and lamproitic magmas resides in the Li isotopic composition of the cores (light and heavy signatures, respectively; Fig. 1). Such large δ^7Li variations are not uncommon in magma systems and have been attributed to diffusive fractionation. This may occur during residence in the crust or in final phases of magmatic activity (cooling). In an open-system, diffusive equilibration essentially depends on the Li gradient between the crystal core and the constantly replenished rim, and time. Modelling predicts that higher Li content at the crystal surface relative to the core should yield to a drop in δ^7Li [12]. However, no such systematic patterns are observed in the samples we have investigated. The diffusive relaxation should yield to values similar to those recorded in the rim. Incomplete diffusive equilibration may still strongly modify the original profile (i.e., extreme δ^7Li negative values are unlikely to be primary [11,12]), but initial differences in δ^7Li may still be distinguishable, which is of critical importance in a regional geodynamic context, such as studied here. Olivines in Roman-type magmas tend to have light δ^7Li signature, which sharply contrasts with the heavy signature recorded in olivines from the lamproitic magma, with overlap between the two at the rims. A primary – albeit modified by diffusion - signature is further suggested by the linear δ^7Li – Li (and other trace elements such as P) correlation exhibited by lamproitic olivines (Fig. 2a). Olivines in the xenolith (VS27) and the co-sanguineous lava (VS29) (Fig. 1c) have similar heavy Li signature, despite different Li concentration patterns (Fig. 1a, c). This again argues for limited diffusive disturbance of the original magmatic δ^7Li zoning signature, likely to only have affected the rim region during cooling [11,12].

Thus, not precluding an important role of diffusive equilibration in generating the profiles, we rather emphasise that initial Li isotopic heterogeneity may be preserved in volcanic rocks from Central Italy. In particular, the data indicate that mixing between Roman-type (silica undersaturated) and Tuscan-type (silica undersaturated) may effectively have occurred, although the extent of which is difficult to assess. We note, however, that the distinction between Roman and Tuscan magmas may be tenuous in some cases, as indicated by the light signature in crystals from the Capraia shoshonite and andesite (TMP). In the latter case, little δ^7Li variations in plagioclase (not shown) either suggest complete equilibration, or limited diffusive exchange. In the latter case, the range in δ^7Li (average of -5‰) may represent to Li signature of the andesitic magma.

Large δ^7Li variations are inherited from processes occurring in the mantle following subduction [10]. The inferred light δ^7Li in the Roman province (Sabatini and Vulsini) involves material from

subduction-processed oceanic crust in the mantle lithosphere, while heavier signature is typically inherited from slab-related fluids. The trend from heavy to normal mantle values supports the hypothesis that the source of lamproitic magmas was modified by bulk incorporation of continental lithosphere at some stage of its evolution [4,6,7].

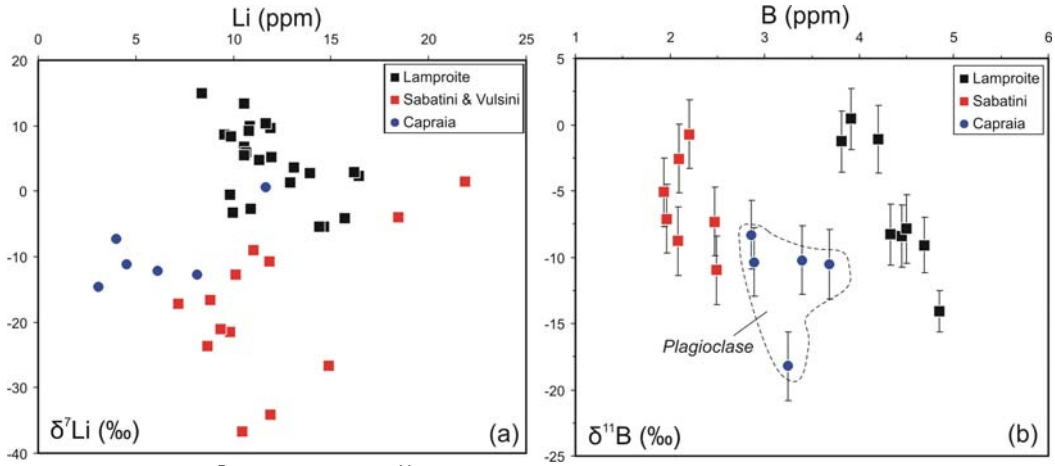

Fig. 2: Olivine δ^7Li - Li (a) and δ^{11}B - B (b) co-variations in lavas investigated in this study.

The significance of the intra-grain Boron zoning patterns requires more data as well as experimental investigations and development of analytical techniques. These preliminary data suggest that δ^{11}B was less affected by diffusive fractionation (**Fig**. 1a, b; 2b), and may thus be relevant to better understand source/differentiation mechanisms (in particular, the interaction between magmas and fluids), as already suggested in other cases by whole-rock data [13].

References

[1] S. Conticelli & A., Peccerillo, Lithos (1990) 24, 305-322
[2] S. Conticelli & A. Peccerillo, Lithos (1992) 28, 221-240
[3] G. Serri, F. Innocenti, & P. Manetti, Tectonophysics 223 (1993) 117-147.
[4] S. Conticelli, P., Manetti, & S. Menichetti (1992) Europ. J. Mineral., 4, 1359-1375
[5] S. Conticelli, L. Francalanci, P. Manetti, R. Cioni, & A. Sbrana, J. Volcanol. Geoth. Res. (1997) 75, 107-136
[6] S. Conticelli, Chem. Geol. (1998) 149, 51-81
[7] A. Peccerillo, Geology 27 (1999) 315-318
[8] T. Moriguti & E. Nakamura, Earth Planet. Sci. Lett. 163 (1998) 167-174
[9] L.H. Chan, W.P. Leeman & C.F. You, Chem. Geol. 182 (2002) 293-300
[10] T. Elliott, A.B., Jeffcoate & C. Bouman, Earth Planet. Sci. Lett. 220 (2004) 231-245.
[11] A.B. Jeffcoate, T. Elliott, S. A. Kasemann, D. Ionov, K. Cooper & R. Brooker, Geochim. Cosmochim. Acta 71 (2007) 202-218
[12] I.J. Parkinson, S.J. Hammond, R.H. James and N.W. Rogers, Earth Planet. Sci. Lett. 257 (2007) 609-621
[13] W.P. Leeman, S. Tonarini, L.H. Chan, L.E. Borg, Chem. Geol. 212 (2004) 101-124.
[14] S.A. Kasemann, A. Meixner, A. Rocholl, T. Vennemann, A. Schmitt & M. Wiedenbeck, Geostandard. Newsl. 25 (2002) 405–416
[15] S.A. Kasemann, A.B. Jeffcoate & T. Elliott, Anal. Chem. 77 (2005) 5251–5257

Distribution of trace elements between zircon, garnet and melt: a key to understanding crustal events and processes (NERC grant NE/B504157/1)

S.L. Harley[1], R.W. Hinton[1], N.M. Kelly[1] and R. Taylor[1]

[1]School of GeoSciences, University of Edinburgh, Edinburgh EH9 3JW, UK

Background

The interpretation of zircon age data in complex high-grade terrains requires detailed textural analysis coupled with in-situ microanalysis of independent chemical criteria for constraining the processes that have affected or controlled zircon behaviour. The distribution of REE and other trace elements between zircon and garnet in natural migmatites has been determined in this project from in-situ microanalysis of texturally-constrained zircon and garnet (and see Harley et al., IMF report 2007). These data have been compared with our new experimental zircon-garnet REE distribution data (Taylor et al., this volume) to provide an assessment of the timing of zircon growth during melting in the deep crust and its implications for melt-related processes in high-grade terrains. Complementary U-Pb, Ti and O-isotope analysis of zircon, and O-isotope analysis of garnet have enabled the zircon growth and modification events to be placed within temperature-time contexts, with implications for the tectonothermal evolutions of both high-temperature and ultrahigh-temperature metamorphic belts.

Results

1. Testing and corroboration of equilibrium zircon-garnet REE distribution relations in UHT leucosomes using zircon Ti contents and zircon-garnet O-isotope fractionation

Two garnet-mesoperthite-quartz UHT leucosomes from the Napier Complex that preserve equilibrium D_{REE}(zrc/grt) have been analysed in detail for oxygen isotopes in the zircons and garnetsusing the Cameca 1270, and for Ti in zircon using the IMS4f and the SX100 electron microprobe. Similar zircon Ti contents (38-60 ppm) are measured by both SIMS and our newly-developed electron microprobe method (Steel & Harley, 2008). Ti-in-zircon thermometry applied to these data yields minimum zircon crystallisation temperatures of 890-920°C, consistent with ternary feldspar thermometry and indicative of leucosome crystallisation during post-peak cooling of the Napier Complex between 2590 and 2550 Ma. The similar $\delta^{18}O$ values for zircon and garnet ($\delta^{18}O \cong 2.5\pm0.5$ ‰) are compatible with UHT equilibrium at >900°C, and the light O-isotopic signatures with a hydrothermally-altered protolith.

A large number of standard garnets have been analysed to allow modelling of instrumental mass fractionation (IMF) with garnet compositional variation. Results indicate that IMF is negligible for garnet compositions with less than 4% grossular component, regardless of variable in Fe-Mg, in contrast to recently published results by other laboratories However, IMF can be expected for increasing Ca in garnet above 4% grossular. The effects of Fe^{3+} on IMF are yet to be evaluated.

2. The use of D_{REE}(zrc/grt): Zircon growth and partial melting processes in the deep crust

The D_{REE}(zrc/grt) data collected in our previous work (e.g. IMF report 2007) have been used in conjunction with new REE data collected in 2007-08 to interpret the context of zircon growth and entrainment in high-grade pelitic migmatites from the Brattstrand Bluffs, east Antarctica. These migmatites underwent biotite-controlled vapour-absent partial melting at ~6 kbar and ~860°C (Fitzsimons, 1996), resulting in production of restitic sillimanite-spinel-garnet melanosomes and segregation of quartzofeldspathic leucosomes. Melts, which have locally migrated to form leucogneiss sheets with variable abundances of entrained residue, have geochemistries equivalent to typical S-type granites. Migmatitic metapelite, leucogneiss and garnet-bearing pegmatite were targeted for analysis. Zircon grains separated from *all* lithology types are coarse, soccerball-style grains characterised by planar banding and sector forms (e.g. Fig. 1), typical of zircon grown in the presence of high-T partial melts. They show consistent zoning from REE-rich cores to REE-poorer outer mantles and rims, correlating with CL patterns (Fig. 1, 2). All zircons are characterised by flat to slightly positively sloping chondrite-normalised HREE patterns, consistent with growth in the presence of garnet.

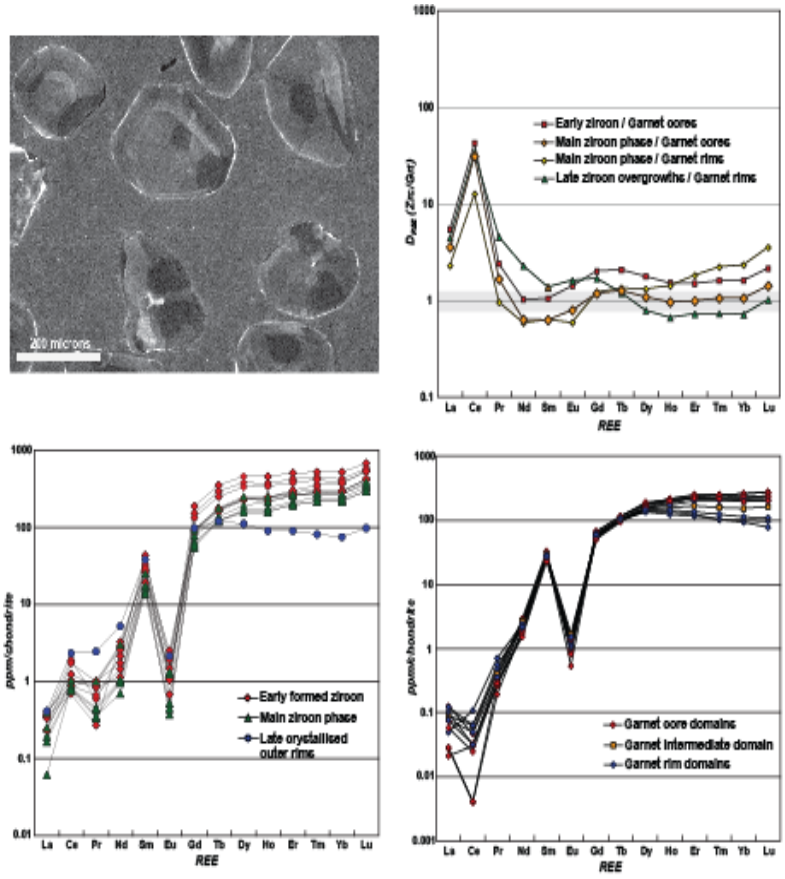

Fig. 1: (Top left) Representative cathodoluminescence (SEM) image of zircon grains from well-segregated leucogneiss (LG1). Zoning in CL images is reflected in a core to rim decrease in absolute REE abundance (bottom left) indicating changing REE availability during zircon growth. (Bottom right) REE abundance in garnet from well segregated leucogneiss. Garnet textures suggest the garnet did not form in situ, but is entrained from the restitic source material. (Top right) D_{REE}(zrc/grt) data for the well-segregated leucogneiss; grey band represents equilibrium values for D_{HREE}. Data indicate that early formed zircon (cores) grew prior to substantial garnet growth (REE-enriched relative to garnet), but that the main phase of crystallisation formed in equilibrium with garnet core domains.

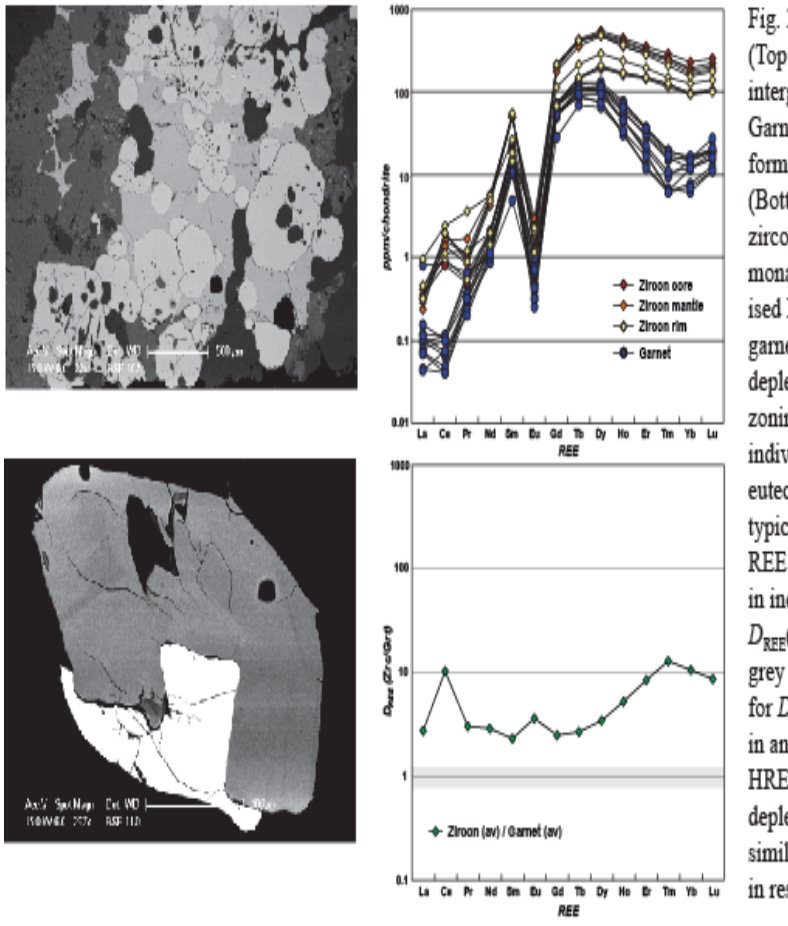

Fig. 2: Planar (undeformed) pegmatite. (Top left) BSE image of eutectic garnet intergrown with late crystallising apatite. Garnet also locally occurs as skeletal forms, indicating late crystallisation. (Bottom left) BSE image of planar banded zircon embayed by late crystallising monazite. (Top right) Chondrite normalised REE cmpositions of zircon and garnet from planar pegmatite. HREE-depleted garnet shows no systematic zoning patterns between core and rims in individual grains or between coarse eutectic and skeletal forms. Zircon typicallu shows a consistent decrease in REE abundance from core to rim domains in individual grains. (Bottom right) D_{REE}(zrc/grt) data for planar pegmatite; grey band represents equilibrium values for D_{HREE}. Data indicate that zircon formed in an environment significantly more HREE-enriched compared with HREE-depleted garnet. Zircon compositions are similar to compositions of garnet observed in restitic portions of the melt source.

Textural and D_{REE}(zrc/grt) data for the leucogneiss and pegmatite dykes indicates that zircon growth occurred in multiple stages and locations within the migmatites. Zircon cores in leucogneiss grew at the source of melting *prior* to substantial garnet growth. The main growth phase of zircon progressed in equilibrium with peritectic (metapelite) garnet prior to entrainment. Late, HREE-depleted zircon rims crystallised within the leucogneiss in close equilibrium with late garnet rims. In contrast, within pegmatites, including late planar dykes (Fig 2), garnet that is strongly HREE-depleted relative to zircon grew late from a Zr-undersaturated melt in which only entrained, slightly older, zircon occurs. This entrained zircon grew in equilibrium with a garnet composition similar to peritectic garnet in metapelite.

Conclusions

The data indicate that zircon growth does not solely occur at a single stage of a P-T path during *terrain-scale* crystallisation of melts, but at various stages during both melt generation, transport and crystallisation. Zircon growth is accounted for by local *domain-scale* compositional and physical parameters that lead to multiple zircon growth events occuring across a terrain at different times and in different textural sites. Early zircon growth occurs as a consequence of locally (i.e. < decimetre scale) controlled melting reactions and transient Zr supersaturation prior to melt coalescence and segregation. Continued melting and melt extraction then allows for entrainment of this previously formed zircon into melts that crystallise *later* in the P-T evolution of the terrain. These considerations indicate that generic P-T-X models will generally fail to accurately predict the timing of zircon growth during the P-T evolution of a terrain and the linkage of U/Pb ages to specific stages on a P-T path. Instead, detailed domain-specific reaction modelling is required, underpinned by textural and geochemical criteria that describe locations of zircon growth and timing relative to associated metamorphic assemblages.

Diffusion in Diamond and the preservation of Carbon and Nitrogen compositions under mantle conditions

B. Harte[1]& T. Taniguchi[2]

[1]School of GeoSciences, University of Edinburgh, Edinburgh EH9 3JW, UK
[2]National Institute of Material Sciences, Tsukuba, Japan.

Introduction

Natural diamonds commonly grow in fluids or melts relatively rich in C, O, H, N and thus diamonds themselves can potentially provide evidence on carbon and nitrogen compositions and sources for those fluids/melts. In the case of common natural diamonds, formed in the mantle, the diamond compositions potentially provide unique evidence of 'deep- Earth' fluid/melt signatures. But under high-temperature deep crustal and mantle conditions the question arises of whether the growth compositions of the diamonds remain unchanged, or whether they are affected by subsequent exchange and diffusion processes in their high-temperature surroundings. Estimates of atomic/isotopic diffusion in diamond show a range of many orders of magnitude (ref [1] and Figure 1); with the faster rates implying relatively rapid diffusion at mantle temperatures given long time scales, whilst the slower rates imply extremely limited atomic mobility under appropriate conditions 950 to 1250 °C. The uncertainty of these data is further compounded by the fact that several of the estimates rely on evidence of nitrogen mobility determined indirectly using infra-red spectroscopy (e.g. [2]).

Figure. 1. Estimated diffusion coefficients for carbon in diamond plotted against 1000/T°K - from various researchers as named, compiled and discussed in ref [1]; selected temperatures in °C indicated. The maximum diffusion coefficients from the new experimental data points of this report are shown as stars.

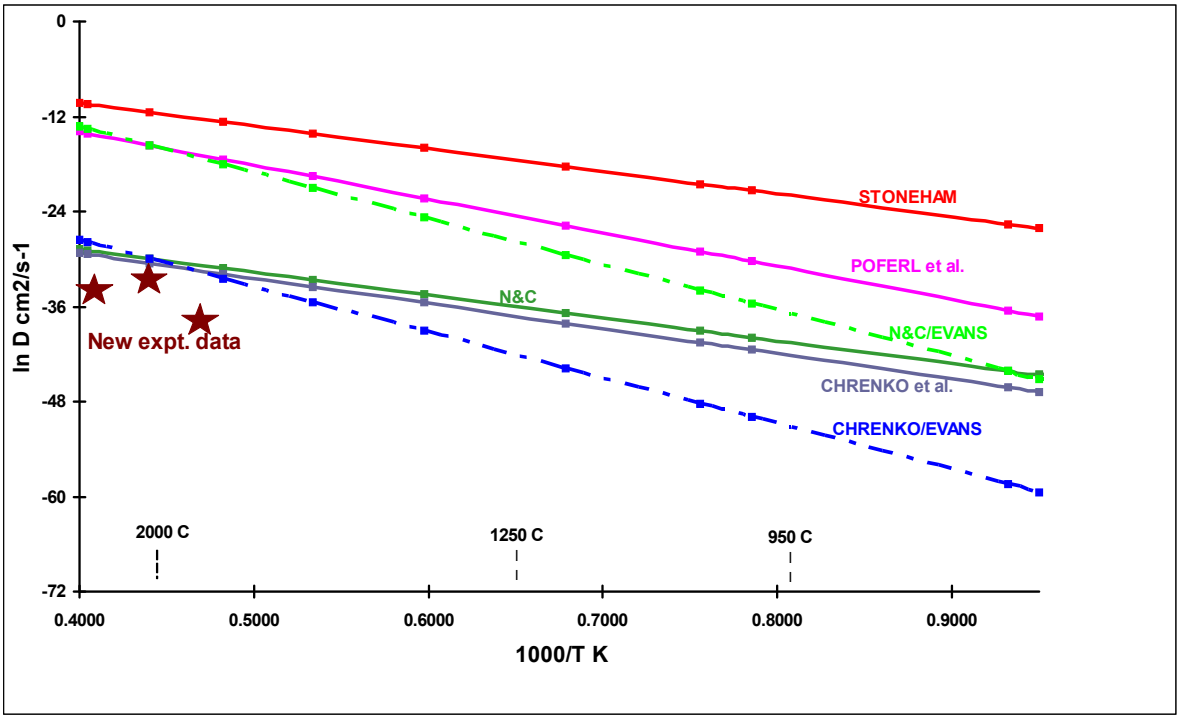

In the present studies we have collected data on carbon isotope mobility in diamonds by conducting high pressure-temperature experiments on diamond plates with a sharp boundary between ^{12}C-rich diamond and ^{13}C-rich diamond, and using the ion microprobe to determine depth profiles of carbon isotope compositions before and after the experiments

Methods

In order to form a diffusion couple of contrasting carbon isotope composition, a diamond plate cut from a natural diamond (largely ^{12}C) was polished and then had a layer of ^{13}C diamond deposited upon it by carbon vapour deposition (CVD). The coated plate was then cut into smaller plates for high P-T experiments. The CVD was carried out with the collaboration of Phillip John of the Department of

Chemistry, Heriot-Watt University. The carbon isotope profiles at right angles to the plates after CVD, and before and after the high P-T experiments were determined by depth profiling using the Cameca

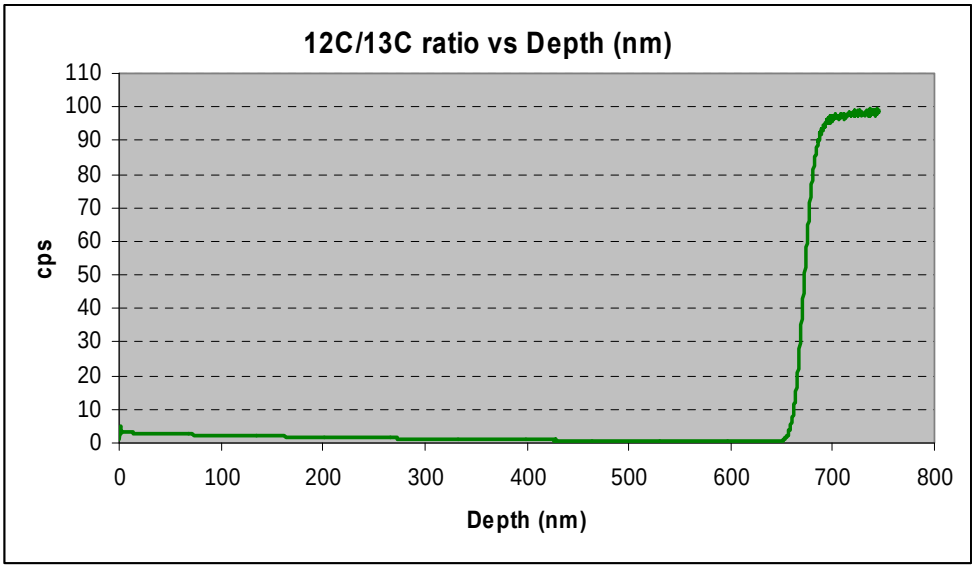

Figure 2. Depth profile of interface between natural diamond (largely ^{12}C to right) and deposited layer of ^{13}C CVD diamond. From the profile the interface between ^{12}C and ^{13}C diamond has a maximum potential thickness of approximately 25nm (see text).

ims 1270 ion microprobe. The depth profile prior to the P-T experiments is illustrated in Fig. 2. The experiments were carried out using the 1500 ton belt apparatus at the National Institute of Material Sciences (NIMS), Tsukuba, Japan. The diamond plates were embedded in CsCl within a tantalum capsule and then placed in NaCl plus 20% ZrO_2 in a graphite furnace. All experiments were done at a pressure of 7.7 GPa for which the apparatus is well-calibrated for the relation of temperature to input current. Three experiments were performed at temperatures of 1800, 2000, and 2200 ºC, for durations of 24hours, 100 minutes and 30 minutes respectively; these run times being dictated by the length of time for which the run conditions remained stable. After the experiments the small diamond plates were recovered and carbon isotope depth profiles determined by ion microprobe.

Results

Despite the high temperatures achieved in the experiments (1800, 2000, and 2200 ºC), no evidence of diffusion was detected in any of the $^{12}C/^{13}C$ depth profiles of the plates measured by ion microprobe after the experiments. Thus all the profiles appeared the same as that obtained prior to high-temperature treatment (as in Figure. 2). If diffusion profiles developed they were narrower than the diffusion interface and the detection limit of the ion microprobe technique. A guide to this limiting thickness is given by the apparent width of the $^{12}C/^{13}C$ interface in Figure 2, which from measurements on several profiles is 20 to 33 nm. Using a value of 25nm, we calculated the potential maximum value for the diffusion coefficient (D) using the approximation $x^2=Dt$ (where x is distance and t is time). The resultant values are plotted on Figure 1, and may be seen to be a little lower than the previously determined lowest estimates.

Conclusions

The null results of the high P-T experiments imply that carbon isotope diffusion in diamond is at least a little slower than the lowest previous estimates of atom mobility presented in Figure 1. Thus the crystal growth signatures of carbon isotopes will be preserved under the high temperature conditions of the upper mantle for hundreds of millions of years. This result concurs with the empirical evidence of limited isotope mobility shown by a matching of isotope distribution patterns with growth patterns (Harte and Craven, IMF report, 2006).

References

[1] B. Harte, I.C.W. Fitzsimons, J.W. Harris, & M.L Otter, Mineralogical Magazine 63, (1999) 829-856.

[2] R.M., Chrenko, R.E.Tuft, & H.M. Strong, Nature, 270 (1977) 141-144.

Annually resolved $\delta^{18}O$ cycles in a Chinese stalagmite: testing and applying SIMS $\delta^{18}O$ measurements

K.R. Johnson[1] & G.M. Henderson[1]

[1]Department of Earth Sciences, University of Oxford, Oxford OX1 3PR

Introduction

Geochemical variations preserved in speleothems are widely used as proxies of past climate[1]. In particular, the oxygen isotopic composition of speleothem calcite can be used to reconstruct past changes in temperature (T) and/or precipitation amount (P) in regions where the rainfall ,and hence drip water, $\delta^{18}O$ is controlled strongly by either T or P. Speleothem $\delta^{18}O$ records from the Asian monsoon region have provided well-dated, high-resolution (decadal to centennial scale) records of summer monsoon intensity over the past glacial-interglacial cycle.

Recently, we observed the presence of seasonal variations in speleothem $\delta^{18}O$ in a 2.5 m long annually banded stalagmite, HS4, from Heshang Cave, China (30.44ºN, 110.42ºE), a site strongly influenced by the East Asian summer monsoon [2]. Rainfall $\delta^{18}O$ in the convective weather system of central China is controlled by the "amount" effect and becomes more negative with increasing precipitation. This imparts a strong seasonal cycle to rainfall $\delta^{18}O$, with the most negative values occurring during the intense rains of the summer monsoon. Measurement of the seasonal $\delta^{18}O$ cycle in speleothems provides a sub-annual resolution record of summer monsoon intensity as well as providing seasonal tie-points, marking the period of maximum summer monsoon. This is extremely useful as it helps constrain the seasonal phasing of other measured chemical proxies such as Mg/Ca and $\delta^{13}C$. In addition, detailed analysis of seasonal $\delta^{18}O$ cycles may help determine how calcite precipitation rate varies throughout the year.

We conducted SIMS measurements of the seasonal $\delta^{18}O$ cycles in two sections of HS4, one from about 7 ka and one from the recent past (about 1995-2000 AD), to assess the potential of *in situ* methods for oxygen isotope analysis. We had previously measured $\delta^{18}O$ in micromilled samples (50 μm resolution) from the 7 ka section by conventional gas-source mass spectrometry. SIMS measurement of this sample therefore enables us to directly compare these two analytical methods. In addition, we measured two growth bands in greater detail to assess the spatial variability of $\delta^{18}O$ along individual growth bands.

Results and discussion

SIMS $\delta^{18}O$ values measured every 30 μm across an 8.8 mm transect of the 7 ka section reveal 21 clear annual cycles in speleothem $\delta^{18}O$ (Figure 1). The conventionally measured $\delta^{18}O$ values of samples micromilled at 50 μm resolution are shown for comparison (Figure 1). While we observe similar cycles in each time series, there are significant differences between the two methods. The SIMS data reveal higher amplitude variability, which is to be expected given the higher spatial resolution achieved. Speleothem $\delta^{18}O$ measured via SIMS varies from -13.8 to -8.3‰ (5.5‰ range) compared with -11.0 to -8.5‰ (2.5‰ range) in the micromilled data. Removal of 3 outliers reduces the SIMS range to 4.4‰, still significantly higher than the micromilled range. Assuming the 7 ka range in rainfall $\delta^{18}O$ is the same as in modern rainfall (5.6‰), the SIMS measurements suggest that a large fraction of the range in rainfall $\delta^{18}O$ is recorded in the speleothem growth bands. Mixing in the epikarst may account for the slightly decreased range observed in the speleothem. The mean SIMS $\delta^{18}O$ (-10.8 ± 0.8‰) is somewhat offset from the mean micromilled $\delta^{18}O$ (-10.0 ± 0.5‰). There is a somewhat systematic offset observed from about 4600 to 8000 mm (Figure 1) that may be related to instrumental conditions on this particular day (June 7th) or problems with standardization. Nevertheless, the amplitude of the variability is consistently large throughout this section. Results from the 1995-2000 AD section reveal similar differences between the two methods.

Figure 1. SIMS $\delta^{18}O$ record across a 7 ka section of the HS4 stalagmite. $\delta^{18}O$ measured in micromilled samples via gas-source mass spectrometry are shown for comparison.

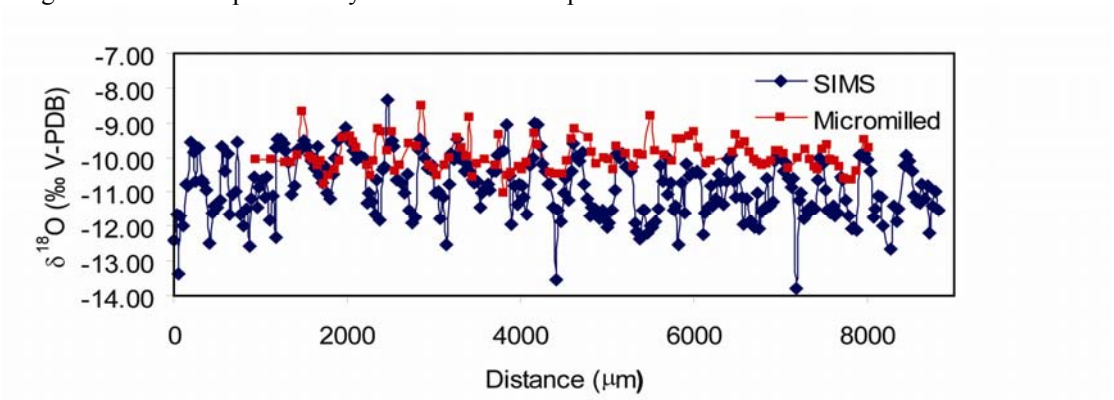

SIMS $\delta^{18}O$ measured in a grid across 2 growth band couplets and along a single growth band for 6 mm reveal some complex spatial variability. Along individual dark or light bands, $\delta^{18}O$ may vary by as much as 1‰. While some of this variability may be due to instrumental variations, there are also potential crystallographic effects which should be investigated further.

Figure 2. SIMS $\delta^{18}O$ measured in a grid across 2 growth bands (A) and along one growth band (B).

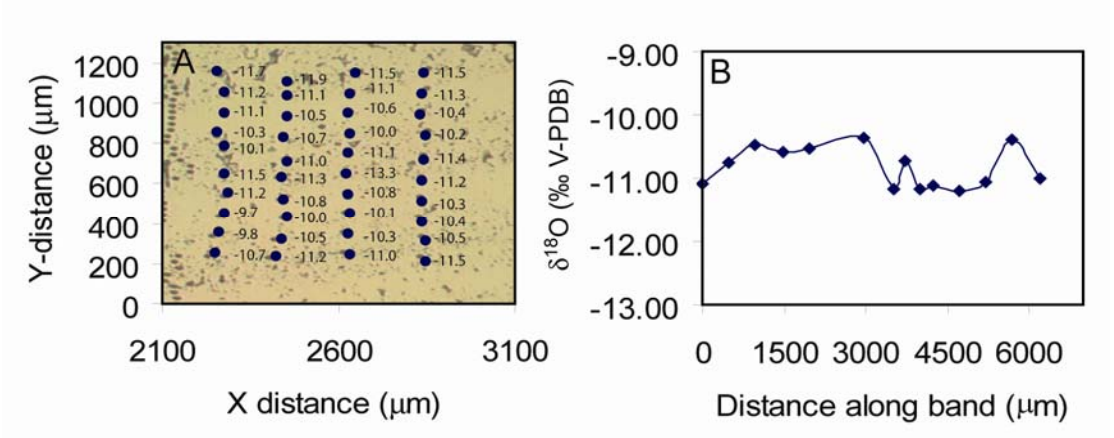

Conclusion

SIMS $\delta^{18}O$ measurements may be useful for investigating sub-annual variations along speleothem growth axes. The full amplitude of these variations is more clearly resolved with SIMS than with traditional micromilling techniques. In addition, micro-scale investigations of speleothem $\delta^{18}O$ could provide new insights into speleothem crystal growth mechanisms as well as improve our understanding of temporal and spatial $\delta^{18}O$ variability in speleothems.

References

[1] I.J. Fairchild, C.L. Smith, A. Baker, L. Fuller, C. Spotl, D. Mattey, F. McDermott & E.I.M.F., Earth-Sci Rev 75 (2006) 105-153.

[2] K.R. Johnson, C.Y. Hu, N.S. Belshaw & G.M. Henderson, Earth and Planetary Science Letters 244 (2006) 394-407.

Quantifying the release of base metals into hydrothermal ore forming systems

S.M, Jowitt[1], G. R. T. Jenkin[1] & L. A. Coogan[2]

[1]Department of Geology, University of Leicester, University Road, Leicester, LE1 7RH
[2]School of Earth and Ocean Sciences, University of Victoria, Victoria, British Columbia, Canada,

Introduction

Understanding the source rock-deposit relationship for Volcanic Hosted Massive Sulphide (VHMS) deposits is fundamental for future mineral exploration and to increase our understanding of ancient and modern day ocean floor hydrothermal processes. Ion microprobe analysis was undertaken to quantify the distribution of base metals (Ni, Co, Cu, and Zn) and other elements (Sr and Zr) in minerals within a series of sheeted dyke samples that have been proposed to be source rocks for VHMS deposits [1]. These samples, from the Troodos ophiolite, Cyprus, show a range in intensity of hydrothermal alteration.

Project Background

The aim of this project was to test the hypothesis that as hydrothermal alteration progresses the mineralogical changes inherently linked with alteration directly input base metals (Ni, Co, Cu and Zn) into ore-forming hydrothermal systems. New whole-rock geochemical data indicate a direct relationship between the progress of alteration to form epidosites (epidote-quartz rocks) and the release of Zn and Co into ore-forming hydrothermal fluids. Epidosites are thought to develop from chlorite-actinolite-quartz-epidote units formed during earlier, less intense alteration [1], and through increasing alteration progress towards an epidote-quartz end-member. The decreasing modal proportion of chlorite (Figure 1) correlates strongly with decreasing Zn and Co, two important metals in Cyprus-type ore deposits, but Cu appears to be decoupled from alteration. A simple interpretation of these data is that Zn and Co are contained mainly in chlorite within these altered rocks. Alternatively, these elements may be distributed between epidote and chlorite with the correlation being due to progressive leaching of metal and progressive decrease in the modal proportion of chlorite, both of which could be attributed to increased fluid-flux.

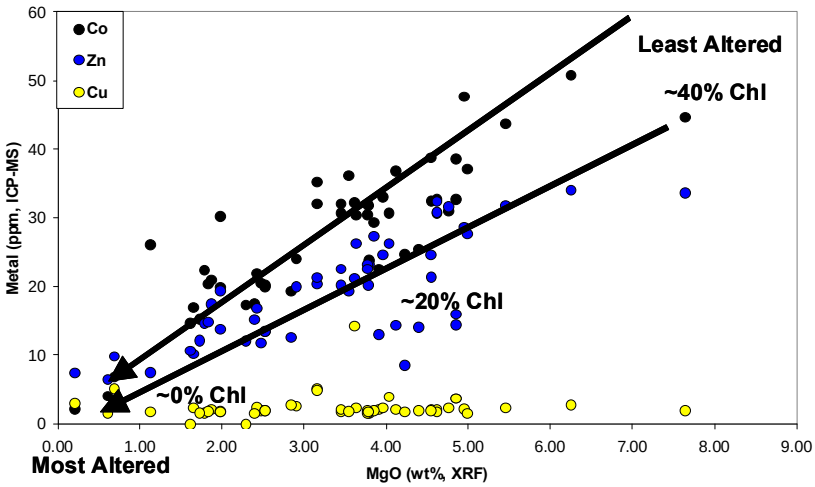

Figure 1. Whole rock metal abundance against MgO (as a proxy for chlorite abundance) for altered samples from the sheeted dyke complex of the Troodos ophiolite.

In order to be able to develop a quantitative model of the release of ore metals into hydrothermal fluids we need both: (i) a model of the progressive mineralogical changes during hydrothermal alteration, and (ii) an understanding of the partitioning of metals among the mineral phases present. Petrographic studies, in combination with bulk-rock chemistry, have been used to develop (i). Ion microprobe analysis was used to try and determine (ii), to enable the quantification of the concentration of metals within differing minerals in a series of rocks at different stages in the overall alteration process, ranging from fresh through to end-member epidote-quartz facies epidosite. The samples analysed were

fine-grained sheeted dykes that are thought to represent source rocks for ore deposits – this means that, by their very nature, they contain low metal concentrations (Figure 1). One of the major aims of this project was to characterise the concentrations of base metals in chlorite and epidote within varying facies of epidosite units.

Results and Discussion

As can be seen in Figure 1, the concentrations of Zn and Co (and to a more limited extent other metals such as Ni) can be related to the modal concentration of chlorite present in the samples examined here. Ion microprobe analysis shows that of the minerals present only chlorite and actinolite contain significant quantities of base metals (>10 ppm). Within the epidosites in the system, only chlorite is present, and as alteration progresses towards an epidote-quartz dominated end-member, this chlorite is removed from the system. This dissolution of chlorite releases base metals into hydrothermal solutions; however, the ion microprobe results here suggest that the removal of chlorite is not the only way of introducing metals into hydrothermal systems. As the modal proportion of epidote increases, the concentration of zinc decreases within individual chlorites (Figure 2). The opposite is true of the cobalt concentration in chlorite which increases with increasing modal proportions of epidote. A similar relationship is seen between Ni and Zn; with decreasing zinc correlating with increasing nickel. These results suggest that as alteration progresses, it is not just the removal of chlorite which controls the release of base metals into hydrothermal fluids. These data indicate that changes within the chlorite, whereby more mobile elements such as zinc move into solution, whilst more immobile elements such as cobalt and nickel move into or are preferentially retained by chlorite. This must have had a significant influence on the concentration of base metals in ore-forming hydrothermal fluids during the time this system was active.

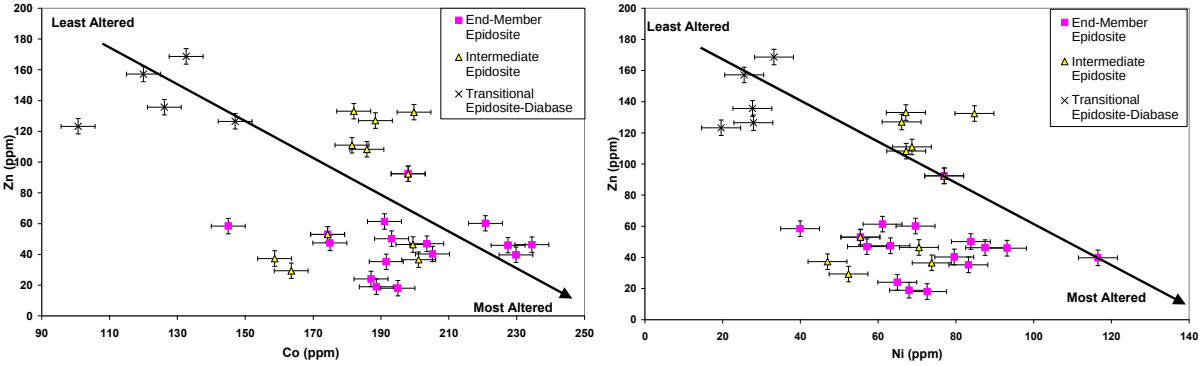

Figure 2 Concentrations of base metals in chlorites determined by ion microprobe, showing variations in Zn vs Co (left) and Zn vs Ni (right) during progressive alteration from Transitional Epidosite-Diabase facies to End Member epidosite facies.

Conclusions

These new data greatly improve our knowledge of the processes occurring within VHMS and ophiolitic hydrothermal alteration systems, and have implications both for mineral exploration and our understanding of mid-ocean ridge hydrothermal systems. The ion microprobe data presented here, combined with field and geochemical data, has enabled the tracking of base metal mobility at a range of spatial scales and with progressive alteration.

References

[1] C. J. Richardson, J. R. Cann, H. G. Richards, J. G. Cowan, EPSL, 84 (1989) 243-253.

Constraining the Pliocene climate record in Taiwan

L.A. Kirstein[1]

[1]School of GeoSciences, University of Edinburgh, Edinburgh EH9 3JW, UK

Summary

A major modern controversy in tectonic geomorphology relates to the interaction between climate and tectonic forcing on mountain uplift, erosion and hence the evolution of landscape topography. Currently little is known about climate in regions of accelerated uplift during the Cenozoic (65 – 0Ma). Commonly the sedimentary archive is incomplete such that evaluating the significance of climate versus tectonic forcing on topography is extremely difficult. Taiwan, located in the western Pacific, is the best example of a modern orogenic system where the interplay between climate, tectonic and erosion can be studied. The 4 km high Central Ranges of eastern Taiwan result from the collision of the Luzon volcanic arc and the south China passive margin since the late Miocene (~8 Ma). Studies have shown a general agreement between long term exhumation rates (5-7 mm/year) (Willett et al., 2003) and present day erosion rates (3-6 mm/year) (Dadson et al., 2003) signifying a dominant tectonic forcing. However, erosion rates from individual catchments can vary up to 68 mm/year (Dadson et al., 2003) suggesting that climate change in at least the Quaternary (< 2 Ma) has had a dramatic effect on local erosion rates.

The Coastal Range of eastern Taiwan contains volcanic igneous rocks and reef carbonates unconformably overlain by Plio-Pleistocene sediments. The reef carbonates are locally termed the Kangkou and Tungho limestones and vary in age from 5.2 Ma to 2.9 Ma respectively. They formed as fringing reefs on the Luzon volcanic islands and contain coral fragments, rhodoliths, molluscs and foraminifera. These limestones are therefore a valuable palaeo-environmental archive which can potentially be unravelled using a combination of high resolution in situ oxygen and trace element analyses. The hypothesis is a simple one. If climate in the Early Pliocene was similar to that today then similar sea surface temperatures (SST) will be obtained. If however there was a progressive cooling in the region during the Pliocene then the palaeotemperatures recovered from the two reef carbonates will be different from each other.

Oxygen isotope ratios, recorded in fossil foraminiferal shells, have been the paleoceanographers' principal tool for constraining glacial-interglacial variations in sea level and continental ice volume. The analysed samples are lithified which means conventional mass spectrometry methods are unsuitable for providing oxygen data for individual species. The size, shape and importance of avoiding micritised material within or adjacent to the foraminifera make the use of high resolution in situ ion microprobe analyses key to the success of obtaining detectable differences in SSTs. Successful oxygen isotope analyses will have an error on analyses is <0.5‰ making variations in SST of the order of 2°C detectable.

Results

Two samples from the Pliocene Kangkou (~5 Ma) and Tungho (~3 Ma) carbonates (CH1 and TH1) were selected so that a preliminary investigation could be undertaken to establish the potential of reconstructing past temperature variation using Mg/Ca and O isotopes. Examination of the carbonates using cathodoluminescence has revealed limited micritisation of the carbonates suggesting minimal diagenesis has occurred (Mn < 0.1 wt. %; Sr below detection). Scanning electron microscope (SEM) work also allowed the identification of intact, large unaltered benthic foraminifera including the genera Amphistegina, Gypsinia and Lepidocyclinia.

The foraminiferal tests are Mg calcite (MgO: 0.5-1.5 wt. %) with a systematic difference in Mg/Ca ratios between the two limestones. These preliminary Mg/Ca data suggest a detectable difference in palaeotemperature (Kangkou - 29 °C versus Tungho - 27°C) between the two reef carbonates consistent with a cooling of the region in the Late Pliocene.

Stable isotope analyses on individual foraminifera is relatively new and recent advances in analytical techniques enable in situ analyses of stable isotopes with the required spatial resolution and analytical accuracy. As part of the pilot study O isotopes were measured *in situ* in foraminifera from two samples using the Cameca 1270 ion microprobe facility at the University of Edinburgh and indicate $\delta^{18}O_{PDB}$ values of -0.7 to -1.6 in the Kangkou sample and in the Tungho limestone $\delta^{18}O_{PDB}$ values of -0.2 to +0.9. These values appear consistent with the palaeotemperature estimates from Mg/Ca ratios for these two limestones signifying a cooling in the region in the Pliocene. The Kangkou O isotope values are within the range estimated from planktonic foraminifera Globigerinoides sacculifer in mudstones from southwestern Taiwan which were considered to have a pristine environmental signature (Shieh et al., 2002). The present data are limited however they highlight the immense potential of the proposed approach.

Future work

This work has formed a proof of concept with the principle aim of demonstrating that the techniques are appropriate and capable of providing the sensitivity required for a larger project which I have since submitted to the New Investigators grant 2008 deadline.

References

[1] S.J. Dadson, N. Hovius, H. Chen, B. Dade, M.L. Hsieh, S.D. Willett, J.C. Hu, M.J. Horng, M.C. Chen, C.P. Stark, D. Lague, & J.C. Lin, Nature 426 (2003) 648-651.

[2] S.D. Willett, D. Fisher, C. Fuller, Y. En-Chao, L. Chia-Yu, Geology 31 (2003) 945-948.

[3] Y-T. Shieh, C.F. You, K.S. Shea, C.S. Horng, Jour. Asian Earth Sci. 21(2002) 1-5.

Vent mussel shells as indicators of environmental conditions at hydrothermal vents

J. Libertinova[1], L. J. Clarke[1], and H. Kennedy[1]

[1]School of Ocean Sciences, Bangor University, Askew Street, Menai Bridge, Isle of Anglesey, LL59 5AB

Introduction

The geochemical composition of biogenic carbonates can yield information about the ambient environment in which calcification occurred. Marine bivalve molluscs are a particularly useful archive because the incremental manner in which their shells are deposited allows for high temporal resolution reconstructions of oceanographic parameters, e.g. temperature and water chemistry. Marine bivalves also are widely distributed throughout the oceans, from the tropics to the poles and from coastal waters to the deep-sea mid-ocean ridge environment. However, very little work of this nature has been completed on species that inhabit the hydrothermal environments of mid-ocean ridges.

Investigations of the chemical composition of shells of the deep-sea hydrothermal vent mussel species, *Bathymodiolus azoricus* and *Bathymodiolus puteoserpentis*, which dominate the fauna of the Mid-Atlantic Ridge, have potential to inform us about historical changes in the hydrothermal environment. Deep-sea hydrothermal vent mussels live in continuous darkness, close to vents that discharge hot (≤10–350°C) fluid enriched in trace elements, methane and sulphide. The mussels live in temperatures that rarely exceed 10–15°C, but can experience rapid temperature (and seawater chemistry) fluctuations on the timescale of seconds to days. Measurement of differences in the chemical composition of *Bathymodiolus* shells by sequential sampling along the growth axis of individual specimens therefore allows a better understanding of changes in their growth environment.

Sclerochronological techniques reveal distinct microgrowth increments, ~5–100 μm, in the calcite outer shell layer of the vent mussel *Bathymodiolus azoricus* (see Figure 1B). Similar microgrowth increments in *Bathymodiolus brevior*, from the North Fiji Basin, western Pacific Ocean, have been reported as daily shell growth increments and for some shell portions growth increments have been found to be controlled by tidal variability [1]. Consequently, the objective of this one-day pilot ion microprobe study was to determine whether periodicity is evident in *Bathymodiolus azoricus* calcite shell element/Ca ratios and to compare elemental records with the internal shell growth increments.

Results

Mg/Ca, Mn/Ca and Ba/Ca ratios are shown in Figure 1C. Statistical program PAST [2] has been used to complete spectral analyses, using the Lomb periodogram, for each element/Ca ratio after removal of linear trends. Periodicities are observed for Mg/Ca, Mn/Ca and Ba/Ca ratios across a number of microgrowth increments (Figure 1D). For Mg/Ca ratios spectral analysis showed a statistically significant peak for a period of 181 μm ($r^2 = 0.19$; expressing fit to a sinusoidal model). In contrast, Mn/Ca ratios had periods of 208 μm and 463 μm ($r^2 = 0.42$), with the best fit for Ba/Ca ratios at a period of 463 μm ($r^2 = 0.50$). All element/Ca ratios also show a statistically insignificant peak at a period of 83 μm, but which improves fits to sinusoidal models for Mg/Ca ($r^2 = 0.22$), Mn/Ca ($r^2 = 0.46$) and Ba/Ca ($r^2 = 0.55$) ratios. Relationships between Mg/Ca and Mn/Ca ($r^2 = 0.08$), Mg/Ca and Ba/Ca ($r^2 = 0.06$) and Ba/Ca and Mn/Ca ($r^2 = 0.21$) ratios are weak but significant ($p < 0.001$).

Conclusion

High spatial resolution ion microprobe data illustrate periodicities for Mg/Ca, Mn/Ca and Ba/Ca ratios in the calcite outer shell layer of *Bathymodiolus azoricus*. There seems also to be a relationship between element/Ca ratios and growth increments, e.g. between 0–225 μm distance and especially for Mg/Ca ratios. These observations suggest a common control on geochemistry and shell structure, which most likely reflects changes in the temperature and chemical composition of the seawater surrounding the mussels, due to fluctuations in hydrothermal activity and/or tidal influences.

References

[1] B.R. Schöne and O. Giere, Deep-Sea Res. Part I. 52 (2005) 1896-1910.

[2] O. Hammer and D. Harper, Paleontological Data Analysis, Blackwell (2005) http://folk.uio.no/ohammer/past

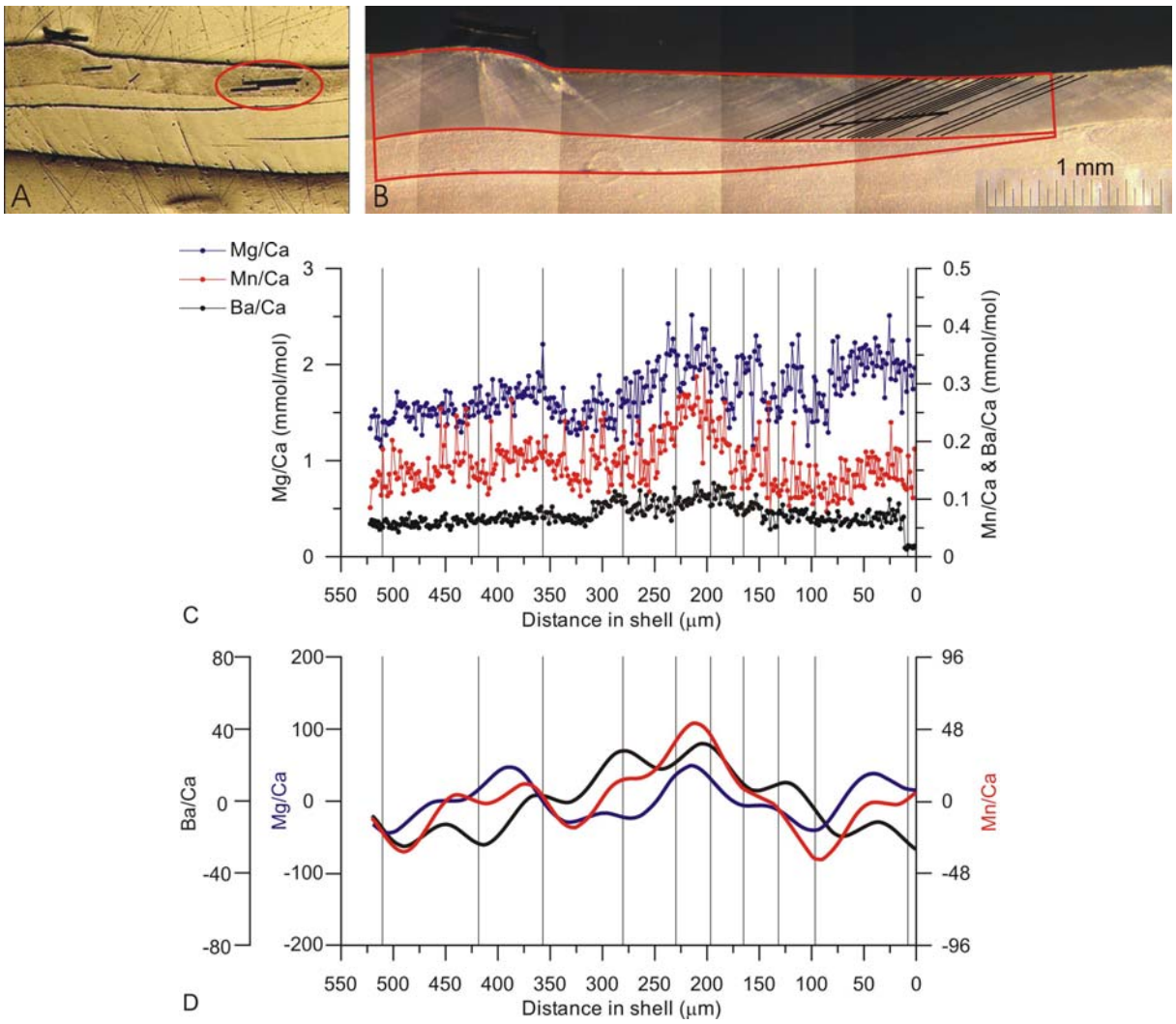

Figure 1: Light microscope photographs of (A) polished cross-section of a *Bathymodiolus azoricus* shell, coated with a thin layer of Au, and location of SIMS profile (circled) for which data are presented (bottom two tracks being merged together) and (B) re-polished shell cross-section, after SIMS analyses, etched by Mutvei's solution (1% acetic acid and 25% glutaraldehyde, mixed 1:1, without alcian blue staining) with marked microgrowth increments and location of SIMS profile. (C) SIMS Mg/Ca, Mn/Ca and Ba/Ca ratio profiles in the calcite outer shell layer of the *Bathymodiolus azoricus* shell (specimen #RB1A-1). (D) Periodicities found in the SIMS Mg/Ca, Mn/Ca and Ba/Ca ratio profiles, after removal of any linear trend. Vertical lines in Figures C and D represent lines revealed within the outer calcite shell layer after etching and delineate shell microgrowth increments. Direction of shell growth is from left to right, and the SIMS sampling direction is from right to left, in the images and the graphs.

A preliminary stable carbon isotope study of the graphite crystal morphologies in the volcanic-hosted epigenetic deposit at Borrowdale in Cumbria, UK

D. Millward[1] & F. J. Luque[2]

[1]British Geological Survey, Murchison House, Edinburgh EH9 3LA, UK
[2]Department of Crystallography and Mineralogy, Faculty of Geology, Complutense University, Madrid, Spain

Scientific Report

Graphite structure consists of a continuous bidimensional array of six-fold rings of carbon atoms stacked along the c-axis, and most commonly results in a laminar (platy) habit. In spite of the layered structure, other morphologies have been reported and the widest range of morphologies known within a single paragenesis is from the Borrowdale graphite deposit in Cumbria, UK. There, graphite mineralization is hosted within volcanic rocks, one of only two examples known worldwide of such an association. The crystal morphology of any mineral is controlled by the physico-chemical conditions prevailing during nucleation and growth; on the other hand, some geochemical features are also dependent upon the conditions of crystal growth. The present study on the Borrowdale deposit was aimed at testing the hypothesis that the different graphite morphologies have distinct isotopic compositions. This study complements a wider investigation by the authors and their colleagues, of the mineralogical and geochemical characteristics of this unusual fluid-deposited graphite occurrence, with the aim of unravelling the evolution of the mineralizing process.

Geological and mineralogical features

The Borrowdale graphite deposit consists of mineralised faults hosted by andesite lavas and sills belonging to the upper Ordovician (Caradoc) Borrowdale Volcanic Group, the geochemical characteristics of which show evidence of assimilation of pelitic material from the underlying Skiddaw Group[1]. The richest graphite deposits are developed at the intersections of the faults within steeply inclined pipe-like bodies up to 1 x 3 m in cross-section and from a few metres to over 100 m in length. The pipe-like bodies contain nodular masses and patches of graphite, typically 1-2 cm across, but ranging from a few millimetres to 1 m or more. The mineral association of the deposit includes graphite, chlorite, epidote, and quartz.

The wide diversity of graphite morphologies recognized within the deposit can be grouped into three categories: laminar, cryptocrystalline, and spherulitic. Laminar graphite crystals (up to 300 μm long and 50 μm wide) are by far the most abundant (≈ 90%). Along fault zones, "graphic-like" intergrowth textures, consisting of thin curved and tapering graphite flakes or "vermiform" graphite crystals within chlorite have been observed. Cryptocrystalline graphite may form: 1) "composite nodules" consisting of both flaky and cryptocrystalline graphite, 2) rounded patches within flaky graphite, and 3) "colloform" bands and globules dispersed within the host rock. Spherulites occur in four different settings: 1) as individual forms, 5-40 μm in diameter, within flaky graphite, 2) as individual forms, 1-3 μm in diameter, included in quartz fragments, 3) as individual forms, 1-5 μm in diameter, or aggregates disseminated within the volcanic rock, and 4) as aggregates, 5-10 μm in diameter, associated with chlorite along fault zones.

The structural characterization of these morphologies by Raman spectroscopy indicates a high degree of crystallinity (large crystallite size along the basal plane), except for the cryptocrystalline graphite forming colloform textures within the host rock that displays significantly lower crystallinity. The study of fluid inclusions within quartz associated with graphite indicates that the mineralizing fluids evolved from H_2O-CO_2-CH_4 mixtures ($X_{H2O} = 0.646$; $X_{CO2} = 0.244$; $X_{CH4} = 0.114$; $X_{NaCl} = 0.006$) circulating at temperatures close to 340 ºC to H_2O-CH_4 ($X_{H2O} = 0.93$; $X_{CH4} = 0.02$; $X_{NaCl} = 0.05$) fluids at temperatures close to 200 ºC.

Ion probe work

Secondary ion mass spectrometry (SIMS) analyses were performed at the Grant Institute of Geology, University of Edinburgh, using a Cameca ims-1270 ion microprobe. Gold-coated polished thin

sections were analysed using negative secondary ions sputtered with a positive charged Cs+ beam. The spot size was 20 µm, and hence stable carbon isotope data were obtained only for those morphologies displaying sizes larger than this. The results were checked using international standards, including graphite USGS24 (δ13C = -16.05 ‰). Five measurements were made on the standard at the start and end of each 20 analyses – thus enabling calibration of the sample measurements against 10 standard measurements. Under these conditions, the precision of the point analysis is close to 0.2 ‰.

It is noteworthy than the analyses of each morphological type show very homogeneous values, thus falling within narrow ranges (Table 1). Graphite flakes have one of the heaviest isotopic signatures (average $\delta^{13}C$ = -30.26 ‰). Such values are close to those found in graphite spherulites within chlorite (average $\delta^{13}C$ = -30.15 ‰). On the other hand, cryptocrystalline graphite in composite nodules has significantly lighter isotopic signatures (average $\delta^{13}C$ = -33.70 ‰) with no apparent zoning across the banded texture (Fig. 1). The lightest carbon isotope ratios correspond to vermicular graphite within chlorite (average $\delta^{13}C$ = -34.49 ‰).

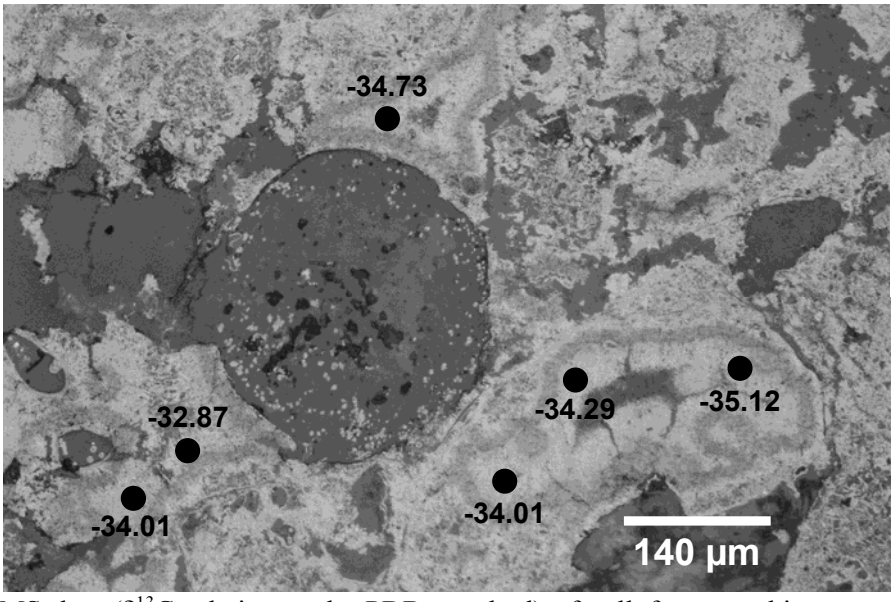

Figure 1: SIMS data ($\delta^{13}C$ relative to the PDB standard) of colloform graphite around quartz. The quartz grain contains small graphite spherulites. Note the narrow range of $\delta^{13}C$ values.

Discussion

The light isotopic signatures of the different morphologies of graphite from the Borrowdale deposit suggest that the carbon was derived from a biogenic source. This is in good agreement with the evidence of assimilation of Skiddaw Group metapelites by the volcanic host rocks, and with the presence of zones within the metapelites that have been depleted in carbon and other elements during hydrothermal alteration[2]. Independent bulk carbon isotopic analyses of Skiddaw metapelites yielded values close to -28‰. In addition, the small differences in the $\delta^{13}C$ values suggest that graphite precipitated over a narrow temperature interval.

According to classical theories of nucleation, spherulites and colloform textures represent heterogeneous nucleation on pre-existing substrates under high supersaturation conditions. Laminar graphite should nucleate later, probably as a result of homogeneous nucleation from fluids with lower supersaturation. In the fractionation that occurs between two carbon-bearing phases, the more oxidized species of the pair becomes relatively enriched in the heavier isotope, i.e. ^{13}C. Thus, graphite precipitating from CO_2-rich fluids would be lighter than CO_2 in equilibrium. This agrees with the fact that the earlier morphologies (colloform) crystallizing in the pipe-like bodies display lighter signatures than flaky graphite that formed somewhat later. However, graphite within chlorite from fault-fills points to an inverse relationship: the isotopic ratio of spherulitic graphite within chlorite is heavier than in the vermicular intergrowths. This suggests, though does not prove, that graphite-chlorite veins represent a slightly later mineralizing event related to deposition from lower temperature, CH_4-rich fluids. Since graphite is the oxidized phase with respect to methane, the earlier crystallizing

morphologies (i.e. spherulites), retained heavier isotopic signatures than those precipitating later (vermicular graphite).

Table 1: Results of the ion probe analysis of graphite morphologies.

Vermicular intergrowths in chlorite	**$\delta^{13}C$**	**Cryptocrystalline**	**$\delta^{13}C$**	**Flakes**	**$\delta^{13}C$**
F2@1.asc	-34,87	P0@1.asc	-33,72	P0@17.asc	-29,26
F2@2.asc	-33,76	P0@2.asc	-32,56	P0@18.asc	-31,89
F2@3.asc	-33,99	P0@3.asc	-34,45	P0@19.asc	-28,97
F2@4.asc	-35,29	P0@5.asc	-34,09	P0@20.asc	-28,65
F2@5.asc	-34,20	P0@6.asc	-34,45	P0@21.asc	-29,72
F2@6.asc	-35,20	P0@7.asc	-33,87	P0@22.asc	-28,71
F2@7.asc	-35,15	P0@8.asc	-33,60		
F2@8.asc	-33,92	P0@9.asc	-31,60	G2C@1.asc	-30,85
F2@9.asc	-34,05	P0@10.asc	-32,10	G2C@2.asc	-31,31
		P0@11.asc	-34,29	G2C@3.asc	-30,56
AVERAGE	***-34,49***	P0@12.asc	-35,12	G2C@4.asc	-31,01
		P0@13.asc	-34,01	G2C@5.asc	-30,75
Spherulites in chlorite	**$\delta^{13}C$**	P0@14.asc	-32,87	G2C@7.asc	-30,23
F2@11.asc	-29,87	P0@15.asc	-34,01	G2C@8.asc	-30,22
F2@12.asc	-30,02	P0@16.asc	-34,73	G2C@9.asc	-28,97
F2@13.asc	-30,98			G2C@10.asc	-31,55
F2@14.asc	-29,76	***AVERAGE***	***-33,70***	G2C@12.asc	-31,61
F2@15.asc	-31,11				
F2@16.asc	-29,18			***AVERAGE***	***-30,26***
AVERAGE	***-30,15***				

References

[1] B.J. McConnell, J.F. Menuge & J. Hertogen, J. Geol. Soc. Lond. 159 (2002) 417-424.
[2] D.C. Cooper, M.K. Lee, & 5 others, J. Geol. Soc. Lond. 145 (1988) 523-540.

Causes of porosity heterogeneity of quartz arenites: Evidence from $\delta^{18}O$ by SIMS analysis of quartz cement in Cambrian sandstones, Baltic Basin

Nicolaas Molenaar[1] & Jolanta Cyziene[2]

[1]Department of Geology and Mineralogy, Vilnius University, K.M. Čiurlionio 21/27, LT-03101 Vilnius, Lithuania
[2]Geological Survey of Lithuania, S.Konarskio 35, LT-03123 Vilnius, Lithuania

Scientific Report 2007

Porosity is one of the most important properties of sandstones both as hydrocarbon reservoirs and as groundwater aquifers. The present day porosity is a function of primary porosity upon deposition and of postdepositional diagenetic processes such as compaction and cementation. These processes are largely a function of the detrital composition of the sandstones, and the latter influences the general mineralogy of the cement. Quartz-rich sandstones, the most common type of sandstone, dominantly have quartz cement, occurring as syntaxial overgrowths on detrital quartz grains. Porosity therefore is commonly inversely related to the amount of quartz cement. Understanding the mechanisms and controls of quartz cementation is therefore crucial for predicting reservoir quality and constructing reservoir models.

Decades of measurements in the oil industry have demonstrated that sandstone bodies have a rather large variation in porosity and degree of quartz cementation. In outcrops this tends to cause differential weathering and therefore is often clearly visible. This heterogeneity is more a rule than an exception. To improving recovery of hydrocarbons, good petrophysical models are essential and thus also to understand and thereby possible to extrapolate and predict the porosity heterogeneity. Inversely, the heterogeneity may comprise clues to understand quartz cementation.

Despite a lot of research on the timing of quartz cementation and the sources of the silica, not much consensus has been reached and neither the heterogeneous nature of quartz cementation has been solved. For instance the emplacement of oil has been mentioned as cause of the heterogeneity. If true, this would have tremendous consequences for the occurrence of reservoirs and the timing and pathways of oil migration would be essential for exploration. The argument for this has not been very convincing, including the paucity in numerical data to support it. Some studies used O isotopes of quartz cement and explain observed vertical variations in terms of changing temperatures (increasing T with depth in the reservoir) during precipitation or changes in porewater composition due to the slow filling of the reservoir with oil and/or gas.

However, most sandstones show a rather wide variation in properties even at similar conditions. Just because of this natural depositional variability, and the possibility that cementation did proceed at different rates as depending on the silica supply by pressure solution in the adjacent shales, only a sufficient number of data can lead to robust conclusions about changes in temperature or pore water chemistry in the system. Part of the literature suggests that oil emplacement hinders or even inhibits quartz cementation and therefore the filling of the reservoir would lead to different temperatures of the quartz cement.

The subsurface of Lithuania offers a unique opportunity to deal with this question in a fundamental way. Cambrian quartzarenites contain a number of small but economic oilfields at a depth of about 1600 to 2100 metres. In order to check the effect of oil emplacement, the present study focuses on an oilfield in Cambrian quartzarenites in the Baltic Basin (quartz-cemented, very-fine grained sandstones in sheet-like sandstone bodies, and with variable content of intercalated silty shales) with about 18 boreholes available for research. The studied field is a brachyanticline (a domal structural trap). The SIMS technique has been used to acquire a sufficient large database on $\delta^{18}O$ of quartz cement in the reservoir sandstones. The $\delta^{18}O$ data of quartz cement will be combined with a 3D lithological model, pore fluid compositional data, and petrophysical-sedimentological properties. Analyzed samples are from the main sandstone reservoir bodies throughout the oilfield at various distances above and below

the oil-water contact (OWC). An extensive database of petrophysical properties and sedimentological properties comprising grain-size distributions has been collected. The same samples used for SIMS $\delta^{18}O$ measurements have been studied by SEM-CL for quantification of the content of quartz cement. A lithological model based upon correlation of natural gamma logs and core studies of the field is under preparation. Later this year, the various databases will be combined with the lithological model giving a 3D distribution pattern of properties in the main sandstone bodies as a function of the distance to the OWC and the position in the oilfield. The internal architecture of the sandstone bodies can be characterized by thickness and shale content and interconnectivity.

The use of stable oxygen isotope compositional data is very common in sedimentary geology in particular for diagenetic studies**.** The $\delta^{18}O$ values of authigenic quartz cement is a function of the temperature (fractionation being T depend) and the isotopic composition of the pore water during quartz precipitation, both parameters basically being unknown. In this study, the $\delta^{18}O$ values will initially only be used for comparison of the quartz cement within the oilfield, i.e., the isotopic composition of the quartz cement within the oil zone and within the water leg of the oilfield.

The initial SIMS results (see figure with a plot of $\delta^{18}O$ values of quartz cement, N=237, against the distance to the OWC) show that $\delta^{18}O$ is variable but does not differ in the sandstones below and above the OWC, and no specific trend in $\delta^{18}O$ values with depth is present. There is thus no effect from the presence of oil on quartz cementation. This implicitly also confirms the fact that the silica for quartz cementation is derived from local sources.

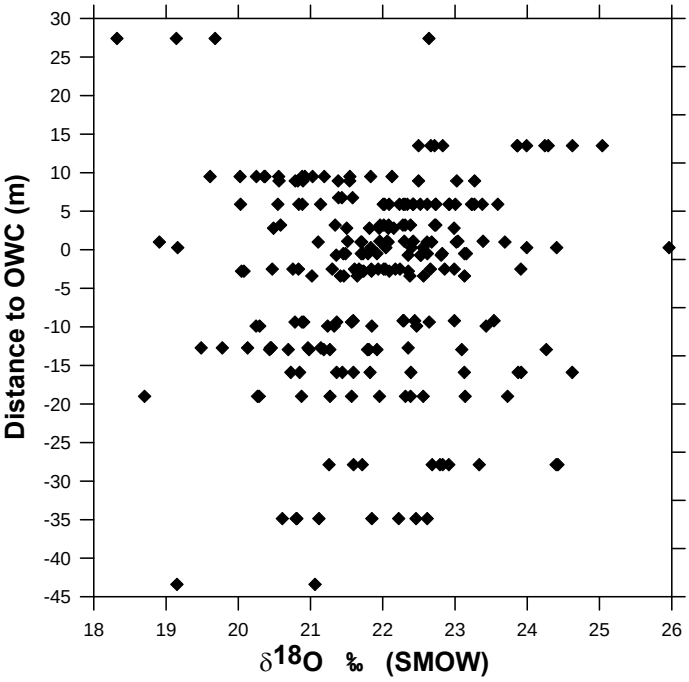

Modelling of the maturation of organic matter and the burial history showed that quartz cementation took place largely in the oil window and filling of the reservoir was largely contemporaneous with quartz cementation. Since the $\delta^{18}O$ data of quartz cement does not show any trend with respect to the distance to the OWC, the conclusion is that oil emplacement had no effect on quartz precipitation and other explanations have to be found to explain the porosity heterogeneity.

Striking is the rather large range of $\delta^{18}O$ cement compositions despite of the constant mineralogical composition of the sandstones and the limited variation in grain-size distribution. The only parameter changing laterally and vertically within the sandstone bodies and the reservoir as a whole is the architecture of the lithology (the thickness of sandstone beds and the amount and thickness of shale intercalations). Within a specific sandstone body, with similar chemical and physical general conditions in terms of pore water and temperature, the measured range in $\delta^{18}O$ can only be explained in terms of slight differences in the onset and temperature interval during development of the quartz cement as related to differences in rate of local supply of silica. Later in the study the architecture will be characterized and correlated to the variation in cement $\delta^{18}O$ values to find more numerical prove of the former conclusion.

Volatiles in magmas quantified by Ion-probe analysis of silicate inclusions

N. Oskarsson[1]

[1]Institute of Earth Sciences, University of Iceland, 101 Reykjavik, Iceland

Outline of the project

The actual volatile content of magma is of basic importance in a) modelling magmatic equilibrium at different depths and b) estimating the release of volcanic gases to the atmosphere. Quantification of pre-eruptive volatiles in magma is, however, at early stages. Present understanding of their role in magmatic evolution and eruption mechanism is derived from a limited number of solubility experiments and analysis of volcanic gases. These constraints apply to extreme scenarios; saturation with respect to volatiles and irreversible degassing of species with different solubility in magma. It is inferred from quantification of volatiles in silicate inclusions, published so far, that magmas are rarely saturated with respect to all volatiles and that composition of volcanic gases is rarely representative for the pre-eruptive volatile content. The present project aims at quantifying volatiles in magmas from the Icelandic rift system. Three short Ion-Probe sessions during 2005-2007 were aimed at volatile inclusions from early equilibrium minerals (olivine. clinopyroxene and plagioclase) in evolved rocks (rhyolite to qz-tholeiitc), normal olivine tholeiites (MORB) and primitive mantle derived basalts (picrite). It has to be emphasized that the Ion-Probe analyses of hydrogen, carbon, fluorine and chlorine are a small but essential part of this project. The main workload involves the characterization of naturally quenced equilibrium-minerals (rapidly cooled volcanic ash and pillow-rims) and electron microprobe analysis of representative silicate inclusion populations. Correlation of electron microprobe analysis and Ion-Probe analysis is based on analysis of titanium by both methods.

Release of volcanic gases to the Atmosphere.

Only generalized tentative results, unpublished so far, can be reported. It is already confirmed that magmas of the Icelandic rift system comprise three distinct groups with respect to total volatile content. These groups are rhyolites (3-5 Wt%), evolved basalts (0.3-0.6 Wt%), and the olivine tholeiites (0.05-0.2 Wt%), that are the principal building material of the oceanic plates. This division was clearly expected from general geochemical studies but the quantification of volatiles within each group opens a new dimension in estimating the volcanic pollution of the atmosphere. It is confirmed that in large explosive (Plinian) eruptions that have occurred in Iceland, gas plumes of tens of cubic kilometres have formed. In our times, such eruptions would create an alarming situation for air traffic across the N-Atlantic.

Petrological Modelling

The very low water content of the most primitive basalts indicate that petrological modelling based on dry silicate melts closely resembles natural conditions during early fractionation. During prolonged fractionation, however, the actual water content has ever increasing effects on liquidus temperatures and mineral stability. An example of the significance of Ion-Probe analysis in petrological modelling appears in the first published contribution from this project [1]. Dissolved water is the most important volatile in silica saturated magmas due to its effect upon equilibrium temperatures (liquidus) at different pressure (depth). Ion-Probe analyses of hydrogen in glass inclusions in olivine, were used to calculate the water content of the basaltic andesite magma that erupted from Mount Hekla, Iceland, in year 2000. It turns out that that the (unexpectedly) high water content favours multisaturation of minerals that are, indeed, observed as micro-phenocrysts in the erupted basalt andesite. This convincing result permitted a realistic depth estimate for magma-segregation prior to eruption. I turns out that this depth estimate conforms well with the results from ground deformation studies around the volcano.

References

[1] A. Hoskuldsson et al., Bull. Volcanol. 70 (2007) 169-182

Investigating volatile saturation pressures and degassing in the plumbing system of the 1783 AD Laki fissure eruption

E. Passmore[1], J. Maclennan[2] & J.G. Fitton[1]

[1]School of GeoSciences, University of Edinburgh, Edinburgh EH9 3JW, UK
[2]Department of Earth Sciences, University of Cambridge, Cambridge CB2 3EQ, UK

Justification: Understanding the causes and consequences of large basaltic eruptions

Volatiles are elements or compounds that form gases at relatively low temperatures and pressures, and it is the rapid exsolution of volatiles at low pressure that is the driving force behind volcanic eruptions. Millions of tonnes of volatiles are released into the atmosphere annually by volcanic activity, with basaltic volcanism accounting for 10-15% of the total volcanic gas budget [1]. The importance of volatiles in magma is twofold: firstly, volatiles act to modify the physical properties of magma, such as viscosity, density and temperature, and play a vital role in its ascent and eruption; secondly, volcanic volatiles contribute to the global gas budget, and large eruptions can have significant short and long term impacts on climate. Water and CO_2 are by far the most abundant gas species produced at erupting volcanoes, and, along with Cl and F, act as greenhouse gases in the upper atmosphere. Estimating gas fluxes for eruptions that have occurred in the geological past is possible by measuring the concentrations of volatile elements trapped in melt inclusions hosted within minerals in the erupted lava. Olivine is the first mineral to form in basaltic lavas at upper mantle temperatures and pressures, and will therefore host melt inclusions with volatile concentrations most similar to those of the early, undegassed, magma reservoir.

Iceland has been the site of the two largest basaltic eruptions to have occurred in human history. The most recent was the 1783 A.D. Laki fissure eruption in southeast Iceland, which produced 15 km^3 of basalt and tephra over 8 months and is estimated to have released in total 122 Mt of SO_2 (producing 250 Mt of H_2SO_4 aerosols), 15 Mt of HF and 7 Mt of HCl, which were lofted into the troposphere by 0.8 – 1.4 km high fire-fountains [2]. Reliable contemporary accounts from the Laki eruption document the effects of the notorious Cl and F rich 'dry haze' that lingered over the island during and after the eruption, killing much of Iceland's livestock, and causing famine and disease that resulted in the death of 25% of the island's population. Recent studies of Laki have focussed on the volcanology of the eruption and on petrological estimates of the total flux of volcanic gases to the atmosphere [2]. Better constraints on these numbers using direct measurements from melt inclusions gives a better estimate of the total flux of volcanic gases to the atmosphere during the eruption. Understanding the evolution of the volatile content of magma before the eruption is key to understanding the driving processes behind the eruption. It has been suggested that the Laki magma must have exsolved 50-75% of its original volatile content to drive fire-fountaining in the early stages of the eruption [3], but the extent of pre-eruptive degassing of the magma reservoir has not yet been investigated. This study aims to address this problem by comparing the volatile contents of melt inclusions to the composition of the olivine crystals in which they are hosted, to show the relative timing of degassing in comparison to crystallisation. Saturation pressures at the time of melt entrapment were calculated using measured H_2O and CO_2 concentrations, giving pressure and depth estimates for melt inclusion formation. Both naturally quenched (NQ) inclusions and re-homogenised (CC or CH depending on the gas-mix at time of heating) inclusions were analysed for this study.

Results and interpretations

VolatileCalc 1.1 [4] was used to calculate the saturation pressure for each melt inclusion based on its measured CO_2 and H_2O concentrations. Input parameters were set at 48 wt% SiO_2 (average of the melt inclusions measured by electron probe), and T =1200°C. Results from this study show a poor correlation between CO_2 and H_2O (R^2=0.0135). Melt inclusion CO_2 concentrations vary by a factor of ten (~100–1000 ppm CO_2), and H_2O concentrations by a factor of two (~0.1–0.2 wt%). The saturation pressures calculated here using VolatileCalc are less than half those calculated using clinopyroxene-liquid equilbria equations for major elements [5]. The re-homogenisation process did not affect the melt inclusion volatile contents as NQ inclusions display the same range in H_2O and CO_2 concentrations as CH and CC inclusions. The water contents of the melt inclusions have probably been reset by low pressure diffusive exchange between the inclusions and the surrounding melt through the

olivines: H diffuses particularly rapidly in olivine. The melt inclusions are therefore recording low pressure degassing, possibly in the sub-volcanic conduit, rather than the saturation pressures at melt entrapment in the deep magma chamber. Laki matrix glass (Fig. 1.) is almost completely degassed, and has H_2O and CO_2 concentrations lower than any of the melt inclusions measured in this study.

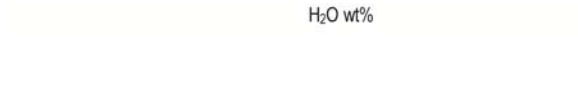

Fig. 1. Melt inclusion saturation pressures calculated using VolatileCalc 1.1 for Laki melt inclusions. Grey lines are isobars, with pressure in bars. Grey filled triangles are NQ inclusions, black filled squares are CH inclusions, and open circles are CC inclusions. The green filled diamond is Laki matrix glass from [6]. Red filled squares are melt inclusions from [7] measured by FTIR, giving water contents approximately twice those measured in this study, yet comparable CO_2 concentrations. Error bar at the top left shows absolute precision (1σ) based on repeats on standards.

The forsterite content of olivine is controlled by the temperature and extent of crystallisation of melt. As the temperature drops, and crystallisation proceeds, the composition of the crystallising olivine becomes less forsteritic. Modelling the concentrations of volatiles against the concentration of forsterite in the host olivine shows how volatiles behave during olivine crystallisation.

Fig. 2. C/La ratio versus Fo mol% in host olivine for Laki melt inclusions. Grey filled triangles are NQ inclusions, black filled squares are CH inclusions, and open circles are CC inclusions. The error bar on both diagrams shows absolute precision (1σ) based on repeats on standards.

Fig. 3. Positive correlation between F and La in Laki melt inclusions. Triangles are NQ inclusions, squares are CH homogenised inclusions and circles are CC homogenised inclusions. Each analysis is shaded according to the Fo content of the host olivine: white = Fo_{82-87}; blue = Fo_{75-82}; black = Fo_{68-75}.

Fluorine correlates with La in the melt inclusions, and increases with decreasing forsterite content of the host olivine (Fig. 2.). Therefore, fluorine behaves as an incompatible trace element, becoming enriched in the residual melt as crystallisation proceeds and was therefore not degassing before or during olivine growth. This fits well with the fact that F is very soluble, and will remain dissolved in the melt until at very low pressures. Conversely, C does not correlate well with La (C versus La R^2 = 0.002), and the C/La ratio shows a large range in the most forsteritic olivines, which steadily decreases as forsterite in the host olivine decreases. The average C/La ratio also decreases as Fo decreases, showing that the destruction in the range is not simply due to mixing, but to concurrent degassing of C from the melt as mixing occurred, and as olivine crystallisation progresses. This captures pre-eruptive degassing of carbon. Carbon is the least soluble of all the volatile phases, and rapidly degasses from the magma as pressure decreases. The observation of pre-eruptive degassing of C is important not only for volatile budgets but may also provide a new tool in forecasting volcanic eruptions in Iceland.

References

[1] M.M. Halmer, H.-U. Schmincke & H.-F. Graf, J. Volcanol. Geotherm Res. 115 (2002) 511-528.
[2] T. Thordarson, S. Self, N. Óskarsson, & T. Hulsebosch, Bull. Volcanol. 58 (1996) 205-225.
[3] L. Wilson & J.W. Head, J. Geophys. Res, 86 (1981) 2971-3001.
[4] S. Newman & J.B. Lowenstern, Comput. Geosci. 28 (2002) 597-604.
[5] K. Putirka, M. Johnson, R. Kinzler, J. Longhi & D. Walker, Contrib. Mineral. Petrol. 123 (1996) 92-108.
[6] N. Óskarsson, K. Grönvold & G. Larsen, Mál og Menning, Reykjavik (1984) 67-80.
[7] N. Metrich, H. Sigurdsson, P.S. Meyer & J.D. Devine, Contrib. Mineral. Petrol. 107 (1991) 435-447.

The melt inclusion record of magma degassing at Etna, Sicily

D.M. Pyle[1], S.J.Collins[2]& J. Maclennan[2]

[1] Department of Earth Sciences, University of Oxford, Oxford, OX1 3PR, UK
[2] Department of Earth Sciences, University of Cambridge, Cambridge, CB2 3EQ, UK

Introduction

Mt Etna, Sicily, is a persistently active volcano responsible for 5-10% of global annual volcanic emissions of CO_2 and SO_2[1]. Activity on Etna has changed dramatically since 2001[2]. From 2001 – 2003, eruptions were vigorous and volatile-rich marking the arrival of a new batch of magma[2]. In contrast, eruptions in 2004 and July 2006 started with the slow effusion of gas-poor magma[1].

In recent years, understanding of the gas geochemical behaviour of Etna has been transformed, following developments in gas chemical sampling[1]. However, there is continuing disagreement over the extent to which gases at Etna either accumulates at depth before eruption; and or loses gas at shallow levels. We have therefore used olivine hosted melt inclusions to better understand magma storage and degassing at Europe's largest and most active volcano; Etna, Sicily. One feature of many melt inclusion volatile data sets is that it is very rare that samples follow simple patterns of either closed-system equilibrium or open-system degassing. Indeed, in many cases it is abundantly clear that there must be an alternative explanation. Here we present evidence that shows how melt which was stored in the edifice after the 2003 eruptions was dehydrated by flushing and re-equilibration with CO_2-rich gases prior to entrapment as melt inclusions, and eruption in 2004, 2006 and 2007.

Each melt inclusion was analysed for major elements by electron microprobe on a CAMECA SX100 at the University of Cambridge and for volatiles (H, CO_2, F, Cl, S) and trace elements (Li, Zr, La) by SIMS, on a Cameca IMS-4f ion microprobe at the University of Edinburgh. Subsequently a selection were analysed for trace metals (Cu, Zn, Pb) by LA-ICP-MS at the University of Cambridge.

Results

Major element compositions of melt inclusions and matrix glasses from samples erupted between 2001-2007 form a continuous trend from more primitive glasses, erupted in 2001, through to the more evolved 2001 glasses and to the most evolved products of the 2006 eruption. The involatile and incompatible trace elements are strongly correlated and along with the major elements show that the samples form a coherent rock suite linked by fractional crystallisation, (Fig. 1). H_2O concentrations of melt inclusions from samples post 2003 are all <2wt%, similar to the most degassed samples measured in the 2001-2002 products[2,3]. Dissolved H_2O contents of matrix glasses are low, <0.14wt%, as expected. Dissolved CO_2 contents range from <60-4000ppm in the melt inclusions and <60-250ppm in matrix glasses. In contrast to the published data from the 2001-2002 samples[2,3] however, CO_2 concentrations remain high in those melt inclusions which have low water concentrations (Fig. 2). The semi-volatile trace elements such as Li show significant variability. This variability can not be completely explained by the partitioning properties of the element, since their changes in concentration do not correlate simply with any of the in volatile incompatible elements (Fig. 1), so we suggest that their distribution reflects a control by the volatility.

Discussion

By integrating our new melt inclusion data sets with prior geochemical and geophysical constraints on gas fluxing, we propose that the melt inclusions sampled in the erupted products since 2003 record the effects of a CO_2-rich gas equilibrating with a stored melt in the shallow edifice. In contrast to the 2001-2002 eruption products, which show clear evidence for syn-eruption degassing and melt inclusion entrapment over a range of depths[2,3] (Fig. 2), the 2004-2007 samples show no clear trends of dissolved CO_2 vs. H_2O. We propose that the dissolved volatile pattern of the post-2003 samples reflect magma storage, and gas exchange, of magmas residual from the 2001-2002 activity, at shallow depths for up to 4 years. This hypothesis is consistent with the major and trace element trends (Fig. 1) and the more evolved nature of the later eruptions compared to the 2001-2002 samples.

We propose that during the extended period of storage, the residual magmas equilibrated with the

passing flux of CO_2 rich gas, which was derived from degassing at depth, leading to progressive isobaric dehydration of the samples. Prior to eruption, melt inclusion samples were trapped in growing olivine crystals, and the degassing/re-equilibration record was thus preserved.

Further evidence for gas fluxing can be observed when the distribution of the semi volatile elements is studied. Semi volatile elements such as Cu and Li show variability which is not consistent with fractional crystallisation trends instead it can be explained by both enrichment by a gas flux and degassing in the shallow reservoir by Cl complexing. Shallow level degassing is also evident by the enrichment of these elements in the aerosol particles of the Etna plume and the depletion of Cu in matrix glasses.

Conclusions

The ion microprobe has enabled us to track multiple volcanic processes in melt inclusions. One outcome of our work is discovering that volatile data sets do not simply track just open or closed system degassing representative of a melt which has ascended rapidly from depth and erupted but rather shows scatter representative of multiple processes. By comparing volatile data sets to trace elements within the same inclusions however we have been able to separate out the affects of storage, degassing and gas fluxing on the concentrations of elements analysed for the recent eruptions of Mt Etna.

Figure 1: Trace element systematics of the post 2003 melt inclusions: The analysis of trace elements has tracked storage and crystallisation, degassing and enrichment of semi volatile elements in the post 2003 melt inclusions. Calculated fractional crystallisation trends have been plotted assuming D=0 for La, in grey and Cu in black. Semi volatile trace elements including Cu show greater enrichment than is possible by fractional crystallisation, as well as depletion by degassing.

Figure 2: Magmatic volatiles: Previous analysis of MI'S from the 2001-2003 eruption, show the typical degassing path expected for rapidly ascended melts. 2004-2007 melt inclusions deviate from this path due to an isobaric gas fluxing event which enriched the shallow melt in CO_2. Grey diamonds 2001-2002 data from Ref. 3. white diamonds 2001-2002 data from Ref. 2. 2004-2007 data from this study. Isobars, isopleths and degassing paths were calculated using Volatile Calc Ref. 5.

References

[1] Aiuppa, A., et al. J. Geophys. Res. - Solid Earth, **111** (2006)
[2] Metrich, N., Allard, P., Spilliaert, N., Andronico & D., Burton, M. Earth Planet. Sci. Lett. **228** (2004) 1-17
[3] Spilliaert, N., Allard, P., Metrich, N. & Sobolev, A.V. Journal of geophysical research-solid earth, **111,** (2006)
[4] Aiuppa, A., Dongarra, G. & Valenza, M. **139** (2003) A.G.U Washington, DC, 2003
[5] Newman, S., and Lowenstern, J.B. Comput. Geosci. **28**, (2002) 597-604

Ocean acidification during the Palaeogene hyperthermals

A.J. Ridgwell[1] & D.N. Schmidt[2]

[1]School of Geographical Sciences, University of Bristol, University Road, Bristol BS8 1SS
[2]Department of Earth Sciences, University of Bristol, Bristol, BS8 1RJ, UK

Variation of boron isotopes and trace elements in foraminifers: biomineralisation or ecology?

D. N. Schmidt[1]

[1]Department of Earth Science, University of Bristol, Bristol Uk; d.schmidt@bristol.ac.uk

Rationale

Changes in CO_2 concentrations in the earth's atmosphere are believed to be one of the largest challenges for our future climate, leading to an increased greenhouse effect and global warming but also to an increase CO_2 absorption of the ocean and hence ocean acidification. There are two established ways to asses past CO_2, using organic biomarkers (alkenones) and boron isotopes in the carbonate of planktic foraminifers [5,7]. The applicability of the boron isotope proxy and the precision of the CO_2 assessments depends on our understanding of the incorporation of boron into foraminiferal carbonate. Physiological processes, such as photosynthesis, respiration and calcification, modify the micro-environmental *p*H of the planktic foraminifera and thus exert an important influence on the $\delta^{11}B$ of their shells.

I analysed specimens of *Globigerinoides ruber* and *G. sacculifer* from sediment traps off Cape Blanc in the subtropical East Atlantic at 719 meters. Figure 1 shows the temperature and pH profiles of three WOCE stations in the vicinity of the sediment trap. I analysed samples from the same month in 1997, 2000 and 2003 to test for interannual reproducibility and from July, October and March (2003-2004) to rest for intra-annual variability. Based on the variability in the measured data (Fig. 2), the $\delta^{11}B$ data should all be within the analytical error.

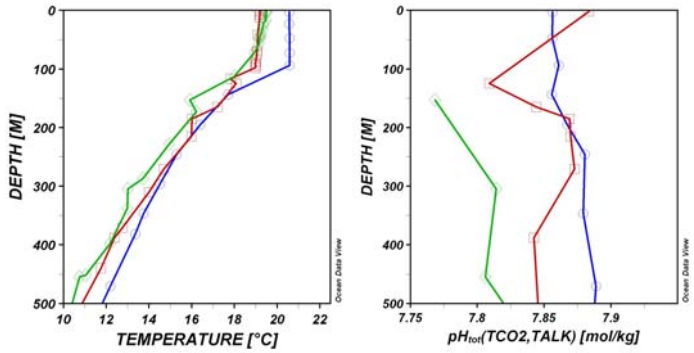

Figure 1: Temperature and pH profile for the top 500 meters of three GLODAB stations in the vicinity of the Cap Blanc sediment trap

Next to Boron isotopes, I analysed Mg/Ca, Ba/Ca, Li/Ca, B/Ca and Sr/Ca ratios. The measured isotopes and elements in the foraminiferal test are correlated to measured environmental data during time of carbonate precipitation to test their applicability as environmental proxies.

Results

G. ruber shows a high variability in the pH reconstructions. This is mainly due to the fact that the test is very thin, and hence the small number of reliable measurements result in large errors. In contrast, *G. sacculifer* allows much better reconstructions of pH. Repeat measurements of two specimens from the same two week interval show that the reproducibly of the measurement is much better than the error indicates, i.e. the difference is around 0.1 pH units. Most reconstructed pH values, though, are slightly too high as indicated by the fact that they fall outside the two lines on Figure 2 indicating surface and 200 m pH values. There are two possible reasons for this deviation. Firstly, the organism is altering the pH of the seawater due to symbiont activity. The symbionts assimilate CO_2 during photosynthesis therefore making the seawater more alkaline. Microelectrode measurements showed a resulting change of the ambient pH from 8.23 to 8.62 [3]. The empirically determined deviation i.e. the specific vital effect though the effect is assumed to be much smaller ie 0.2 pH units [2, 6], as expressed in the calibration equation $pH = pK_B - \log(-(\delta^{11}B_{seawater} - \delta^{11}B_{sample} - a)/(\delta^{11}B_{seawater} - \alpha*(\delta^{11}B_{sample} + a) - \varepsilon)$ with a being the species specific offset from equilibrium and ε the difference between sea water and carbonate.

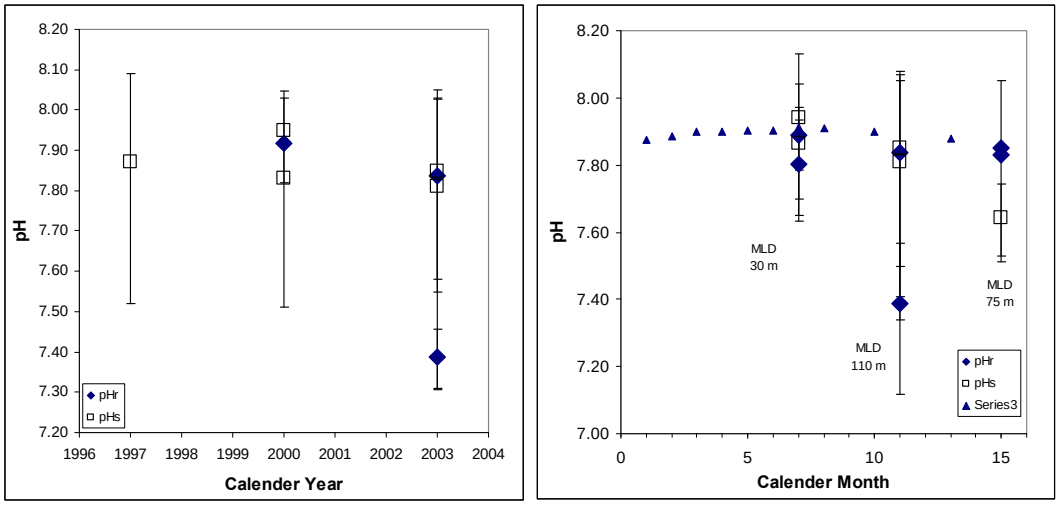

Figure 2: Measured pH during the year 1997, 2000 and 2003 and the seasonal variation during 2003/2004 for ESTOC (European time series station north of Cap Blanc) in comparison to measured pH of *G. sacculifer* (open sqares) and *G. ruber* (filled diamonds). Error bars represent standard errors of the mean.

The culture based vital effect, though, is smaller than the one using microelectrodes. I suggest that the incomplete compensation of the vital effect in the Hönisch et al [2] and Sanyal et al [6,7] papers compared to the microelectrode measurements lead to the too high pH values. If true, this would suggest that the foraminiferal cultures are under stress and do not represent natural conditions.

Secondly, the calculation of the pH depends on the fractionation between sea water and carbonate ε, the boron isotope equilibrium constant. Recently, ε has been determined theoretically in contrast to previous empirical calculations changing the value from 19.4 [1] to 27 [4]. Using the empirical values of [4] computes to species specific vital effects of 2.5 for *G. ruber* and 3.5 for *G. sacculifer*. Unfortunately, no microelectrode measurements are available for these species to test if our empirical vital effects fit our understanding of biology, though *G. sacculifer* is the nearest relative to *O. universa* which has been used for the above mentioned analysis. The similarity of the values, 0.4 pH units using microelectrodes versus our 0.36 pH empirical data provides confidence in the fact that for surface dwelling foraminifers symbiont density and activity is the only important vital effect offsetting the $\delta^{11}B$ in the foraminiferal from theoretical calcite values.

The large intro test differences in *G. truncatulinoides* (see last report), therefore, are likely to be related to the formation of the large amount gametogenic calcite enveloping the foraminiferal test. This layers is not just different in boron isotopes but also trace elements and therefore indicates a different calcification behaviour

References

[1] Hemming, N. G. and Hanson, G. N. (1992) Geochmi. Cosmochim. Acat **56**, 537-543
[2] Hönisch, B., Bijma, J., Russell, A. D., Spero, H. J., Palmer, M. R., Zeebe, R. E., and Eisenhauer, A. (2003) Marine Micropaleontology **49**, 87-96.
[3] Jørgensen, B. B., Erez, J., Revsbach, N. P., and Cohen, Y. (1985) Limnology and Oceanography **30**, 1253-1267
[4] Klochko, K., Kaufman, A. J., Yao, W., Byrne, R. H., and Tossell, J. A. (2006) Earth Panet. Sci. Lett. **248**, 276-285.
[5] Pearson, P. N. and Palmer, M. R. (2000) Nature **406**, 695 - 699.
[6] Sanyal, A., Bijma, J., Spero, H. J., and Lea, D. (2001) Paleoceanography **16**, 515-519
[7] Sanyal, A., Hemming, N. G., Hanson, G. N., and Broecker, W. (1995) Nature **373**, 234-236**.**

Open system processes recorded in plagioclase phenocrysts from Nevado de Toluca, Mexico

V.C. Smith[1], J. Blundy[1] & J.L. Arce[2]

[1]Department of Earth Sciences, University of Bristol, Wills Memorial Building, Bristol BS8 1RJ, UK
[2]Instituto de Geologia, UNAM Cd. Universitaria, Coyoacan, Mexico

Introduction

The aim of this study was to use the 10.5 ka Upper Toluca Pumice (UTP) eruption deposits to gain more of an understanding of the magmatic systems that feed dacitic volcanoes. We have used the invaluable record provided by the plagioclase crystals and their trapped melt inclusions (MI) to gain insight into the accumulation and eruption of a large volume of dacitic magma.

Summary of results

Whole-rocks, phenocrysts, matrix glass and MI have been analysed and have provided information on processes such as crystallisation, recharge, and eruption triggering. SIMS techniques were used to analyse melt inclusions, matrix glass (melt), and plagioclase phenocrysts.

The plagioclase-hosted melt inclusions display compositions that are similar to matrix glass, suggesting that they were connected to the melt during most of the crystallisation history, and only provide a partial record of the magma evolution. However, plagioclase crystallises over a wide range of magmatic compositions and conditions, continuously recording variations in composition of the melt during crystallisation, thus profiles provide a more complete record of magmatic processes.

Considerable major and trace element variation is observed across the plagioclase phenocrysts (Fig. 1). The observed and often simultaneous fluctuations in Mg, Sr and Ba in the plagioclase and melt compositions (determined using partition coefficients) cannot be generated in closed-magmatic system via the crystallisation of typical phases. These trends imply that the magmatic system was open and received periodic influxes of less evolved magma. The rims of the plagioclase phenocrysts are generally calcic and enriched in Mg and Ti indicating a recharge event occurred prior to the eruption. The lack of significant diffusion of these elements from the rim indicates the more mafic magma entered the chamber within months of the eruption, and suggests it triggered the eruption. The presence of some more mafic whole-rock and matrix glass analyses, and the wide range in temperatures and oxygen fugacities (determined from Fe-Ti oxides), also indicate the influx of hot, less evolved melt into the chamber occurred immediately prior to the eruption.

Entrapment pressures calculated from the volatile elements in the MI indicate magmatic system was located ~4-6 km below the surface. Even though the entrapment pressures do not vary much, considerable variation is observed in XH_2O. Most analyses have an XH_2O of ~0.8, but about 18 of the 80 analyses have much lower values (~0.5). These variations suggest that a more CO_2-rich gas was fluxed through the system.

The unusually large volume of (8 km^3) dacitic melt under Nevado de Toluca prior to the Upper Toluca Pumice eruption was constructed through the amalgamation of numerous magma batches in the upper crust. Eventually a hot, gas-rich, more mafic batch intersected the voluminous accumulation of magma and triggered the eruption. Variation in composition, temperature and pressure are observed throughout the eruption sequence, which suggests that the magmas mixed thoroughly within the system and/or the eruption violently evacuated magma from all levels in the system almost simultaneously.

Future work

All analyses have been completed and these data are currently being interpreted and written up for publication.

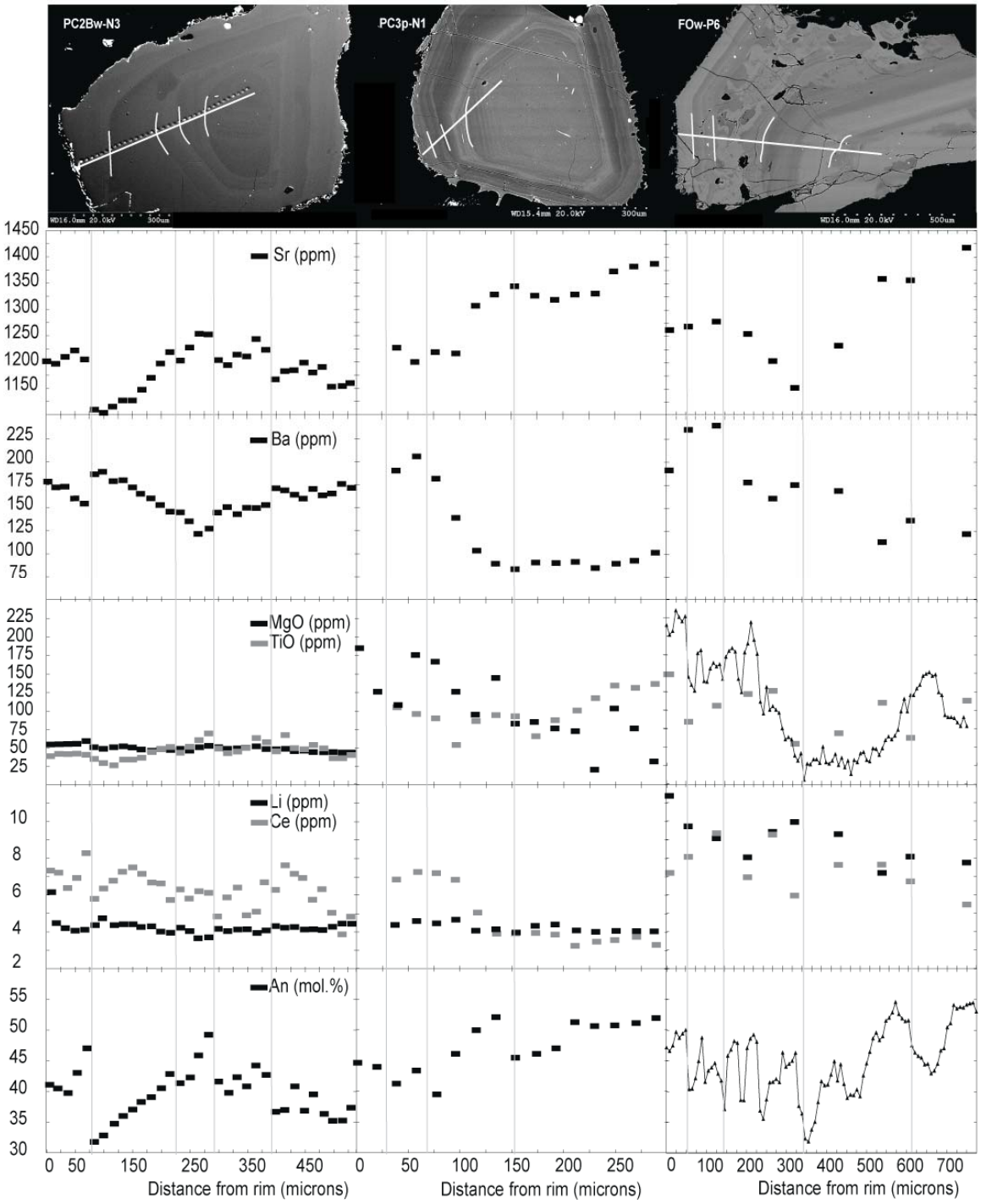

Fig. 1: BSE images, and major and trace element profiles across plagioclase in the Upper Toluca Pumice deposits. Three groups are distinguished based on texture: (1) crystals with rounded sodic cores; (2) crystals with calcic cores; and (3) crystals a prominent zone displaying sieve textures. Noticeable, major resorbtion horizons are marked with dashed lines on BSE images, and as vertical lines across the graphs. Zones within the groups cannot easily be correlated, with each group displaying a somewhat different and complex history, suggesting the magmatic system was compositionally heterogeneous or that the plagioclase in each group mostly crystallised within distinct batches of magma. Most crystals have calcic, compositionally similar rims, implying that the batches had amalgamated and/or the system was actively convecting during the last stages of crystallisation.

Melt inclusions in a Baffin Island high-^{3}He/^{4}He picrite: source variability or crustal contamination

N.A. Starkey[1,2] & J. Maclennan[3]

[1] School of GeoSciences, University of Edinburgh, Edinburgh. EH9 3JW. UK
[2]Isotope Geosciences Unit, SUERC, East Kilbride. G75 0QF. UK
[3]Department of Earth Sciences, University of Cambridge, Downing Street, Cambridge. CB2 3EQ. UK

The work at the IMF carried out in May 2007 was intended as a one-day feasibility study prior to submission of a full proposal for IMF time which has now been secured and is due to take place in April 2008.

Justification

Lava flows erupted 60mya in Baffin Island, Canada represent the start-up phase of volcanism in the North Atlantic that continues today in Iceland. The reason for the sudden onset and huge volumes of lava erupted in such a short timescale in this region is the matter of debate. The fact that these lava flows contain the highest magmatic ^{3}He/^{4}He ratios measured on Earth [1] makes them a particularly interesting and potentially informative case study for mantle evolution. Several recent studies have shown an apparent link between high ^{3}He/^{4}He ratios and depleted mantle [2,3] which is inconsistent with prevailing orthodoxy that considers an uppermost depleted, degassed mantle and a lower undegassed 'primordial' mantle.

Recently, new data from a PhD project based at Edinburgh University show further high ^{3}He/^{4}He ratios from a new suite of samples from Baffin Island and from contemporaneous West Greenland lava flows. Interestingly, despite most high ^{3}He/^{4}He samples displaying MORB-like ^{143}Nd/^{144}Nd, a few samples have distinctly lower Nd isotope composition. Variations in whole-rock ^{143}Nd/^{144}Nd in high ^{3}He/^{4}He samples may reflect crustal contamination of the whole-rock or the presence of a population of olivine xenocrysts that do not belong in their transporting magma, having precipitated from an earlier magma batch. If these two factors can be ruled out then the variations in ^{143}Nd/^{144}Nd at high ^{3}He/^{4}He are more likely due to mantle source heterogeneities. Compositions of melts trapped within olivine crystal inclusions have the potential to record the small scale effects of crustal contamination and/or the presence of xenocrysts. Major elements in melt inclusions are not very sensitive to mantle source variation and measurement of ^{143}Nd/^{144}Nd on individual melt inclusions is beyond current capabilities. We can therefore use Rare Earth Element (REE) concentrations as a proxy for ^{143}Nd/^{144}Nd. In general, in terms of the wider PhD project, we seek to investigate whether high ^{3}He/^{4}He is associated with a wide range of mantle source compositions. However, in the May 2007 feasibility study we were simply testing one Baffin Island sample to analyse the range in melt inclusion REE and trace element compositions to assess whether a more detailed study was viable on the Baffin Island and West Greenland data sets.

Results

The concentrations of 19 elements including selected REE's, Mg, Si, K, Ca, Ti, Rb, Sr, Y, Zr, Nb and Ba were obtained on 20 melt inclusions in one high ^{3}He/^{4}He Baffin Island sample, PAD6 (Fig.1).

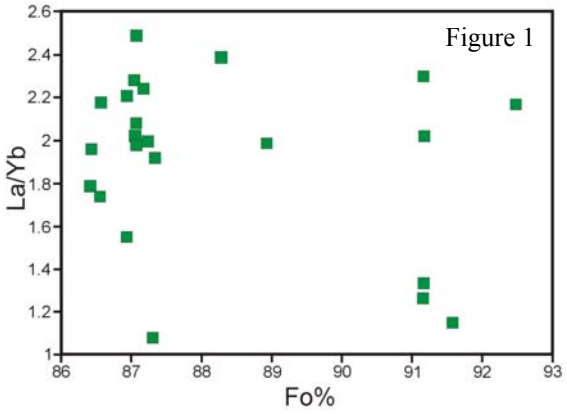

Figure 1. La/Yb vs. Fo% for melt inclusions analysed in PAD6 during the pilot study in May 2007. Range in La/Yb for high and low forsterite crystals is similar indicating no significant crustal contamination, which would be expected to have a bigger effect on those crystals (with lower forsterite contents) that grew later at lower temperature in the crust.

Melt inclusions were generally small (~25µm in diameter on average) and were measured in a range of olivine crystals with different shapes and different forsterite contents. Averaged REE profiles of melt inclusions in PAD6 are very similar to the whole-rock composition (Fig.2). Melt inclusions from low forsterite olivine crystals are relatively more enriched than the whole-rock and melt inclusions from high forsterite olivine crystals are relatively more depleted (Fig.2). One of the reasons we intend to measure melt inclusions from both high and low forsterite olivine crystals was to assess whether they had different trace element ratios. A difference in melt inclusion compositions may indicate either gradual crustal contamination of melts picked up by the crystallising olivines or that olivine crystals were growing from melts of varying composition due to source heterogeneity. The limited data collected in the feasibility study (only 6 melt inclusions were measured hosted by high forsterite olivine crystals) appear to indicate that there is not a large difference between compositions of melt inclusions hosted by high and low forsterite olivine crystals (Fig.1). However, many more inclusions were measured from low forsterite crystals and they show a larger spread in trace element ratios (Fig.1). In addition, it would appear that none of the melt inclusions measured are hosted in xenocrystic olivines since we would expect these melt inclusions to differ hugely and appear as outliers. More measurements will be needed to confirm the results of this study and these will be completed on not only this sample but 5 further samples from the same dataset in April 2008.

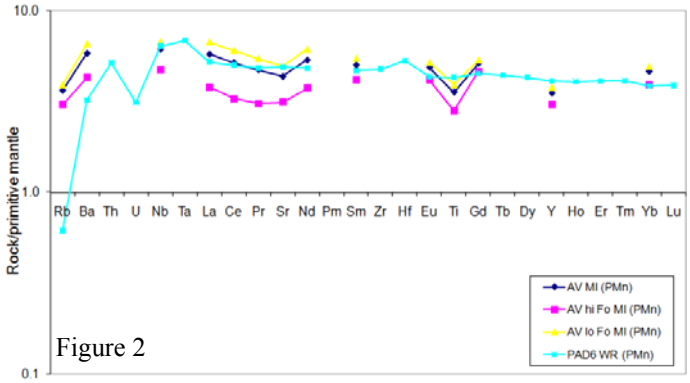

Figure 2. Primitive mantle normalised trace element variation diagram comparing average melt inclusion compositions of high and low forsterite olivines and average melt inclusion to the bulk rock of the same sample measured previously.

Interpretation

Due to the small number of measurements made during a one-day study we are unable to provide any firm conclusions on the data and therefore can only speculate concerning our interpretation of these data. Firstly, we expect to see a wider range in trace element ratios between melt inclusions from high and low forsterite olivine crystals since at the very least it would be expected that they sample a range of different melt compositions trapped by olivine growing during melt fractionation. This would mean that high forsterite olivines (those that grow first and from higher temperature melts) would trap less fractionated melts than melt inclusions hosted in low forsterite olivine (that grow later and trap more fractionated melts). The fact that this gradual fractionation is not observed in the limited data collected in May 2007 indicates that more data are required, especially from melt inclusions hosted by high forsterite olivine. It is hoped that a more extensive study on this sample and others from the dataset will provide the detail required to then assess if variations in melt inclusion trace element ratios and REE patterns are affected by crustal contamination and source heterogeneity in addition to the expected normal fractionation of melt during cooling. If the new data agree with the data of this feasibility study then it would suggest that the melt inclusions do not record small scale effects of crustal contamination and therefore that variations in $^{143}Nd/^{144}Nd$ measured in the whole-rock at high $^{3}He/^{4}He$ are instead due to source heterogeneity. This in turn suggests that high $^{3}He/^{4}He$ is not associated with a discrete mantle composition, in disagreement with earlier studies [1,3], and is instead capable of dominating mixtures irrespective of the initial heterogeneity of the upper mantle into which it is mixed. Such a conclusion would carry important implications for the evolution and composition of Earth's mantle.

References

[1] Stuart, F.M., Lass-Evans, S., Fitton, J.G., & Ellam, R.M. Nature, 424 (2003) 57-59.
[2] Ellam, R.M & Stuart, F.M. Earth and Planetary Science Letters, 228 (2004) 511-523.
[3] Class, C & Goldstein, S.L. Nature, 436 (2005) 1107-1112.

Probing the birth and growth of continents via isotopic records in titanite

C.D. Storey[1] and C.J. Hawkesworth[1]

[1] Department of Earth Science, University of Bristol,
Wills Memorial Building, Queen's Road, Bristol, BS8 1RJ

Introduction

Titanite is a common accessory mineral in intermediate to acid igneous rocks and metamorphic rocks. It generally contains 10-50ppm U and variable amounts of common Pb. It has a closure temperature for Pb of around 650-700^{o}C [1] and similar for O [2] and is, therefore, one of the more robust accessory phases for dating old rocks that may have suffered medium to high grade metamorphism. Titanite also contains up to several thousand ppm Nd and is therefore a potentially useful for mineral for crustal evolution studies since Nd isotopes, corrected for radiogenic ingrowth from Sm, can be used to determine the evolution of the continental crust and complementary depleted mantle. The advantage over whole rock studies is that titanite can be precisely dated and is robust with respect to elemental and isotopic exchange. The further advantage is that at these concentrations the isotopic ratio measurements can be made precisely on small volumes of material, opening up the possibility of in-situ measurement. This can be used in conjunction with in-situ zircon U/Pb-O-Hf studies that have already offered much promise for studies of the secular evolution of the continental crust (e.g. [3]). However, titanite also has the advantage that it contains appreciable Ca (27wt% CaO) and negligible K, thus opening up the possibility of measurements of radiogenic Ca isotopes, which are extremely sensitive to the presence of earlier formed evolved continental crust (e.g. [4]). Thus, the purpose of this study is to monitor the evolution of the very earliest formed continental crust on Earth via U/Pb, O, Nd and Ca isotopes within spatially controlled volumes of titanite.

Samples were selected from West Greenland and the Slave Province of northern Canada, together with reference materials, for in situ O isotope analysis on the Cameca ims-1270 multi collector ion microprobe at Edinburgh. Three potential standard titanite samples were analysed prior to the session by conventional laser fluorination isotope ratio mass spectrometry at University of Wisconsin, Madison, by John Valley. Of these, sample TIBOR (conventional analysis $\delta^{18}O = -0.3 \pm 0.2‰$ 2SD) gave the most reproducible results by ion microprobe across and within separate chips. In the samples discussed below all analyses have been normalised to TIBOR by sample-standard bracketing, using a linear drift function where appropriate. Standards and unknowns were also analysed for major and selected trace elements and the composition of TIBOR was found to most closely approximate those of the unknowns, reducing the potential risk of matrix effects. A sample from the Fish Canyon Tuff was analysed by ion microprobe during the session as some published data exist from titanite and zircon (zircon $\delta^{18}O = 5.61 \pm 0.04‰$, titanite $\delta^{18}O = 4.75‰$; [5]) and so a first order check of accuracy could be made.

Results

The Fish Canyon Tuff results yield a mean of $4.29 \pm 0.38‰$ (1SD), which is close to the published value and is considered to verify the results of the unknowns reported below. Repeat conventional O isotope analysis of this sample is being prepared currently.

Titanite $\delta^{18}O$ analyses can be corrected as a function of assumed equilibration within an igneous melt between zircon and titanite (average Δzrn-ttn $= 1.2 \pm 0.3‰$, whereas equilibrated zircon and titanite in the metamorphic or hydrothermal environment gives a larger fractionation of $2.1 \pm 0.4‰$). This allows comparison with mantle $\delta^{18}O$ in zircon ($5.3 \pm 0.3‰$; [6]) and, providing the assumption of equilibration with igneous zircon is rigorous, a first order assessment of the likelihood of the protolith magma to have assimilated pre-existing crust with either elevated $\delta^{18}O$ (c.f. modern-day low-temperature surficial processes) or low $\delta^{18}O$ (c.f. modern-day high-temperature subaqueous processes). Moreover, subsequent co-existing zircon analyses from these rocks could be measured in the most instructive samples to examine the veracity of these assumptions; this will proceed in May 2008.

Samples from West Greenland were selected from the collection of Stephen Moorbath of Oxford University. The samples come from the region to the south of the Isua Supracrustal belt where well-documented, weakly deformed tonalitic gneisses have reproducible zircon ages of c.3.8 Ga. Some of these samples have also been analysed for whole rock ^{142}Nd, and have a resolvable 5-10ppm anomaly [7] and many have been analysed for Pb isotopes in whole rock and feldspar separates, with ^{206}Pb/^{204}Pb ratios typically of 11-12, representing some of the most unradiogenic Pb ever measured on Earth [8]. Analyses are displayed in Fig 1 with 2SD error bars (typically 0.4-0.6‰). Sample SM/GR/98/2 (tonalite) has a mean of 3.55 $\pm$ 0.38‰ (1SD) and for this one sample zircon δ^{18}O data are available, measured by Tony Kemp on the Edinburgh Cameca 1270 (Tony Kemp, Pers.Comm.), giving a mean of 5.26‰. The fractionation factor is c.1.7‰ and since the analysed zircon is undoubtedly igneous and crystallised at c.3.8 Ga, the fractionation between zircon and titanite can not have been in equilibrium during metamorphism; either the this result represents igneous fractionation or else the titanite is not coeval with the zircon. The mean value for tonalite sample SM/GR/00/2 is 4.86 $\pm$ 0.42‰ (1SD), which would correspond with a zircon value of 5.06‰ given ideal igneous equilibrium fractionation. The final Greenland sample is from a discordant diorite sheet, sample SM/GR/00/13, which gave a mean of 4.32 $\pm$ 0.61‰ (1SD), corresponding with a zircon value of 5.53‰. All of these samples, corrected to zircon, are within error of the zircon mantle value. This result implies that no detectable presence of earlier sediments is present within the parental melts.

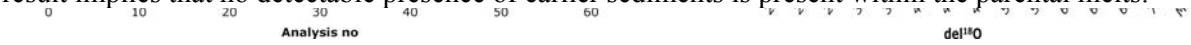

Fig 1. δ^{18}O data from West Greenland samples. a) Plotted with individual error bars (2SD) and 1SD mean error margins for individual samples. All data corrected assuming igneous equilibration between zircon and titanite (+1.2‰) and mantle zircon plotted for comparison with error margin. b) Plotted on a histogram with bins set at 0.4‰ widths for comparison between samples, not corrected for igneous fractionation.

Samples from the Acasta Gneiss of the Slave Province of northern Canada were selected from the collection of Tsuyoshi Iizuka of Tokyo Institute of Technology. Amongst the Acasta Gneiss are believed to be the oldest remnants of rock on Earth, with zircon dates as old as 4.03 Ga [9] and even older xenocrystic cores to 4.2 Ga [10]. Thus, these samples are excellent candidates in the search for Hadean titanite. All data are shown in Fig 2. Two tonalitic gneiss samples were analysed and give similar means of 3.93 $\pm$ 0.6‰ (1SD; sample AY199) and 4.08 $\pm$ 0.77‰ (1SD; sample AC023). Corrected to zircon these values are around 5.2‰, in excellent agreement with zircon mantle values. Hence, a similar conclusion can be derived from the Acasta Gneiss as from the West Greenland samples and, as such, no detectable earlier re-worked sediments have yet been recognised within parental melts from Hadean gneisses as recorded within titanite.

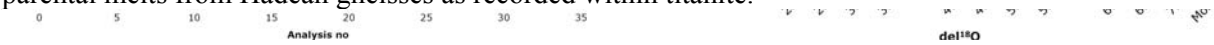

Fig 2. δ^{18}O data from Acasta samples. Parameters as per Fig 1.

Summary

A new technique for in situ δ^{18}O analysis of titanite has been developed on the Cameca IMS 1270 ion microprobe at Edinburgh that gives accurate and precise (0.4-0.6‰ 2SD) data in spatially controlled ellipses c.30μm in diameter. The first application on titanites from c.3.8 Ga (Hadean) gneisses from West Greenland and the Slave Province implies that titanite could have crystallised in equilibrium with igneous zircon and that no detectable earlier contribution from sediments was present within the parental magmas. Further work will look more closely at the issue of equilibrium conditions between zircon and titanite in these samples. All titanite samples will be dated by U-Pb methods and selected samples chosen for Nd and Ca isotope analysis.

References

[1] R.T. Pidgeon, et al, Earth. Planet. Sci. Lett. 141 (1996) 187-198.
[2] X.Y. Zhang, et al, Chem. Geol. 235 (2006) 105-123.
[3] A.I.S. Kemp, et al, Nature 439 (2006) 580-583.
[4] K. Kreissig & T. Elliott, Geochim. Cosmochim. Ac. 69 (2005) 165-176.
[5] E.M. King, et al, Geochim. Cosmochim. Ac. 65 (2001) 3165-3175.
[6] J.W. Valley, et al, Contrib. Mineral. Petrol. 133 (1998) 1-11.
[7] G. Caro, et al, Geochim. Cosmochim. Ac. 70 (2005) 164-191.
[8] B.S. Kamber, et al, Contrib. Mineral. Petrol. 145 (2003) 25-46.

[9] S. Bowring & I. Williams, Contrib. Mineral. Petrol. 134 (1999) 3-16.
[10] T. Iiuzuka, et al, Geology 34 (2006) 245-248.

Geochemistry and boron isotopic composition of tourmalines from gold-bearing and barren rocks in SW Finland – a pilot study

M. Talikka[1], S. Vuori[2], R. Lahtinen[2]

[1]Polar Mining Oy, Käärmesaarentie 3B, 02160 Espoo, Finland
[2]Geological Survey of Finland, PL96, 02151 Espoo, Finland

Tourmaline is a common mineral with several significant aspects. For example, tourmaline is an important constituent in the boron cycle on the Earth, it is closely connected to a number of hydrothermal ores, and provides information on associated ore forming processes. Tourmaline is present in a number of gold and other metal occurrences around Finland. At the moment, the amount of REE and isotopic data on tourmalines from the Finnish ore deposits is limited. O'Brien et al. [1] published isotope (O, H, Sr) data on tourmalines along other minerals from the late Archean Hattu Schist Belt located in eastern Finland. According to them, the primary composition of minerals was affected by Proterozoic overprint, which made the interpretation of the data challenging. The present study area is located in southwestern Finland within the Proterozoic Svecofennian domain that hosts a large number of gold occurrences and showings. As a result of high demand for raw materials, considerable exploration for metallic ores, particularly for gold, is in progress within the study area. So far, the Kutemajärvi gold deposit at Orivesi, which is one of the study sites, is the only operating gold mine in southern Finland.

Objective of this study is to produce new geochemical and isotopic data, which will enlighten the relation between the formation of tourmalines and mineralisation processes. The study is a joint effort by the Geological Survey of Finland and University of Helsinki, Department of Geology. In order to obtain geochemical data on tourmalines, the selected samples were analyzed using electron microprobe device at the Geological Survey of Finland. In addition, Dr. Simone Kasemann made boron isotopic measurements (Table 1) at the Ion Microprobe Facility of the University of Edinburgh. The interpretation of the geochemical and the boron isotopic data is in progress and the data is yet to be published. It is, however, to be noted that both the geochemical and isotopic data demonstrate values of reasonable scale, and provide completely new information on tourmalines from the barren and mineralised Finnish bedrock.

References

[1] O'Brien, Hugh E., Nurmi, Pekka A,. & Karhu, Juha A., 1993. In: Nurmi, P. A. & Sorjonen-Ward, P. (eds.) Geological development, gold mineralization and exploration methods in the late Archean Hattu schist belt, Ilomantsi, eastern Finland. Geological Survey of Finland. Special Paper 17, 291-306

Table 1. Boron isotopic results for tourmaline samples.

Sample	*11B/10B*	*SD(mean)*	*delta 11B*	Sample	*11B/10B*	*SD(mean)*	*delta 11B*
tourmaline1-1a	3.8605	0.0038	-10.7	tourmaline7-4b	3.8662	0.0039	-10.8
tourmaline1-1b	3.8554	0.0020	-12.1	tourmaline7-3a	3.8596	0.0031	-12.5
tourmaline1-3a	3.8534	0.0029	-12.6	tourmaline7-3b	3.8557	0.0023	-13.5
tourmaline1-3b	3.8585	0.0032	-11.2	tourmaline8-4a	3.8559	0.0022	-13.5
tourmaline2-3a	3.8489	0.0038	-13.7	tourmaline8-4b	3.8583	0.0020	-12.8
tourmaline2-3b	3.8570	0.0023	-11.6	tourmaline8-2a	3.8610	0.0018	-12.1
tourmaline2-2a	3.8503	0.0035	-13.4	tourmaline9-1a	3.8648	0.0023	-11.2
tourmaline2-2b	3.8477	0.0035	-14.1	tourmaline9-1b	3.8667	0.0023	-10.7
tourmaline3-3a	3.8611	0.0020	-10.6	tourmaline9-3a	3.8624	0.0031	-11.8
tourmaline3-3b	3.8616	0.0010	-10.5	tourmaline10-1a	3.8671	0.0023	-10.5
tourmaline3-4a	3.8609	0.0026	-10.6	tourmaline10-1b	3.8697	0.0035	-9.9
tourmaline3-4a	3.8642	0.0020	-9.8	tourmaline11-3a	3.8718	0.0024	-9.3
tourmaline3-3c	3.8711	0.0025	-9.5	tourmaline11-3b	3.8724	0.0032	-9.2
tourmaline4-3a	3.8723	0.0019	-9.2	tourmaline12-3a	3.8778	0.0020	-7.8
tourmaline4-4a	3.8626	0.0019	-11.7	tourmaline12-3b	3.8777	0.0011	-7.8
tourmaline4-4b	3.8626	0.0019	-11.7	tourmaline12-2a	3.8699	0.0018	-9.8
tourmaline5-4a	3.8517	0.0039	-14.5	tourmaline12-2b	3.8714	0.0020	-9.4

tourmaline7-4a	3.8715	0.0037	-9.4

Distribution of trace elements between zircon, garnet and melt: a key to understanding crustal events and processes

R.J.M. Taylor[1], S.L. Harley[1], R.W. Hinton[1] & S. Elphick[1]

[1]School of GeoSciences, University of Edinburgh, Edinburgh EH9 3JW, UK

Background

The interpretation of zircon age data in multiply-deformed and polymetamorphosed high grade terrains presents a significant problem in geochronology because the response of zircon to metamorphism is highly variable even on the microscale. The reliable interpretation of zircon age data must be founded upon detailed textural analysis coupled with in-situ microanalysis that yields independent chemical criteria for constraining the processes that have affected or controlled zircon behaviour. The distribution of REE and other trace elements between zircon and garnet in high-temperature crustal processes is being determined in this project, using both an empirical approach, based on in-situ analysis of zircon, garnet and co-existing phases in natural granulites and migmatites, and high-PT trace element doped experiments that yield zircon-granitic melt, garnet-melt and zircon-garnet-melt products. The distribution data are applied to evaluate the event significance of zircon ages in HT and UHT terranes, the responsiveness of zircon to post-peak mineral-melt reactions, and the relative importance of zircon recrystallisation versus new growth in metamorphism. Examples of such applications are provided in this report, and in a separate but parallel report in this volume (Harley et al.).

Results – Experimental Data

A series of experiments simulating granitic, crustal melts from pelitic rocks at high pressure and temperature are used to grow zircon and garnet in trace element equilibrium, to determine REE partition coefficients at a variety of relevant conditions.

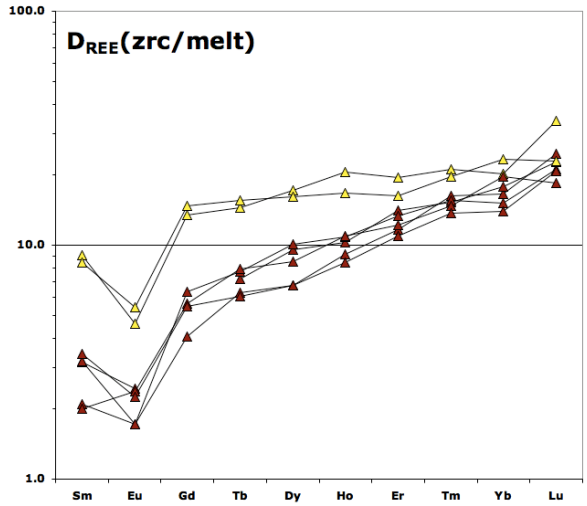

Fig.1. Edinburgh IMS-4f partitioning data for the REE between zircon and granitic melt in experimentally produced samples, at 5Kbar and 850-1000°C.

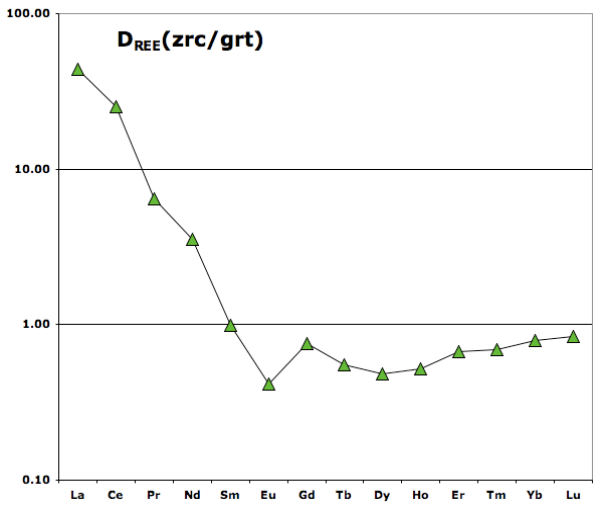

Fig.2. Edinburgh IMS-4f partitioning data for the REE between zircon and garnet in an experimentally produced sample at 7Kbar and 900°C.

REE values for experimentally produced zircon and garnet in granitic melt are obtained using the Edinburgh IMS 4f ion microprobe. Zircon grains are not large enough for single analyses, therefore a mixing line is used, ranging from clean melt to ~40% zircon, to extrapolate zircon REE concentrations.

D_{REE}(zrc/melt) data (fig.1) show a consistent pattern within the temperature range 900-1000°C (red triangles), with a positive slope in the M/HREE (D_{Gd} = ~4-7, D_{Lu} = ~20). D values for the 850°C experiments (yellow triangles) show a slightly more flat pattern (D_{Gd} = ~15, D_{Lu} = ~20-30). This data matches well with previous figures using similar melt compositions, and provides a more complete dataset.

D_{REE}(zrc/grt) data (fig.2) shows an approximately flat pattern for the M/HREE (D_{Gd}/D_{Lu} = ~1) with values close to unity, representing a close to even distribution of these elements between the two minerals, slightly favouring garnet. This experimental data can be matched to natural rock data, providing chemical criteria for showing zircon-garnet equilibrium in high-PT rocks, which is difficult to prove texturally.

Results – Natural Rock Data

As a complimentary dataset, samples of natural crustal melts from pelitic rocks in the Kerala Khondalite Belt (KKB), Southern India were obtained for comparison with the experimental data. Careful selection of leucosome samples from the KKB and detailed study using the combined techniques of textural observation, in-situ chemical analysis and accessory mineral geochronology has provided D_{REE}(zrc/grt) data which correlates very well with the experimental data (fig.3). The fact that the partitioning values for the M/HREE match the experimental example suggests these KKB samples represent equilibrium growth of zircon and garnet.

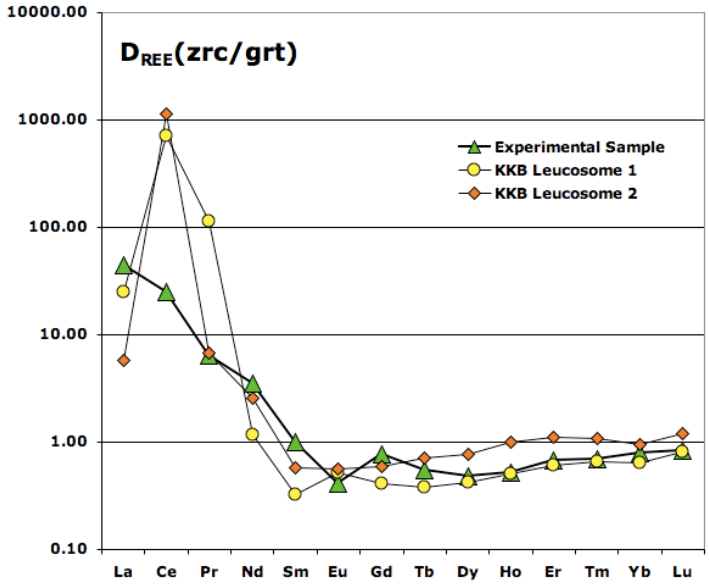

Fig.3. Edinburgh IMS-4f partitioning data for the REE between zircon and garnet in natural crustal melts from the KKB in comparison to experimental data produced in equivalent conditions.
Both the shape of the pattern and the partitioning values are very similar, suggesting these examples match the equilibrium partitioning values from the experimental data.

This matches other data in this volume (Harley et al.) which has consistently shown that D_{HREE}(zrc/grt) patterns of near unity represent equilibrium values for high P-T terrains, and that in-situ trace element analysis must be used, in conjunction with other techniques, to match up thermobarometric data obtainable from garnet, to U-Pb ages from zircon grains in the same rock.

Trace element analysis of Neoproterozoic metazoan embryos

C. W. Thomas[1] & P.C.J. Donoghue[1]

[1]Department of Earth Sciences, University of Bristol, Bristol BS8 1RJ, UK

Introduction

Fossilized eggs, embryos and larvae of marine animals have been found within Neoproterozoic to Lower Ordovician aged phosphorites, from localities in China, Siberia, Australia and North America. Comparative studies between the embryology of living organisms have facilitated major insights into the evolution and development of multicellular animals, thus the presence of such data in the fossil record is unquestionably fundamental to our understanding of this crucial juncture in life history. Eggs and embryos are preserved by permineralization and encrustation with hydroxyapatite, however, preserved biological structures such as subcellular tissue may be overprinted by diagenesis in some cases, thus necessitating a means of discriminating late diagenetic signatures to validate data and assess it's true value to future research. Synchrotron X-ray tomographic microscopy (SXRTM) has been employed to achieve submicrometer scale resolution of embryos [1], and variations in attenuation spectra within individual specimens have revealed differences in the mineralization chemistry. Such differences in mineral chemistry could yield valuable information pertaining to the mode and nature of diagenesis within specimens and could subsequently account for the disparity in preservation quality inherent in the fossil assemblages. However attenuation differences under synchrotron analysis alone are incapable of identifying and quantifying chemical species. A one-day project was therefore proposed with the aim of identifying qualitative differences in mineral chemistry within five diagenetically distinct embryos from the Neoproterozoic Doushantuo formation from South China in order to assess the feasibility of extending the analysis to a wider stratigraphic range of specimens. Four specimens were chosen from a distinct upper 'grey' facies within the Doushantuo Formation containing very high numbers of eggs and embryos. One specimen from this horizon contained well preserved sub-cellular structures while the remaining three displayed varying degrees of diagenetic overprinting.

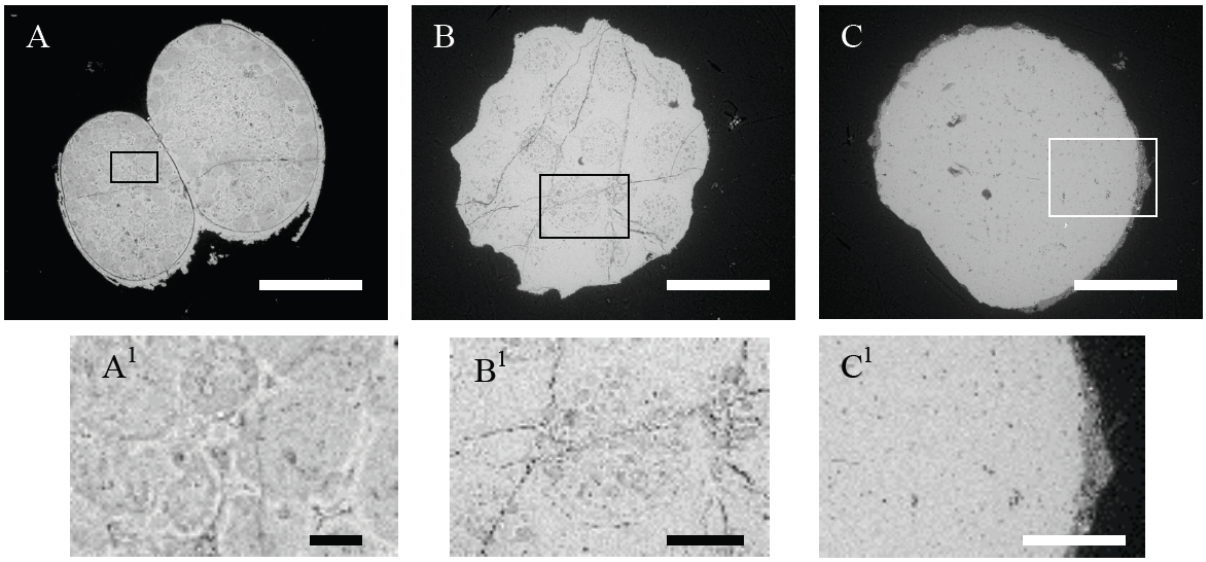

Figure 1. Backscatter electron images of exemplar specimens illustrating degrees of diagenetic overprinting. A) 2-cell embryo with internal darker regions, interpreted as preserved lipid vesicles [1]. A1) Enlarged view of box in A showing internal sub-cellular structures, highlighting differences in attenuation which can also be seen under SXRTM. B) Multi-celled embryo where internal structures have been diagenetically altered. B1) Enlarged view of box in B showing preserved sub-cellular structures surrounded by a region of diagenetic overprinting. C) Specimen from lower black facies (LBF) showing no preservation of biogenic structures. The darker outer region indicates multiphase mineralization. C1) Enlarged view. Scale for A, B, C, = 250μm, scale for A1, B1, C1 = 50μm.

The final specimen was taken from a different horizon directly underlying the first,which characterised a distinctly different facies (named the lower black facies) and contained markedly less fossil material (Figure 1). Ten mineral species were analysed for each specimen; Mg, Al, Si, P, Ca, Sr, C, F, Si, Cl, Ca, Ti, and analyses were taken in point form at various positions of interest over the polished surfaces of the embryos.

Results and concluding remarks

The resulting data highlighted significant disparities in the abundance of certain chemical species between embryos from different facies: There were lower abundances of Al and Cl and marked elevations in Sr in the embryo from the lower black facies, yet the relative abundances of calcium and phosphate remained constant throughout all of the specimens analysed and the remaining elements studied displayed little inter-specimen variance (Figure 2). There was very little variation in the abundance of mineral species within individual specimens, which may have resulted from using a spot size that was too large to achieve the resolution necessary to differentiate between the attenuation variance demonstrated by SRXTM analysis. Subsequently, further analyses using a smaller spot size may be necessary in order to resolve this. However, overall, this study has demonstrated that preservational quality among the fossil assemblages in question is likely to be controlled by differing diagenetic regimes, not by the initial mode of apatite precipitation or the chemical nature of the apatite precipitated.

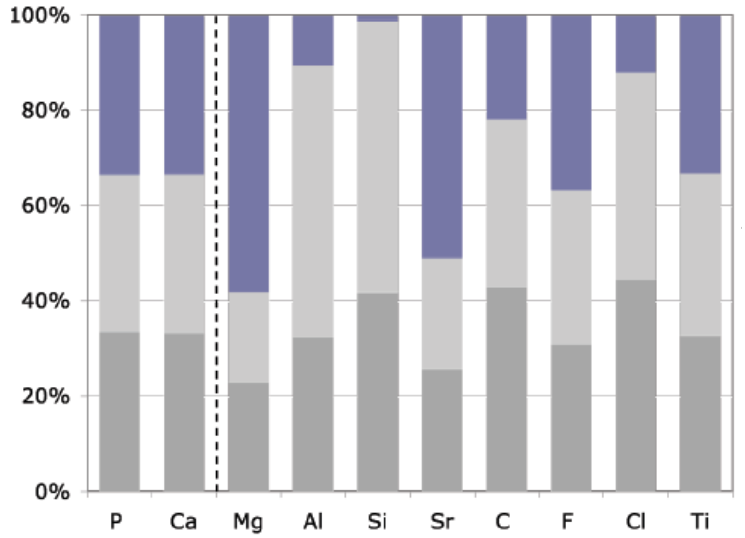

Figure 2. Graph showing averaged relative percentage abundances for calcium and phosphate and other accessory minerals (separated by a dashed line). Dark blue portions represent the specimen from the lower black facies. Grey portions correspond to two representative specimens from the upper facies.

References

[1] J. W. Hagadorn *et al*. Science 314 (2006) 291-294

The carbon isotopic composition of diamonds from Juina, Brazil

M. Walter[1] and G. Bulanova[1]

[1]Department of Earth Sciences, University of Bristol, Bristol BS* 1RJ, UK

Introduction

Natural diamonds are transported from Earth's deep mantle to the surface, and some of these contain mineral inclusions. These inclusions have highly variable major element stoichiometries and indicate a wide range of mantle parageneses. The chemistry of the inclusions along with mineral phase relations yield important information about their mantle protoliths, and constrain the conditions of diamond formation. Rare among these inclusions are those with chemical compositions consistent with deep mantle mineral precursors in the mantle transition zone (400 – 660 km) or lower mantle (>660 km), e.g. [1,2]. Certain inclusions have a clear chemical affinity with mantle peridotite, while others share a pedigree with subducted lithosphere or oceanic crust [3]. We are currently studying sets of inclusion-bearing natural diamonds from the the Juina area, Brazil. Over the past several years we have carried out mineralogic and geochemical investigations on several dozen inclusions with a wide range of paragenesis. We have found that the major and trace element geochemistry of majorite-garnet and rare, Ca-Ti-rich perovskite in several diamonds indicate an origin for some of the diamonds in the mantle transition zone. Our trace element modelling indicates that the equilibration of the inclusions with carbonatitic melt derived from eclogite. The carbon isotopic compositions of these diamonds can provide critical information needed to test our hypothesis, as C isotopes have been used for discriminating between peridotitic diamonds that originate from 'primordial' carbon ($d^{13}C \sim -5$) and eclogitic diamonds that tend to lighter values indicative of organic carbon ($d^{13}C \sim -5$ to -25) presumably injected into the mantle via subduction [4,5]. Further, some diamonds, for example those from Kankan, show carbon isotopic compositions indicating derivation from a carbonate source ($d^{13}C \sim -3$ to $+5$) that may reflect crystallisation from a carbonate-rich melt or fluid. This is particularly relevant for hypothesis based on the trace element signature of Ca-Ti-rich perovskite inclusions that indicate possible equilibration with a carbonatitic liquid. Previous work on alluvial diamonds from this part of Brazil yield carbon isotopic compositions extending from the mantle value of ~ -5‰ to lighter values of ~ -12‰ [6], which is consistent with their formation from minor fractionating mantle fluids [7].

Results

Carbon isotopic compositions were measured with the IMS1270 on 27 sectioned and polished diamonds; 14 diamonds from the Collier 4 kimberlite pipe and 13 from the Machado river. Figure 1 shows results of core to rim traverses in 14 diamonds from the Collier 4 mine. The Collier 4 diamonds span a wide range in isotopic composition from 'heavy' mantle values (e.g. J20 with an olivine inclusion) to extremely light values indicative of organic carbon (e.g. J19 with coesite and kyanite inclusions). Importantly, we note that the CaTiSi-perovskite inclusions in diamonds J1 and J10 have relatively uniform and isotopically light carbon (-10‰ to -12‰) consistent with their derivation from subducted eclogite as is indicated by their major and trace element geochemistry. In contrast, several diamonds that contain apparently deep mantle inclusions (CaSi-perovskite and majorites in J8, J9 and J14) show cores with isotopically light carbon (-10‰ to -14‰) indicative of eclogite, to rims with heavier carbon indicative of primordial mantle carbon (~-6‰). One potential explanation for such variation is multiple stages of growth of the diamonds from fluids or melts from different sources. For example, diamond may crystallize from a carbonatitic melt from eclogite in the transition zone, but such melts will invariably freeze when injected into peridotite. Melting of carbonated/metasomatised peridotite at a later stage may then impart a peridotitic carbon isotopic composition during renewed growth of the diamond. The 13 diamonds from the Machado River also show a wide range of carbon isotopic values, but we note that there are several diamonds of apparently ultradeep paragenesis based on their mineral inclusions that have heavy values (0‰ to -3‰) possibly indicative of derivation from carbonates. These results are invaluable for helping to constrain our recent models of carbonatite melt generation and diamond formation in the deep mantle based on mineral inclusions [8].

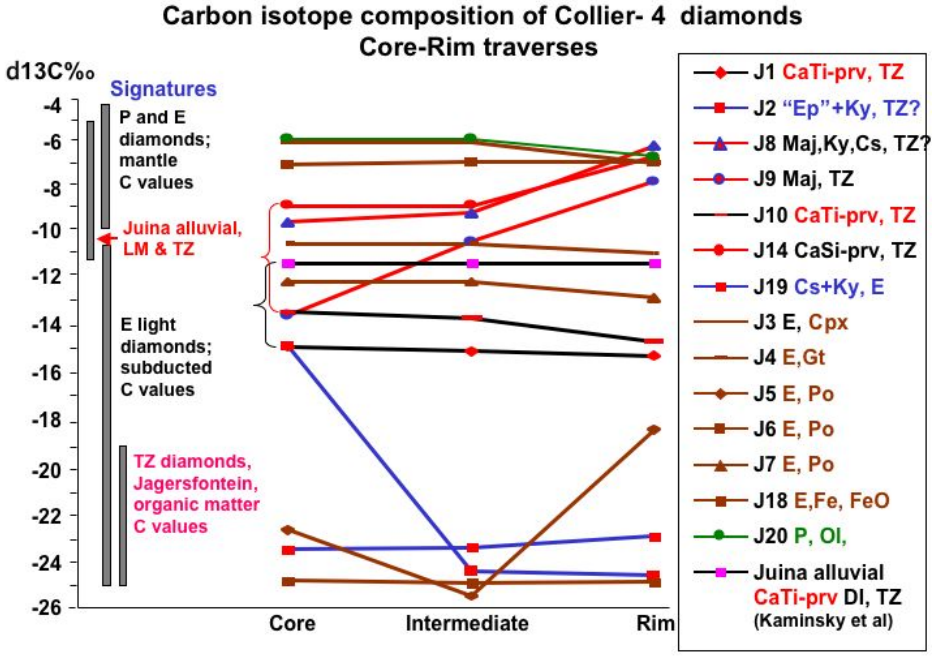

Figure 1. Core to rim traverses in 14 diamonds from the Collier 4 kimberlite pipe, Juina, Brazil.

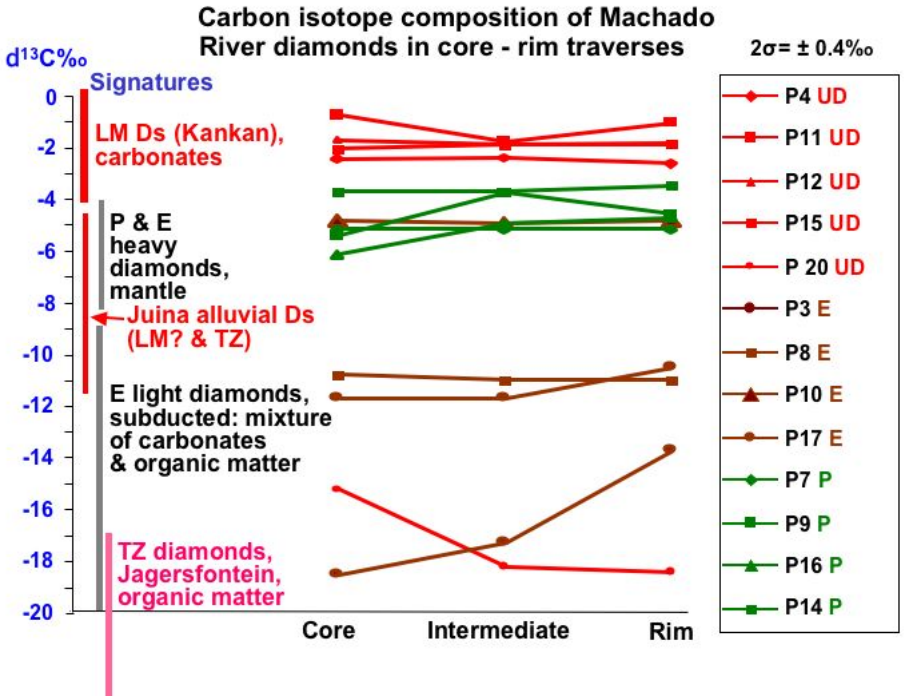

Figure 2. Core to rim traverses in 14 diamonds from the Machado River, Juina, Brazil.

References

[1] Harris, J (1992). In: Field, J.E., (Ed), Academic Press, London, 345-393.
[2] Harte and Harris (1994), Mineralogical Magazine, 58A, 384-385.
[3] Stachel, T.et al (2004) Lithos, 77, 1-19.
[4] Deines, P. (1980) Geochim. Cosmochim. Acta 44, 943- 961.
[5] Tappert et al (2005) Geology 33, 565-568.
[6] Hutchison et al (1999) In: Proc. 7th IKC, Cape Town, SA,V. 2, 372-382.
[7] Stachel et al (2005) Elements 1, 73-78.
[8] Walter et al (submitted) Nature.

Understanding the processes that control diamond formation and their growth histories: a mineralogical, carbon, nitrogen and Re-Os isotope study

D.F. Wiggers de Vries[1], G.R. Davies[1], D.G. Pearson[2] & G.P Bulanova[3]

[1]Faculty of Earth and Life Sciences, Vrije Universiteit, Amsterdam 1081 HV, NL
[2]Department of Geological Sciences, Durham University, Durham DH1 3LE, UK
[3]Department of Earth Sciences, University of Bristol, Bristol BS8 1RJ, UK

Objectives

The study of carbon isotopes in natural diamonds is generally applied to determine the source of the diamond-forming fluid. In our present project we study diamond growth in detail, i.e. at the level of individual growth zones, by combining various techniques. Analysing carbon isotopes along a traverse from core-to-rim enables us to monitor the variability of $\delta^{13}C$ and thus address the temporal variability of the source. Additionally, the time-component will also be accessed by another of our recent projects that focuses on the timescale of diamond growth by Re-Os dating. The key-question is if the varying core-to-rim carbon isotope composition of natural diamonds is produced by source variations and/or modified by kinetic effects.

Methods

The diamonds studied here are from Siberia. Traverses from core-to-rim of 13 diamonds show considerable variability in $\delta^{13}C$. In order to fully understand the significance of any variability in carbon isotope ratios, the homogeneity of a single growth layer, as well as the role of diffusion was investigated. Given that diamonds reside in the mantle at high temperatures (>1000˚C) it is likely that the primary carbon isotope composition is modified by diffusional equilibration and that carbon isotope patterns are smoothed out. If such a process occurs then measured carbon isotope ratios need to be interpreted in the context of diffusional processes. For this reason areas in diamonds that have a significant difference in $\delta^{13}C$ (i.e. >1‰ up to 10‰) are examined. The carbon isotopic ratios are analysed in great detail along a traverse that is at a small angle to the growth zoning in the diamond (and almost perpendicular to the initial core-to-rim traverse) to determine if there is diffusion (smooth-function) or no diffusion (step-function) in this particular area. Due to the angle of these detailed traverses it will effectively rule out or give evidence for diffusion at a sub 5 µm scale.

Results

All diamonds show core-to-rim variability of the carbon isotopes. However, trends can be correlated to distinct groups of CL growth patterns (Fig 1 and 2) and within these groups $\delta^{13}C$ is gradually changing (progressively or retrogressively).

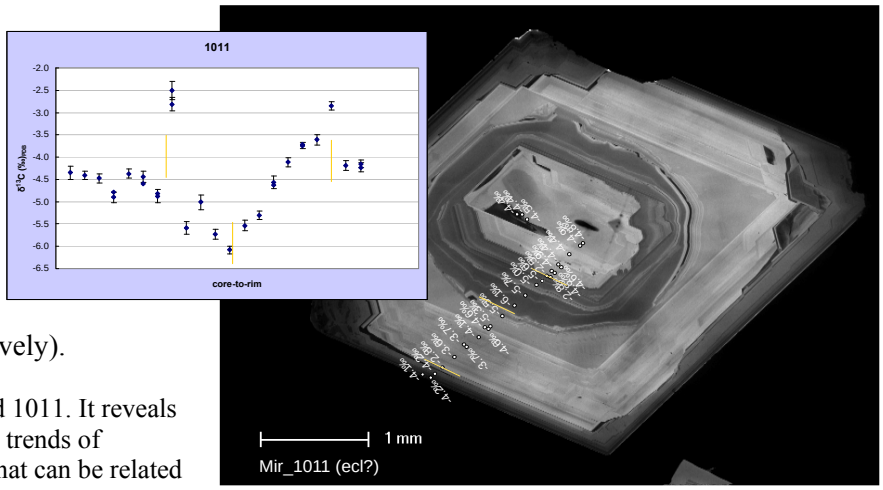

Figure 1. CL image of diamond 1011. It reveals marked variability in $\delta^{13}C$ with trends of increasing or decreasing $\delta^{13}C$ that can be related to specific CL areas.

Importantly, we can confirm that the carbon isotope ratio is constant within a single growth zone (Fig. 2). The detailed traverses perpendicular to the core-to-rim traverse establish there is a step-function of $\delta^{13}C$ between successive growth layers (Fig. 3).

Direct implications

The fact that there is no smoothing of carbon isotopes at the sub 5 um scale (step-function) establishes that the initial carbon composition of the diamonds has not been modified by kinetic processes such as

diffusional equilibration. Hence, it is possible to perform analyses at the micron-scale to study the growth zoning in natural diamonds to obtain isotopic signatures representative of the parental fluid and to understand the details of the variation in parental fluids.

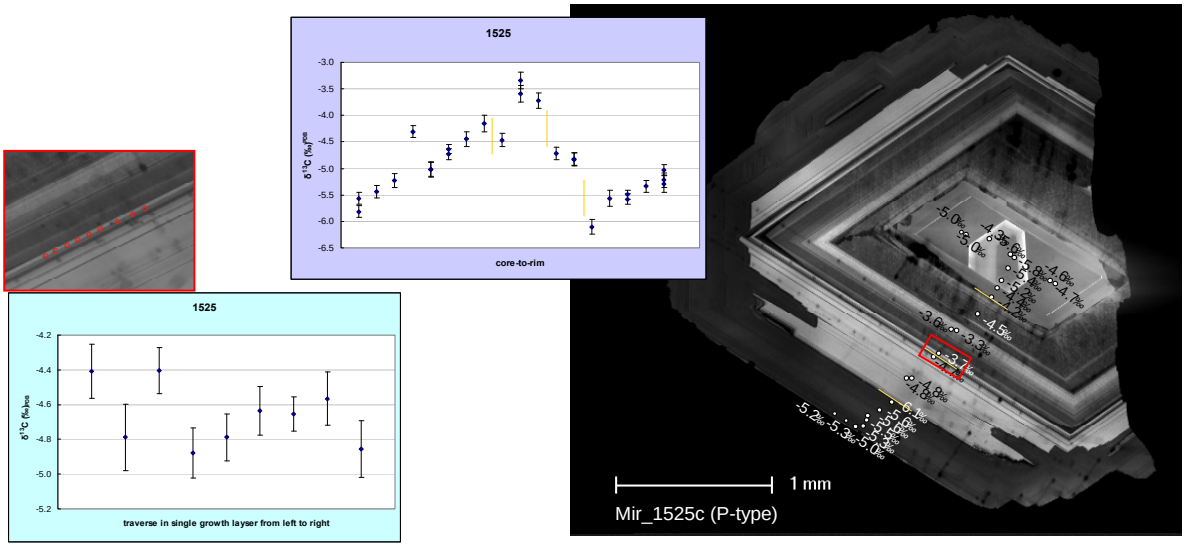

Figure 2. CL image of diamond 1525. Core-to-rim variability and trends in $\delta^{13}C$ like in diamond 1011 are revealed. Additionally, the carbon isotopes are shown to be constant (within error) for a singe growth layer.

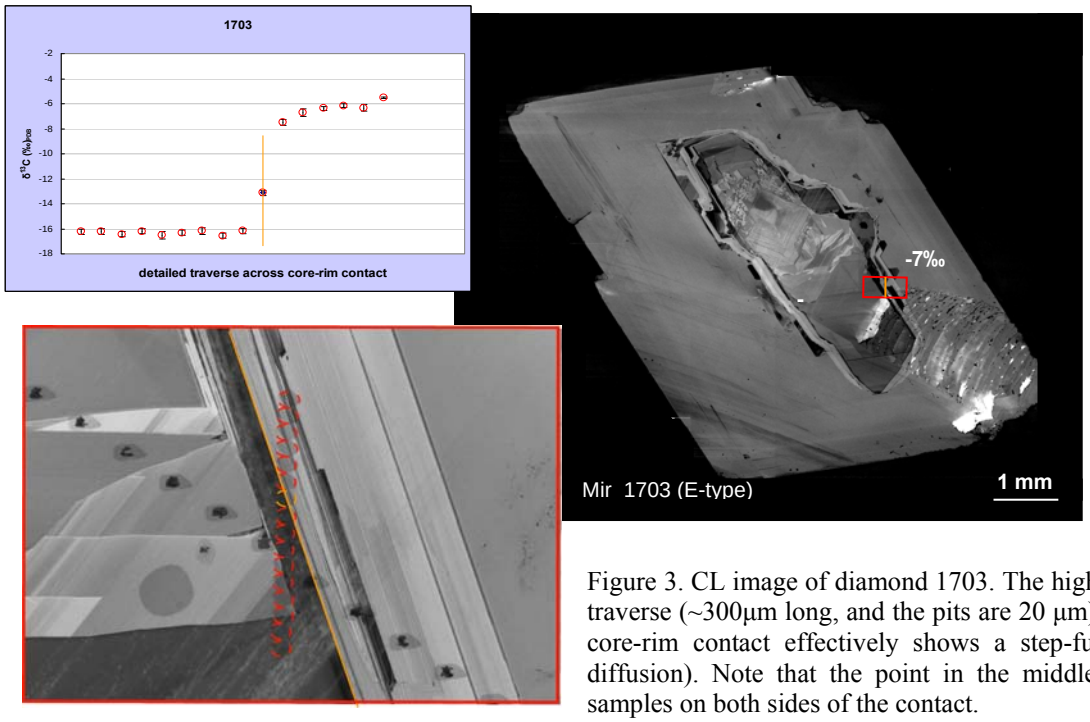

Figure 3. CL image of diamond 1703. The highly detailed traverse (~300µm long, and the pits are 20 µm) across the core-rim contact effectively shows a step-function (no diffusion). Note that the point in the middle of –13‰ samples on both sides of the contact.

Broader implications

The above results are part of a broader study about diamond growth. Re-Os analyses to unravel the timescale of diamond growth have been partly completed and provide clear evidence of age variations within some individual diamonds. Further work is in progress to establish the diamond growth episodes in individual diamonds. In addition, new FTIR spectra that correlate with the SIMS pits, will give another perspective to the temporal $\delta^{13}C$ variability of the C-source from which the diamonds formed. These spectra will in turn provide another anchor for the nitrogen abundance analyses that have been performed at the Cameca ims-1270. Unfortunately the nitrogen isotope analyses performed as part of this project have proved to be difficult to reproduce and as yet are not understood.

Annual sulphate abundance cycles and secular sulphur isotope variations in speleothems

P.M. Wynn[1], I.J. Fairchild[2] and A. Baker[2]

[1]Department of Geography, Lancaster University, Farrer Avenue, Lancaster, LA1 4YQ
[2]School of Geography, Earth and Environmental Sciences, University of Birmingham, Edgbaston, Birmingham, B15 2TT

Introduction

Sulphur emitted into the atmosphere from the combustion of fossil fuels is regarded as a key mechanism in climate forcing at both the local and regional scale. Trace amounts of sulphate in speleothem carbonate at some cave sites show an increase in concentration towards the present day, potentially reflecting the increase in SO_2 emissions since the onset of the industrial era. This suggests speleothems may record local aspects of atmospheric sulphate content where sulphur isotopes can be extracted and used as a tool for provenance. However, speleothem sulphur concentrations are low and manual techniques for sulphur isotope analysis allow only low resolution sampling. Microanalytical techniques are thus required to build a comprehensive record of SO_2 loading in the atmosphere.

Objectives

This work aimed to establish a method for the analysis of sulphur isotopes, present as sulphate within speleothem carbonate at low concentrations (15 – 300 ppm). The method was then used to develop records of sulphur isotopic change in slow growing speleothems where annual laminations were less than 100 μm thick and manual techniques for the extraction and analysis of sulphur isotopes were not suitable. Materials for analysis were obtained from Alpine cave sites in Austria (Obir Cave) and Italy (Ernesto Cave) which have been monitored as part of a larger project (NERC grant NE/C511805/1) to establish sulphur cycling through the cave ecosystem prior to incorporation into speleothem calcite.

Results

Spot analysis at annual resolution encompassing the past 100 years demonstrates an excursion in sulphur isotopic composition from values close to the carbonate bedrock end-member value in the pre-industrial era, to values isotopically depleted in ^{34}S.

Figure 1: $\delta^{34}S$ and Sulphur concentration between 2002 and 1950 in Austrian stalagmite OBi84

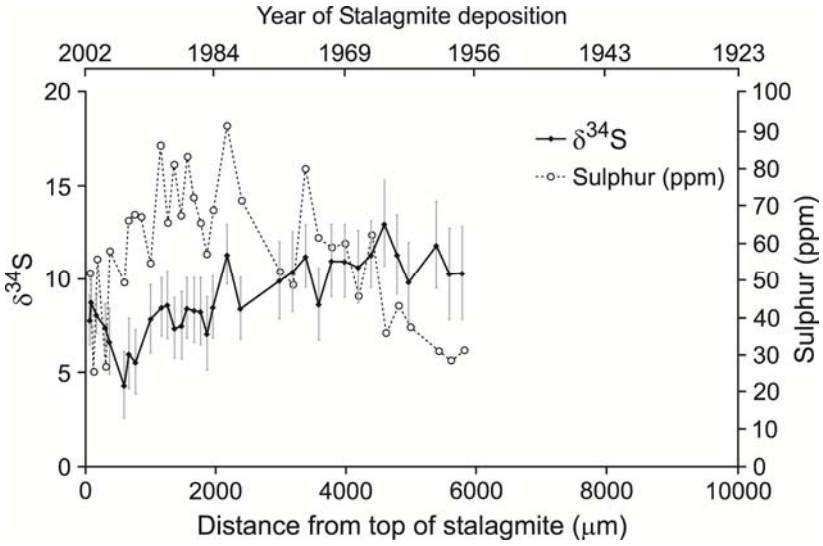

Such depletion in ^{34}S is generally taken to be indicative of sources of industrial pollution where there is an absence of pyrite bearing minerals in the surrounding carbonate matrix. This trend to isotopically depleted $\delta^{34}S$ is mirrored by increasing concentrations of sulphate reflecting the increase in SO_2 emissions with industrial activity (Figures 1 and 2). The subsequent decline in speleothem sulphate

concentrations post 1985, reflects the recent European decline in industrial atmospheric SO_2 content and is thought to be mirrored by the rebound in sulphur isotopic composition to values more enriched in ^{34}S.

Figure 2: $\delta^{34}S$ and Sulphur concentration between 1995 and 1950 in Italian stalagmite ER78

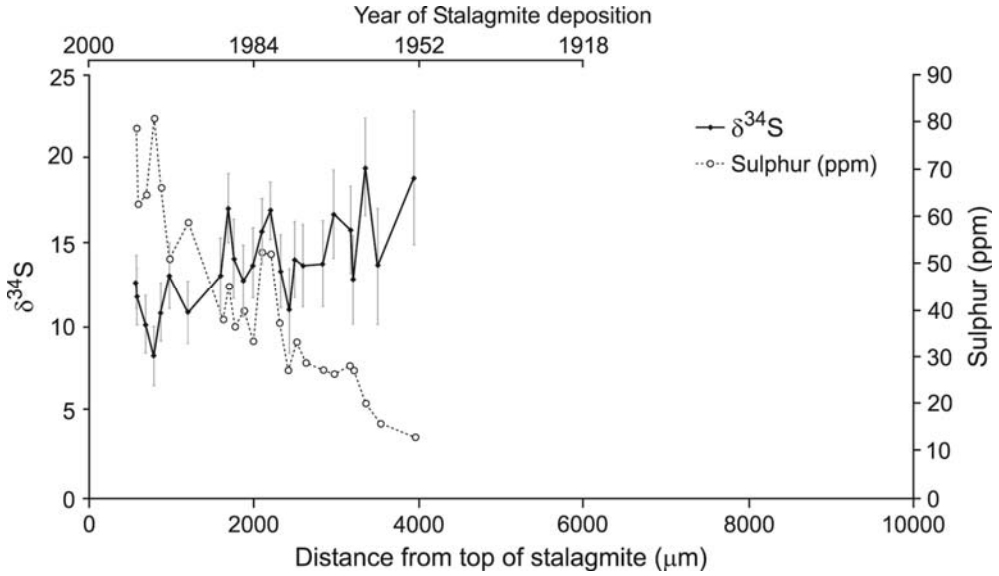

Error bars represent counting statistic errors. For the low sulphur concentrations (~10 ppm) these are ±4 ‰ while for the higher concentrations (~ 70 ppm), these errors approach ±1.5 ‰. The source of this error is related to the need for a more suitable standard material. Results presented here are standardized to Ion Microprobe Facility coral standard M93. However, sulphur concentrations are much greater than those detected within speleothem calcite, and isotope values are enriched in ^{34}S compared to those analysed within stalagmites. New, low sulphur standard material is currently being investigated so that instrumental conditions can be optimized to provide higher precisions at low (10-50 ppm) sulphur concentrations.